MULTI-SCALE AFFINITY ASSAYS FOR THE STUDY OF CARBOHYDRATE INTERACTIONS. EFFECTS OF SIZE, MULTIVALENCY AND SCAFFOLD FLEXIBILITY

Inaugural dissertation

for the attainment of the title of doctor
in the Faculty of Mathematics and Natural Sciences
at the Heinrich Heine University Düsseldorf

presented by

Alberto Camaleño de la Calle
from Valladolid, Spain

Düsseldorf, December 2018

from the institute of Organic and Macromolecular Chemistry
at the Heinrich Heine University Düsseldorf

Published by permission of the
Faculty of Mathematics and Natural Sciences at
Heinrich Heine University Düsseldorf

Supervisor: Jun. Prof. Dr. Stephan Schmidt
Co-supervisor: Prof. Dr. Rainer Weinkauf

Date of the oral examination: 31st January 2019

This work was prepared between October 2015 and March 2018 at the Institute Organic Chemistry and Macromolecular Chemistry of Heinrich Heine Universität Düsseldorf, in the group of Colloidal Bioadhesion of Jun. Prof. Dr. Stephan Schmidt.

a José Miguel e Inés

—Como me quieres bien, Sancho, hablas desa manera —dijo don Quijote—, y como no estás experimentado en las cosas del mundo, todas las cosas que tienen algo de dificultad te parecen imposibles; pero andará el tiempo, como otra vez he dicho, y yo te contaré algunas de las que allá abajo he visto, que te harán creer las que aquí he contado, cuya verdad ni admite réplica ni disputa.

Miguel de Cervantes Saavedra (1615)
Segunda parte del Ingenioso caballero don Quijote de la Mancha
Capítulo XXIII

"Thou talkest in this way because thou lovest me, Sancho," said Don Quixote; "and not being experienced in the things of the world, everything that has some difficulty about it seems to thee impossible; but time will pass, as I said before, and I will tell thee some of the things I saw down there which will make thee believe what I have related now, the truth of which admits of neither reply nor question."

Miguel de Cervantes Saavedra (1615)
Translation by Thomas Shelton (1620)
The History of the Valorous and Wittie Knight-Errant Don-Quixote of the Mancha
Part II, Chapter XXIII

TABLE OF CONTENTS

ABBREVIATIONS

^{1}H-NMR	Proton nuclear magnetic resonance
AFM	Atomic Force Microscopy
APTES	(3-Aminopropyl)triethoxysilane
BSA	Bovine Serum Albumin
CA-SCP	Crotonic acid functionalized SCP
Con A	Concanavalin A
CuAAC	Copper(I)-catalyzed Azide-Alkyne Cycloaddition
D_2O	Deuterium oxide
DLS	Dynamic Light Scattering
DMF	Dimethylformamide
DMSO	Dimethyl sulfoxide
GLYMO	(3-Glycidyloxypropyl)trimethoxysilane
HEPES	4-(2-hydroxyethyl)-1-piperazineethanesulfonic acid
HPLC	High-performance liquid chromatography
HRMS	High-resolution mass spectrometry
LBB	Lectin Binding Buffer
Man	D-Mannopyranose
ManSH	2-Ethanethiol-α-D-mannopyranoside
MeMan	Methyl α-D-mannopyranoside
MES	2-(*N*-morpholino)ethanesulfonic acid
NGPs	Neoglycoproteins
NHS	*N*-Hydroxysuccinimide
PBS	Phosphate Buffered Saline
PEG	Poly(ethylene glycol)

Abbreviations

PEG linker	α-Maleinimidohexanoic-ω-NHS PEG
PEG-dAAm	Poly(ethylene glycol)-diacrylamide
RBITC	Rhodamine B isothiocyanate
RCF	Relative Centrifuge Force
RICM	Reflection Interference Contrast Microscopy
SCP	Soft Colloidal Probe
SM-AFM	Single-Molecule – Atomic Force Microscopy
SMCC	Succinimidyl 4-(*N*-maleimidomethyl)cyclohexane-1-carboxylate
TBO	Toluidine blue O
UV-Vis	Ultraviolet–visible spectroscopy
XPS	X-ray photoelectron spectroscopy

ABSTRACT

Multivalency is a key principle in Nature to overcome the low affinity of biological ligands and receptors involved in crucial processes such as cellular adhesion, signaling, sensing, and infection. Biomedical and pharmaceutical researchers currently investigate how to utilize multivalency for the development of a new class of bioactive compounds. One of the most promising classes of multivalent biomolecules in this regard are glycomacromolecules because multiple sugars are found on a dense carbohydrate layer on the cell membrane, called glycocalyx, serving as an anchoring site to trigger the crucial cell biological processes, as mentioned. Addressing carbohydrate receptors involved in binding to the glycocalyx using synthetic multivalent glycomimetics might become a suitable strategy toward new drug designs, vaccine development or biosensors. However, the precise control of the binding affinity is still very difficult hampering the development of carbohydrates as multivalent ligands. Their affinity has been reported to be affected by various, and partially opposing contributions such as enthalpic gain due to additive binding of subunits at large multivalent scaffolds and entropic loss due to immobilization of mentioned scaffolds upon binding.[1-4] Also, it is speculated that multivalent binding modes could have beneficial effects for binding at larger scales, e.g., using nanoparticles or colloids as scaffolds extending the surface area for the interaction and overall valency.[5-7] Therefore, a better understanding of the influence of multivalence at the molecular as well as the colloidal scale is crucial to optimize and design the new synthetic active compounds.

By making use of the well-known receptor/ligand pair concanavalin A (Con A) / α-D-mannose (Man), this work first presents and validates various methods for the measurement of specific interactions at different size scales, while varying valency, density, length and flexibility of ligand tether to the scaffold. To this purpose, linear polymers (>25 kDa), protein scaffolds (~66 kDa), microgels (~30 µm Ø) and macroscopic glass surfaces (cm^2) are functionalized with previously synthesized sequence-defined glycooligomers of 1.6-2.6 kDa presenting of 1-5 Man units at well-controlled spacing along the oligomer chain. As functionalization techniques, several bioconjugation techniques involving carbodiimides and active esters are adapted. A major focus is devoted to developing methods that could show the overall binding affinity and binding specificity of these constructs. Then, in the second part, the established multivalent scaffolds are used to systematically study the effect of multivalence, scaffold size, and flexibility of the ligand tether:

First, single molecule AFM was used to detect specific binding of Man-presenting oligomers and polymers on the molecular scale, Figure 1 **a)**. The adhesive forces detected in AFM are composed of the non-specific substrate/linker and substrate/tip, as well as the specific Con A/Man

interactions. Therefore criteria are being developed to ensure detection of specific rupture events between Man and Con A complexes. In this respect, the analysis shows that the dissociation force value of Con A/Man grows with the valency and the molecular weight of the ligands, which might be attributed to subsite binding and simultaneous binding of additional Man moieties. Importantly, however, the longer length of the construct, the lower is the frequency of binding, which could be due to the greater steric repulsion or strong coiling of the chains hiding the Man units in the coil. Therefore, coiled presentation of ligands by linear polymers might lead to lower affinity despite their multivalency.

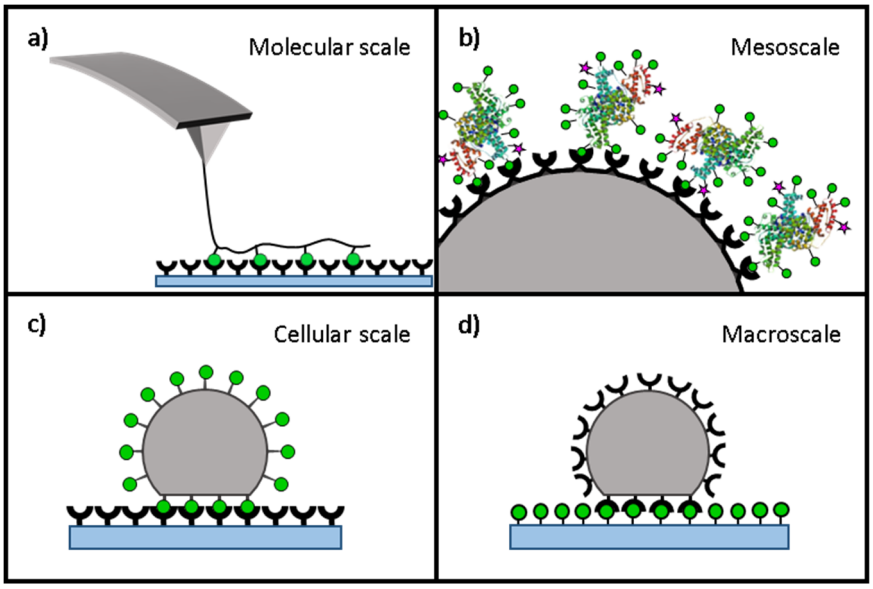

Figure 1- Methods to study multivalent properties at four different scale ranges. a) Molecular scale, using a linear scaffold, analyzed by SM-AFM. b) Mesoscale, using protein scaffolds, analyzed by fluorescence on Con A functionalized SCPs and turbidity measurements (not represented). c) Cellular scale, SCP scaffold bearing sugars, analyzed by SCP-adhesion. d) Macroscopic scale, coverslip scaffold functionalized with sugars, analyzed by SCP-adhesion. Representations are not scaled.

Second, the mesoscopic scale is investigated, between single molecules and colloids. The protein albumin is used as a scaffold onto which Man residues are attached through a linker, to establish so-called Neoglycoproteins (NGPs), Figure 1 **b)**. The overall flexibility of NGPs is altered by the length difference of the used linkers (SMCC ~0.9 nm, PEG ~80 nm). The NGP valency is modified functionalizing them with precision glycooligomers bearing a different number of Man units. As well, fluorescent labeling is introduced to determine the specific binding to Con A functionalized substrates by fluorescence microscopy. An additional turbidity assay highlights the lower activity of the longer flexible PEG linker (10 kDa) when compared to the shorter SMCC linker (334 Da) while clustering a Con A solution. This again indicates the presence of steric repulsion by the higher molecular weight tether and coiling reducing the overall affinity of binding. The lower activity of PEG-functionalized NGPs can be overcome with increasing valency, while a greater

valence for SMCC functionalized NGPs did not improve affinity, indicating that the NGPs scaffold achieves maximum affinity using this analytical method. Lastly, turbidity shows that the mesoscopic scaffolds are more efficient in binding than the molecular-scale ligands used for their functionalization due to the increased size and higher local Man density.

Third, PEG microgels (Ø ~30 µm) are functionalized with Man, to establish so-called Soft Colloidal Probes (SCPs), mimicking the cells glycocalyx, due to the capacity to reproduce their size and elasticity, and serving as cellular scale ligand scaffold, Figure 1 **c)**. Detection of the contact area of these microgels with planar Con A functionalized surfaces yields the adhesion energy between Man and Con A surfaces using the Johnson-Kendall-Roberts model of adhesion (SCP-Adhesion). Special attention is devoted to the development of a reproducible and robust SCP adhesion assay. Then, NGPs and glycooligomers are tested as inhibitors to remove an established adhesion of Man-SCPs on chemically functionalized Con A-surfaces. Both, the ligand scaffold size and the valency increased the adhesion inhibition. The size effect is remarkable, and it is believed that the greater steric repulsion of the NGPs compared to oligomers helped to remove the adhered SCP from the Con A surface.

Finally, Man-functionalized glass coverslips are produced as macroscopic scale ligands to be studied by SCP-Adhesion, Figure 1 **d)**. The functionalization is performed through linkers varying in length (SMCC and PEG). The adhesion assays on these surfaces using Con A functionalized SCPs indicate an effect of the Man linker length, however more detailed studies provide ambiguous results possibly due to large non-specific interactions.

Overall, the effects of size, valency, density and flexibility on multivalent ligand-receptor interactions are investigated. This thesis provides several new assays for studying specific interactions of carbohydrates varying size scale and confirms that the affinity enhancement of multivalent scaffolds grows with the number of moieties and stiffness. As expected, the steric repulsion was shown to also increase with the size and flexibility of ligands. These new insights into material parameters will promote by a combination of them to synthesize feature-defined ligands and control interactions in biological systems.

1 INTRODUCTION

1.1 CARBOHYDRATE-LECTIN AS LIGAND-RECEPTOR PAIR

Ligands and receptors are molecules that bind to form a complex based on non-covalent interactions. The interaction can be described by the lock-key principle since they require structurally matching binding partners. Certain carbohydrates and protein receptors, particularly so-called lectins, have been found to interact specifically and form complexes.

Carbohydrates. Carbohydrates are one of the four main biopolymer classes together with proteins, lipids, and DNA. Carbohydrates are present two remarkable differences compared to the other biopolymers; they can be highly branched and the units are connected by different bonds (N- and O- glycosylation). These features render carbohydrates to exhibit huge structural variations, presumably encoding information. Initially, it was thought that their main function was mostly storage to supply energy as well as mechanical support. In 1988 Dwek et al.[8], coined the term glycobiology encompassing everything concerning the function of sugars in biological systems. Carbohydrate structures are mostly found in glycoproteins and glycolipids, and these are part of the cell membrane among others. The hydrophilic part containing the sugar moieties is exposed to the outer cell serving as docking sites for carbohydrate specific recognition of proteins. Together with structural roles, oligosaccharides also mediate molecular transport to the cell surface and cell-cell and cell-matrix adhesion as well as recognition events. Carbohydrates are essential in numerous biological processes such as inflammation and immune response, viral and bacterial infection or fertilization.[9-10] The biological functions of sugars usually require sugar-binding lectins[11], in which sugar-binding interaction can be ascribed to the carbohydrate-recognition domain (CRD); a module found within the lectin polypeptide.

Lectins. Lectins are non-enzymatic proteins or glycoproteins of non-immunological origin, which typically bind specifically mono-, oligo- or polysaccharides[12] usually in two or more non-catalytic domains, the CRD, whether they are free or part of more complex structures. They also have the ability to bind sugar residues, which are conjugated to lipids or proteins.[13-15]

The classification of lectins can be done by the monosaccharide to which they display the highest affinity. Only six of the many natural sugars are surface constituents of eukaryotic cells; N-acetylglucosamine, N-acetylneuraminic acid (sialic acid), N-acetylgalactosamine, fucose, galactose, and mannose. However, oligosaccharides exhibit association constants 1000-fold higher compared to monosaccharides.[16] Lectins can ubiquitously be found in the majority of organisms,

including plants, animals, viruses, and bacteria, each of which can be further subdivided. Lectins have structural homologies. Many are formed by two or four identical subunits respectively resulting in a dimer or a tetramer. Each subunit consists of around 250 amino acids with a molecular weight of around 25-30 kDa, sometimes carrying up to a couple of N-linked oliogosaccharides. The subunits present a carbohydrate binding pocket (CRD) and two divalent cations (Ca^{2+} and a transition metal such as Mn^{2+}) necessary for carbohydrate binding.[17] Their functions in the kingdom *Animalia* are still not fully understood; it is believed they may play a role in immunological processes; such as mitogenic trigger[18], fungicide preventing mycosis[19], anti-HIV[20] or antitumor[21]). One of the most salient of the lectins is the mannose and glucose specific model lectin concanavalin A, Figure 2. It was isolated from the jack bean in 1919 and today is still one of the most studied lectins.[16, 22-23]

Molecular recognition of lectins. The molecular recognition between lectins and carbohydrates occurs through noncovalent bonding[24]: hydrogen bonding, metal coordination, hydrophobic forces[25], van der Waals forces, dispersive forces. Concanavalin A belongs to the C-type lectins, like most lectins in mammals. Their CRDs are Ca^{2+} dependent providing the sugar recognition activity.[26] Carbohydrate ligands bind through the Ca^{2+} which stabilizes the local conformation of the protein. The cation makes coordination bonds to the protein and key hydroxyl groups of the sugar ring. Amino acid residues that coordinate to the Ca^{2+} also establish hydrogen bonds to the sugar hydroxyl groups, Figure 2. Non-polar interactions between the hexose ring with aromatic lectin side chain groups can also result. As well, the solvent indirectly influences in driving molecular recognition in solution.[27]

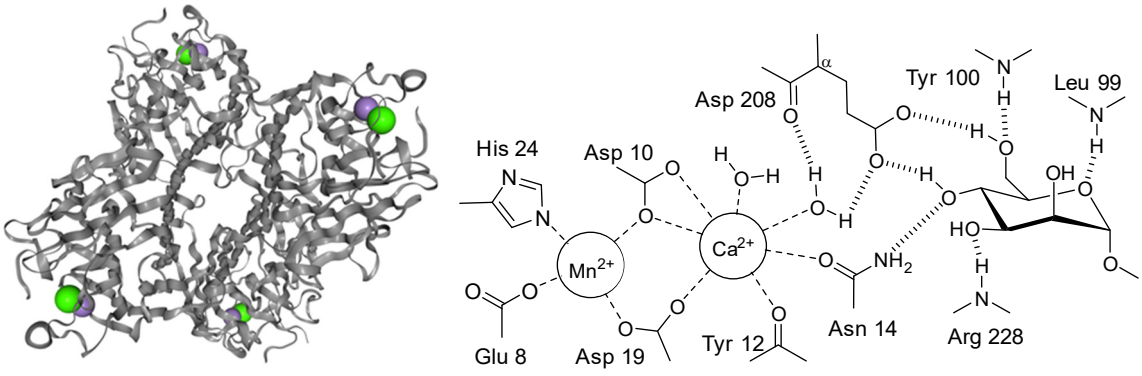

Figure 2- Left) 3D representation of concanavalin A in its tetrameric conformation, green spheres represent Ca^{2+} and purple Mn^{2+}; from [28-29]. Right) Methyl α-mannoside in the combining site of concanavalin A. Adapted from[16, 28-29].

1.1.1 Molecular interactions of solutes

Two entities form a complex when the intermolecular attractive forces between them are greater than the sum of possible unfavorable interactions and the respective solvation energy decrement

of the entities. The established interaction forces between two not-bonded entities are named cohesive interactions, and they include all the non-covalent ones; being this the following:

Ionic interaction. It is a coulombic interaction involving the electrostatic attraction of ions, where equivalently charges repel and opposing charges attract. Molecules usually present ions on the heteroatoms of functional groups, depending on the pH of the media. The ionic interaction is produced by monopoles, and it is not directional. The potential energy depends on the inverse power of the distance.

Dipole-dipole. It is presented between molecules with a permanent dipole. The dipole appears for molecules whose center of mass differs from the electron density. Therefore, it is plausible to present a dipole if they lack high symmetry. Dipoles behave like coulombic attractions. The potential energy of interaction between two polar molecules depends on their dipole magnitude and the relative orientation and drops as a cubic power function of the distance. The interaction strength is maximum for antiparallel, zero for normal and minimal for parallel alignments. It depends on the temperature.

Dipole-induced dipole. Dipoles are induced in a molecule without a permanent dipole by polarizing their electron cloud upon being brought into contact with a permanent dipole. The strength of the induced dipole interaction depends on the magnitude of the permanent dipole, the polarizability of the non-polar molecule and the relative orientation. The potential energy depends on $1/r^6$. The dipole–induced-dipole interaction energy is independent of the temperature because the thermal motion has not got any effect on the averaging process.

Dispersive interactions. These interactions are responsible for nonpolar molecules to attract one another even though neither a present permanent dipole. They are also known as London or induced-dipole–induced-dipole interactions and explain the condensation of argon gas and the liquid state of benzene at room temperature. All non-polar molecules, on timescales shorter than electron reorganization, present instantaneous dipoles which can further polarize another molecule. When a dipole changes its direction, the induced one will follow it resulting in no orientation dependence. The energy of dispersive interactions drops as a sixth power function of the distance ($1/r^6$). The dispersion interaction generally controls all the interactions between molecules other than hydrogen bonds.

Hydrogen bonding. It is a stronger interaction that results from linking two highly electronegative elements, one possessing a lone electron pair and the other linked to a hydrogen atom. It can be understood either as the interaction of partial positive charge of H and a partial negative charge of the lone electron pair or as a delocalized molecular orbital formation. This results in the

lengthening of the σ-bond of hydrogen while shortening its distance to the electronegative atom. Hydrogen bonds are directional and stoichiometric. The interaction is not dependent on the distance, turning zero when the contact is broken.

1.1.2 Molecular interactions in solution

The consequences of adding a solvent to the media bring into consideration the interactions between solute and solvent and not just solute and solute; being solute the ligand and receptor. Water as the most common solvent in biological processes interacts with every kind of solute, decreasing the energy of solvated species. In that respect, the binding of two solutes (ligand-receptor) involves firstly breaking the favorable interactions with the solvent. Water strongly interacts with charged and dipolar species, resulting in less favorable cohesive interactions; energy difference between bound and unbound species is smaller in water media. The strong favorable interactions with water are not always satisfied, preventing cohesive binding. Dipolar interactions are also directional and being improperly satisfied disfavor the cohesive binding, affecting the specificity of ligand-receptor interactions. The energy of hydrogen bonds can be decreased by up to 50 times by simply being present in water. Still, their contact demanding nature and angular dependence increases the specificity of ligand-receptor interactions forming the complex. Dispersion interactions are weak but still contribute to the cohesion. Changes in energy by introducing a solution/solvent depend on the polarizability of it. Water polarizes weakly, and so cohesive interactions between ligand and receptor are greater than to water. Additionally, the distance dependence ($1/r^6$) remarkably orients for ligand-receptor binding.

Hydrophobic interaction. Non-polar molecules slightly dissolve in polar solvents, and individual solute molecules are secluded in solvent cages. This effect is exothermic ($\Delta H<0$) but endergonic ($\Delta G>0$), therefore entropically disfavored ($\Delta S<0$). Hydrophobic molecules are those presenting a positive ΔG to be transferred from non-polar to polar solvents. Surrounding non-polar solvents implies forming hydrogen bonds ($\Delta H<0$) but ordering the media through cage forming, then decreasing the entropy. The net effect for dissolving non-polar molecules is to form larger clusters of non-polar aggregates to increase the entropy of the system presenting fewer solvent cages and so greater entropy of water. The hydrophobic interaction is an ordering process stabilized by a greater disorder of the solvent.

Overall, cohesive forces for carbohydrate-lectin interaction in water are weak, presenting forces of less than a hundredth of the covalent ones. Therefore, nature circumvented the energetic deficiencies with multivalency.

1.2 MULTIVALENT PRESENTATION

Multivalency is an essential molecular feature in biological systems to overcome the weak binding of specific ligand and receptor compounds even preserving reversibility without altering their covalent structures.[13] The cumulative binding events sum up in overall energy gain and in some cases act to support each other (cooperative binding). The overall binding modes depend on parameters, such as size, valence, flexibility and their effect on the resulting affinity can be analyzed.

1.2.1 Thermodynamic contributions

A monovalent ligand can bind to a monovalent receptor, and the system only presents two states; bound and unbound. The number of possible states for a system formed by a monovalent counterpart and a multivalent relative grows to the sum of their valences. Multivalency as a strengthening interaction is presented in systems composed by polyvalent both ligand and receptor, and the number of possible binding states requires of combinatorial calculations to be determined.[30] The polyvalent interaction that happens between N epitopes on a ligand and N binding sites on a receptor is defined as an N^{th}-order.[31] The nomenclature to describe multivalency is wide, so for simplification and to understand the principal contributions, the proposed nomenclature by Whiteside et al. is presented, Figure 3.

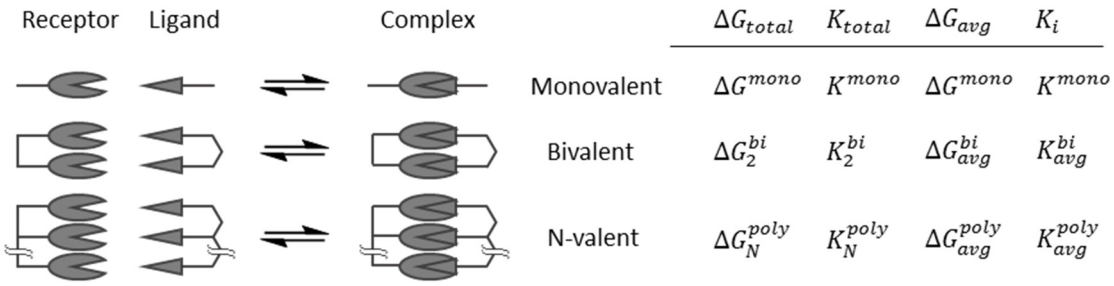

Figure 3- Nomenclature for monovalent and polyvalent systems, with free energies of binding (ΔG) and inhibition constants (K_i). Adapted from [31].

Every molecular recognition process is governed by thermodynamics under the free Gibbs energy;

$$\Delta G = \Delta H - T\Delta S \quad (1)$$

and so is multivalency. Thermodynamics determine the maximum achieved energy after a normal linkage of the maximum possible counterparts. The overall ΔG for the binding of multivalent systems does not necessarily require being greater than the n-times individual processes resulting in a positive cooperation (synergetic, α>1), but also equally resulting in a non-cooperative binding (additive, α=1) and/or lower resulting in a negative cooperation (interfering, α<1).[32]

$$\Delta G_N^{pol} = N\Delta G_{avg}^{pol} = \alpha N \Delta G^{mono} \quad (2)$$

where *N* is the order of the interaction and *α* the cooperativity parameter. This nomenclature was established for biology[33] and criticized because biological samples do not always involve polyvalent systems. As well, it requires to know the order of the polyvalent interaction (N) for deeper thermodynamic analysis, what is not always known. However, this nomenclature is kept for the simplicity of the preface.

Multivalency is closely related to the real structure, and it remarkably affects the thermodynamic process. Regarding enthalpy and as a first approximation that all binding events are independent: the more binding events, the more favorable the overall process is:

$$\Delta H_N^{pol} = N\Delta H_{avg}^{pol} = N\Delta H^{mono} \quad (3)$$

However, the reaction enthalpy is considered to be reduced if any of the binding partners are constrained, for instance suffering strain while binding because of the energetic unfavorable molecular conformation, Figure 4. Then, the binding of one ligand to a receptor with a given enthalpy may cause the following ligands to bind to their receptors with greater or lower enthalpy resulting in the synergetic, additive or interfering cooperation (α≷1); what in literature is also called enthalpically enhance or diminished binding.[31]

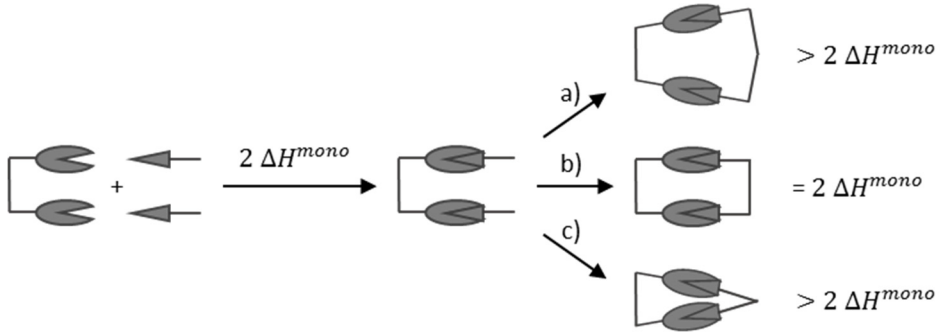

Figure 4- Representation of enthalpy in polyvalent binding interactions. The binding energy of two monovalent ligands can remain unaffected in the multivalent presentation if the spacing between epitopes matches the receptors (b). It can be diminished if the ligand spacing strains the interaction by widening (a) or closing (c) the conformation. Adapted from[31].

The second term of free Gibbs energy refers to the entropy of the process, and it can be affected by different contributions; translation (ΔS_{trans}), rotation (ΔS_{rot}), conformation (ΔS_{conf}) and solvation (ΔS_{sol}) of the receptors and ligands while associating. These contributions are related to the freedom to perform the corresponding translation and rotation, the ability to arrange the conformation and the surrounding water molecules.

The decrement in degrees of freedom for the translational and rotational contributions (ΔS_{trans} and ΔS_{rot}) upon binding is common to every molecule regardless of any property such as valence or size among others, Figure 5 a) and b). The entropic costs are paid once, but their overall contribution affects as a function of mass (size) and concentration. For big multivalent molecules upon binding, the reduction in degrees of freedom from translation and rotation are negligible to the process, because the conformation and solvation contributions are much higher than translation and rotation, and so predominant. For small molecules, there are fewer possible conformational dispositions, and the solvation occurs with fewer water molecules. Subsequently, the translational and rotational contributions are more relevant for the overall. Therefore the ligand size is important.

As well, the translational entropy of ligands and receptors in solution (3D) is greater than constraining the receptors to diffuse across a membrane (2D) while remaining ligands in solution. Therefore, binding a multivalent ligand with N receptors on a membrane can be more favorable than N monovalent interactions in solution.[31] Therefore the substrate and media matter.

The conformational contribution (ΔS_{conf}) is applicable after a first binding event is set among two multivalent bodies. It deals with the entropic expenses arising from the overall available conformations to establish a second linkage within the already linked multivalent entities. These expenses can be lower than the translational and rotational contributions of a second molecule to bind, then favoring an intermolecular binding, Figure 5 c) path A. Otherwise, the binding of a second molecule could entropically be indifferent or more favorable; when matching or exceeding these translational and rotational entropic costs, Figure 5 c) path B. Therefore the flexibility of ligands affects multivalency.

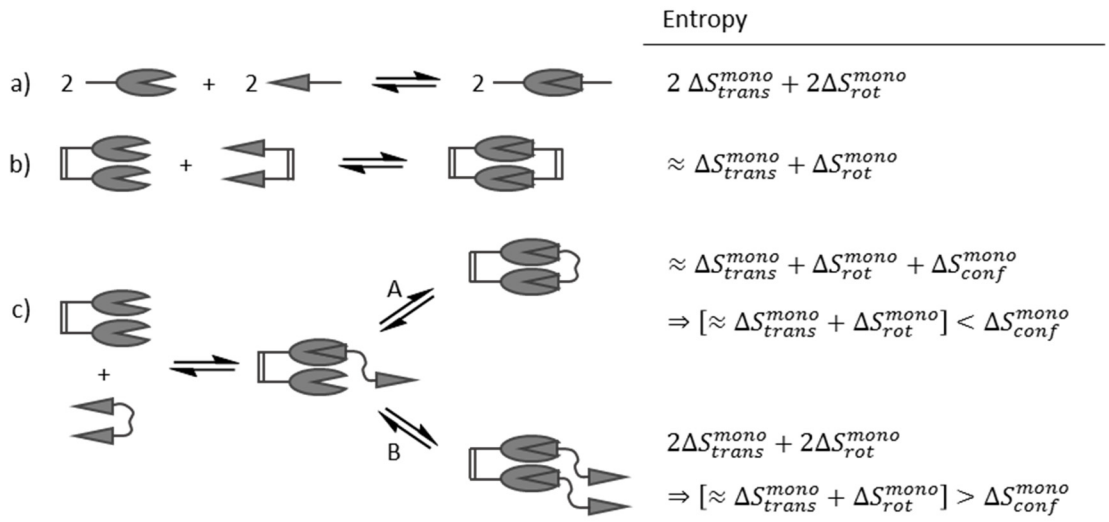

Figure 5- Entropic contributions for two recognition events; for monovalent and divalent systems. Note the differences between binding a rigid ligand (b) and a flexible ligand (c). Adapted from[31].

Solvation (ΔS_{sol}) contributes by releasing the ligand surrounding solvent molecules upon binding. This contribution can be assumed as constant for each binding, independently of their mono- or multivalent presentation, unless the conformational of the ligand changes reduce the solvation area; newly affected by the flexibility.

These thermodynamic contributions are not fully independent and can remarkably influence or compensate each other. For instance, high available conformations increase the entropic expenses (greater ΔS) while rising chances to establish more binding events (greater N) and these occurring without energetic strain (greater ΔH). This is known as enthalpy-entropy compensation and has been discussed in detail.[34]

Regarding kinetics, dissociating multivalent systems requires breaking multiple bindings happening slower than in monovalent systems.[35] The thermodynamic expenses for the first linkage in multivalent systems are of about the same as the monovalent analogous, meaning that the association rates are also similar. Some kinetic studies support that the multivalent binding enhancement between bodies is due to a reduction of its dissociation rate.[36-38]

1.2.2 Multivalent binding modes

The simultaneous presentation of multiple sugars has a key role in overcoming the weak interaction of individual carbohydrate-lectin events. Usually, for a ligand with n-epitopes, multivalent effects present greater binding affinities than n-times the monovalent binding analog.[39] Several multivalent binding effects have been distinguished, some contributing simultaneously to the increase in affinity.

Chelate binding. The chelate binding effect is presented when several sugar ligands occupy more than a single binding site on the same multivalent receptor. Here, the translational and rotational entropic requirements to set the first binding event favor consecutive binding to additional sites.[40] This issue leads to a dramatic increase in the overall binding avidity, K_N^{pol} in Figure 3, from three to five orders of magnitude in comparison to monovalent ligand binding.[41-42] Some studies raise the enhancement to 6000 times over monovalent ligands.[42-44] Chelate binding is remarkably influenced by the ligand conformation, the crosslinker flexibility, and the final relative spacing to match the binding pockets without being strained.[45] An appropriate structure can lead to reaching an increment of a million times greater than monovalent structures, as seen for five-pointed star shape polymers inhibiting pentameric toxins.[46] In contrary, small mismatches of a single bond can drop the affinity six times.[42] It has been reported that flexible crosslinkers, like ethylene glycol, and ligands are advantageous to adopt suitable conformations resulting in binding events[47]; despite rigid ligands dramatically increase the overall binding avidity when perfectly matching the receptor spacing.[41, 48]

Subsite binding. Subsite binding effect is presented by simultaneously binding another sugar moiety on the backbone to a subsite of the receptor binding pocket, leading to an increase in the binding avidity. Similar thermodynamics to the chelate effect is presented for subsite binding; subsite multivalency. Recognition on extended cleft sites is reported for some lectins, including Con A as an example. The binding to adjacent amino acids (Tyr 12, Thr 15, Asp 16) of the Con A binding pocket (Tyr100, Leu99, Arg 228, Asn 14 and Asp 208) was reported to happen in studies with a natural mannose trisaccharide, leading to binding enhancement.[49]

Statistical rebinding. Statistical rebinding effect, also named bind and slide effect[50], is presented in multivalent ligands with a high local sugar density allowing for a fast exchange of the bond sugar in the lectin binding pocket.[45, 50] It is a dynamic process where a sugar in the proximity can replace the released bond sugar. It has been reported to gain affinities in two orders of magnitude.[44]

Cluster formation. Cluster formation is presented upon several receptor molecules bind simultaneously to one multivalent ligand, thereby increasing the effective avidity of it. It results as a consequence of the high number and density of sugar multivalent ligands. This effect is reported to serve as a triggering signal for transduction.[51] Cluster formation is usually observed in solution by a turbidity assay, in where multivalent ligands cluster soluble receptors producing insoluble precipitate forms.

Aggregation is simultaneously affected by other multivalent effects, and so the enhancement of individually clustering formation has not been evaluated yet.[40]

Steric shielding. Steric shielding effect is present when a bonded multivalent ligand sterically shields the binding pockets, preventing competing ligands from binding, thus apparently increasing the binding avidity of the bond multivalent ligand.[31, 52] Steric shielding has being observed while studying the inhibitory potential of multivalent glycoligands and results in a stabilization of the ligand-receptor complex.[53-54]

1.2.3 Synthetic carbohydrate presenting scaffolds

Synthetic multivalent glycoligands and glycoprotein mimetics have risen as an important tool for investigation of ligand-receptor binding. The synthetic analogs can result in better accessibility together with the capability of being modulated to gain greater affinities compared to the natural ligands.[10, 46] Synthetic glycoligands could be constructed efficiently since lectins naturally bind with oligosaccharide presenting glycoproteins at terminal sites, relegating the internal moieties to less involvement.[55] Therefore, synthetic carbohydrate bearing scaffolds can replace the internal sections by inactive, cost-effective scaffolds to mimic natural oligosaccharides.

Literature reports a vast cast of multivalent presenting scaffolds including liposomes, micelles, vesicles, proteins, hard surfaces, cyclodextrins, calixarenes, nanoparticles, peptides, dendrimers, and polymers. Most of the multivalent saccharide ligands can be sorted through conceptual features. A brief description of various groups is provided in the following.

Glycopeptides consist of amino-acid based backbones bearing sugar ligands in the side chain. Sequence-defined, monodisperse structures can be synthesized by solid phase peptide synthesis (SPPS) firstly introduced by Merrifield in 1963.[56] Sugar moieties can be introduced while growing the backbone with glycosylated amino acids[57] or with a post glycol functionalization of certain amino acid side chains.[58] Non-natural amino acids with specific functional groups in the side chains can be introduced for conjugations such as Staudinger ligation.[59] As well, an appropriate design of the peptide can result in defined secondary structures for further applications.[60] Glycopeptides have been used to optimize binding efficiencies to hepatic lectins by presenting ligands in a cluster conformation varying the sugar spacing.[55] The affinity to human mannose-binding receptors was studied with lysine scaffolds, gradually presenting greater sugar amounts[61]. Selectin binding studies with multivalent peptide scaffolds concluded that a determined density is also required[62]. Binding mechanisms were also investigated with sugar bearing peptide scaffolds[63] reporting that multivalent chelate binding can be related to high binding affinities and that the

binding enhancement depends simultaneously on the carbohydrate presentation and the linker nature.

Glycopolymers are synthetic macromolecules bearing sugar moieties.[64] Polymerization techniques such as Reversible Addition-Fragmentation chain Transfer (RAFT) or Atom Transfer Radical Polymerization (ATRP) and forms of Ring-Opening Polymerization (ROP) control over the molecular weight.[65] Common techniques to introduce sugars are the Cu(I) catalyzed alkyne and azide 1,3-dipolar click cycloaddition (CuAAC) which also requires azide-containing carbohydrates to react onto a polymer backbone[66], and the thiol-ene click reaction between polymers with vinyl groups and thiol-functionalized sugars[67]. Biological applications have been reported for galactose-functionalized polymers[68] and N-glycosyl polymers[69] among others. Multivalent binding modes have also been studied. The viral hemagglutinin was inhibited by steric shielding where non-binding carbohydrates on virus-bond glycopolymers prevent from binding to erythrocytes.[54] The crosslinked complex formation was thermodynamically studied binding galactopyranoside polymers to peanut agglutinin.[70] Orientation and spacing of clustering saccharide chains were found requirements for specific multivalent lectin recognition comparing rigid and flexible helical polyglycosyl chains.[71] The Chelation effect was studied through different linear mannose functionalized neoglycopolymers correlating the number of epitopes to the receptor binding affinity [51]

Glycodendrimers are monodisperse molecules with a tree-like shape built in a generation-wise manner resulting in a series of branches emerging from a central core.[72] The size range is of several nanometers.[73] The carbohydrate ligands are linked and exposed on the dendrimer periphery after functionalizing reactions such as amidation or click chemistry. Glycodendrimers have being employed for multiple biological purposes and studies, to name a few; selectin binding[74], hepatic lectin binding[75], inhibition of Escherichia coli[76], as well as studies investigating the multivalent binding effects and mechanisms. As the main tendency, the greater number of presented sugar epitopes, the higher binding affinities are. This affirmation is limited by the experimental setup (solid angle, flexibility) to a certain number of binding epitopes. In this respect, studies are reporting higher affinities for monovalent structures rather than multivalent ones.[77] Together to epitope quantity, the density of these plays a role in multivalent binding. Multivalent dendrimers, from 4x to 178x valence, had yielded hemagglutination inhibition enhancements 600-fold higher per sugar residue when only half of the linking sites were sugar functionalized.[78] Dendrimer structures might not be completely accessible whether presenting a tight and compact outer layer. In this respect, it could be postulated that the epitope flexibility also influences the multivalent enhancement.

Neoglycoproteins are assemblies of several molecules loaded on a protein scaffold. They could be considered as dendrimers with a different core. These compounds were introduced by Monsigny et al.[79] Functionalized carbohydrate derivates are loaded through a myriad of reactions.[80-85] They have been studied as bacteria anti-adherent agents to prevent infections.[86-87] As well, though additional conjugated markers, these kinds of ligands have been proposed to detect surface and endogenous lectins.[85, 88] NGPs in this field are analogous to diagnostically used antibodies.[89] The NGPs are useful in studying the distribution and kinetics of sugar-recognizing moieties because the interaction of single sugar molecules is overcome by the multivalent interactions of labeled NGPs[90] and on the other hand, being smaller than other sugar presenting scaffolds, such as gold or latex particles, prevents them from internalization by phagocytosis.[85]

Hydrogel microparticles are proposed in biological studies because they can be synthesized at the cellular scale objects. Microparticle composition is broad comprising silica, gold or polymers, but are hydrogel materials which keep on growing interest due to their applications in biological sensing, drug delivery, and tissue regeneration among others. Hydrogels are water-swollen hydrophilic networks, which contributes to biocompatibility and results in tissue-like mechanical properties making them highly suitable for *in vivo* applications.[91] Some microgels respond to physicochemical stimuli[92], and others bind determined targets after specific functionalization of the surface.[93-94] Hydrogels microparticles as scaffolds will not differ from dendrimers in shape but size, presenting the opportunity to be microscopically observable. Hydrophilic microgels are used in biological studies as they can be adjusted to the right mechanical properties, sizes and colloidal stabilities.[95] A major application of microgels in biology is the separation of biomolecules like bacteria, proteins or DNA in aqueous solution[93, 96] but they can also be used as biosensors converting molecular binding events into a measurable and quantifiable signal.[97]

Macroscopic planar surfaces can also be used as scaffolds to present carbohydrates. More than 600 glycans have been tethered and used for screening.[98-99] The array support depends on the later detection system; many are made on glass, metals and different plastics. The advantages of using microarrays are their easy handling, fast screening and the possibility to be automatized.[100] There are many protocols to functionalized the arrays, mostly by covalent binding or hydrophobic interactions.[101-102] Due to their properties, glycan arrays have been used to determine the carbohydrate structure that the malectin protein binds.[103] As well, the specificity of a set of lectins against tumor-associated antigens has been tested with carbohydrate arrays.[104-105] Profiling antibody responses in xenotransplants have been identified after organ rejection because of anti-α-Gal antibodies.[106] Glycan arrays are sensitive to antibody levels and are proposed as a diagnostic tool for breast tumor Globo H antigen.[107]

1.3 FORCE-BASED TECHNIQUES FOR MOLECULAR BINDING STUDIES

The quantification of ligand-receptor interactions is a key requirement first to understand and further control all binding processes and biological functions in nature. Some techniques and methods allow studying the interactions among proteins and sugars by tracking the different response of certain physical properties. A vast group of techniques makes use of label-based detection because of common availability of reagents, basic instrument requirements and the ease of use. By this approach, the presence and physical properties of a receptor- or ligand-linked molecular label are determined to quantify the reaction status. This kind of techniques is of great interest while tracking product distributions, e.g., in cell permeating compounds or fate destiny of drug-complexes. Radioisotopes, fluorescent dyes, chemiluminescent molecules and others like inorganic quantum dots have shown promising results[108]; but also may present limitations by the labeling reagent itself, such as altering the native characteristics of the issued molecule, or in the labeling procedure resulting laborious and time-consuming.

On the other hand, label-free techniques are advantageous and can better illustrate the reality of the process avoiding distortion of the results. They rely on measuring an inherent property of the query molecule. Quartz Crystal Microbalance (QCM) correlates the vibration frequency with a deposited mass on the support surface. Ellipsometry determines the light polarization change upon its reflection on or transmission through the sample. Surface Plasmon Resonance (SPR) measures changes in the refractive index of a dielectric medium through an evanescent wave. Dual Polarization Interferometry (DPI) determines the refractive index and the thickness of an adsorbed layer by an interferogram of two polarization modes. The complexity of using these techniques reverts in the selectivity and sensitivity due to measure adsorbed analytes on a surface. For instance, for small molecules with dielectric constants close to water, like sugars, changes in the refractive index (SPR) and masses (QCM) become very small.

Techniques can be shorted by the physical system that supports the analysis; in solution or on a solid support. It is understood that the solid support techniques do also require permanent contact to a liquid phase in order to approach and retract the reactants. Spectrophotometric techniques like Ultra Violet-Visible (UV-Vis) and Turbidity, together with Isothermal Titration Calorimetry (ITC) are some examples of applied techniques in solution, in which agglutination assays determine affinity enhancements rather than adhesion.[109] The main discrepancies confront real systems because many natural processes occur on a fixed support, with mechanical stress resulting in conformational changes affecting binding properties like force transduction.[110-111]

Force-based techniques like Single-Molecule Atomic Force Microscopy (SM-AFM) and the recently developed Soft Colloidal Probe adhesion (SCP-adhesion) provide direct and quantitative insight

into the interaction force between ligand and receptor molecules. Also, they provide a more accurate impression of the biological situation of signaling processes due to surface character and lack of labels, e.g. of the glycocalyx interacting with anchored membrane receptors. They are described below.

1.3.1 Atomic Force Microscopy – AFM

In the early 80s, the scanning tunneling microscope (STM) was developed by Binnig and Rohrer.[112] This technique was revolutionary because it was capable of imaging and modify surfaces; not only the inorganic substrates (metals, semiconductors, covalent compounds, ionic crystals) but also organic ones (polymers, cells, tissues). In brief, the tunnel effect is the transmission of electrons with the consequent loose in energy through a dielectric material, an electronic barrier. The technique is then based in raster a surface with a tip tracking this interaction. Apart from the tunnel effect, there are more kinds of interactions that can be tracked such as evanescent waves and electronic forces. One of them is Scanning Force Microscopy (SFM) that stands nowadays as Atomic Force Microscopy (AFM). It is of high relevance because there is always forces present between two sample surfaces. These forces include magnetic, electrostatic, ionic, van der Waals, hydrogen bonding, and the dipoles. The microscope was developed in 1986 by Binnig et al.[113], and the new implementations allowed it to work in different media like gas, vacuum, and liquid, i.e., scanning force techniques could be applied to biological samples for the first time. It is a versatile tool for surface characterization due to its nanometer/atomic range resolution. The AFM microscope can work in two modes; imaging mode in which a surface is scanned to provide a topographic map of it and force mode in which the cantilever is pressed on samples to determine concomitant surface forces, among others. There is a closely related technique to force-mode AFM for surface analysis, the Surface Force Apparatus (SFA).[114] Similar to AFM, SFA has a vertical resolution of tenths of nanometer with a force resolution of tens of nanonewtons. However, unlike AFM, SFA presents some drawbacks regarding geometry and sample composition. SFA scans areas of square millimeters and requires light-transparent samples; while, AFM can work with opaque samples and can reduce the scanning area to a single molecule spot. These features plus the high force-control and lateral resolution promote AFM to advance applications like force spectroscopy, mapping heterogeneous samples, and nanoelectronics.[115]

Equipment. The AFM microscope[116-117] is mainly divided into three interconnected parts: a chip with an attached probe at the end of a cantilever, the detection system with a laser and a photodiode, and the height control device, Figure 6. The laser beam reflects on the reverse side of the cantilever, and the reflection reaches the photodiode detector. The cantilever acts as a spring thus any flexion while analyzing the surface will change the laser trajectory and so the detected

signal. These signal changes are correlated to the topology of the surface as well as used to correct the distance between cantilever and sample. Cantilever chips are made of silicon, sometimes with metal coatings to obtain or increase some properties such as the reflectivity. Usually, cantilevers present tips made of silicon or silicon nitride with a pyramidal shape ending in a more or less sharp round edge. The cantilever is fixed to a glass block, which is locked within the height-control system. The coarse height move is achieved by electronic motors while the fine move is from a piezoelectric device that also controls lateral X- and Y-movements. Some devices shift (X and Y) the sample remaining steady cantilever.

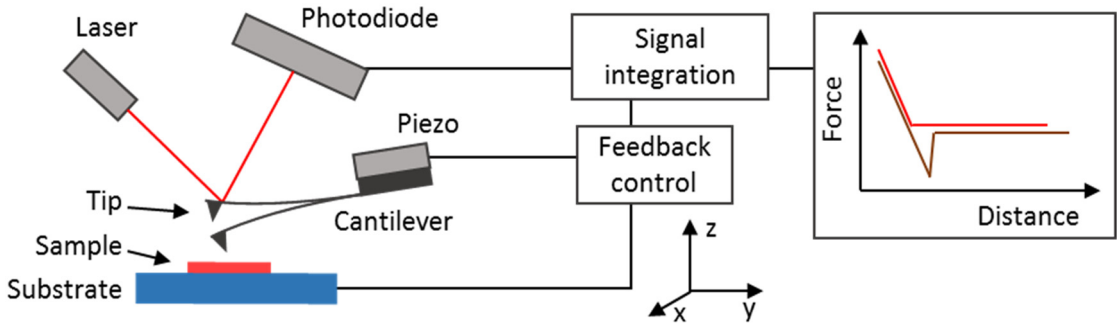

Figure 6- Schematic representation of an atomic force microscope configuration.

Applications. The main applications of an AFM microscope are based on the properties of cantilever and probe: the precise mobility, the flexibility, the loaded force and the possibility of functionalization. The first main application is known as *imaging*, where the probe is scanned across the surface while maintaining a constant force (contact mode), frequency or amplitude (both in vibration mode). A second application is the *sample modification* and arises from pressing harder on the sample surface. The surface can be scratched and modified with a determined pattern with an appropriate cantilever-probe able to load higher forces.[118] The latest main application is called *force spectroscopy*. It provides information about the force properties of the sample, i.e., elastic modulus, attraction/repulsion interactions, internal conformations. The sample can be either the surface, the probe or the interaction between both.

1.3.1.1 Force mode AFM

In force spectroscopy mode, force-distance curves are produced tracking the changes in vertical laser deflection while approaching and retracting a probe functionalized cantilever to the surface, Figure 7. At this mode, the microscope does not oscillate the cantilever. The laser reflection is firstly aligned with the detector and will remain constant while freely moving far from the surface. The cantilever remains unbent until reaching the surface but will bend (concave) once it comes into contact with the surface. The greater compression, the higher flexion of the cantilever.

Differences in the cantilever curvature produce changes in the reflexing laser angle, and therefore, cantilever deflections can be expressed in terms of force after calibration. Retracting from the surface reveals adhesion forces, i.e., attracting interactions hold the probe and surface in contact while retracting. As a result, a convex bent is exerted that also produces changes to the vertical laser deflection; in an opposed way to approach phase. The cantilever recovers its relaxed state after exceeding the adhesive forces. Since the interactions hardly depend on the experimental setup[119], refined material depending bonding and breaking theories have been developed. For example, when analyzing weak noncovalent bonds theory predicts that their binding strength will depend on the loading rates.[119] Hence, it has been proven for a noncovalent binding ligand-receptor pair that the bond survival time decreases and the binding strength increases while increasing the loading rate.[120]

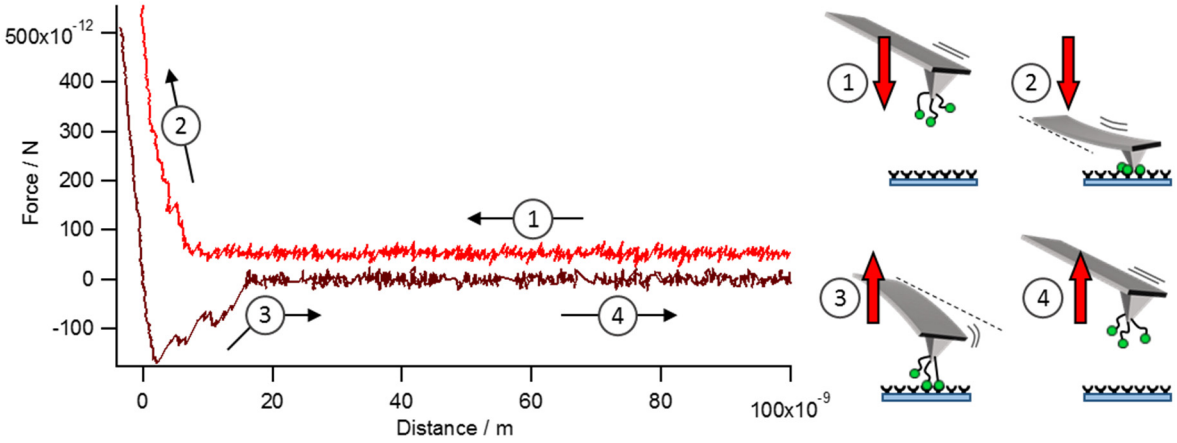

Figure 7- Force-distance curves of a functionalized cantilever on a counter-pair functionalized surface. The cantilever remains straight while approaching to the surface (1) and deflects concave upon compression on it (2). The retraction of the cantilever releases the loaded force, and adhesive interactions result in a convex deflection of the cantilever (3). Successive unbinding events stepwise release of the adhesive forces until free the functionalized cantilever (4). For clarity, the trace curve is y-shifted (+50 pN), and the straight cantilever slope is represented with dash lines next to deflected cantilevers.

Calibrating an AFM for force measurements. Cantilever calibration consists in determining the detection sensitivity and the cantilever spring constant. The sensitivity is directly related to the laser beam reflection point; the closer to the edge it is reflected, the greater angle changes when bending. This first calibration step correlates the detection in volts with the laser reflection distance in meters. The cantilever spring constant is an inherent property that is individually determined through its resonance frequency; this process correlates the oscillation amplitude in meters with the exerted force in newtons. There are few methods for cantilever calibration.[121]

Single Molecule AFM on bimolecular interactions. Many molecules and samples suited for force analysis, among which the principal variables are analyzed and studied; rupture forces, the

position of rupture events, the influence of the media. Florin et al.[122-123] were the first to perform force experiments on biomolecular interactions. The Si_3N_4 tip was functionalized with physisorbed BSA protein carrying avidin and faced to biotin functionalized agarose beads. The adhesion energy was found to be ~20 nN. The force histogram was found to present multiples of 160±20 pN which was presumed to be the disconnection force for individual avidin/biotin pair. The specificity of the interaction was proven by inhibiting with free avidin. Strands of DNA molecules were firstly analyzed by Lee et al.[124], and the complementary oligonucleotides were covalently linked to flat mica surfaces and mica spherical probes. Four kinds of signals were detected. While one was attributed to non-specific interactions, the other three were assigned to interactions between oligonucleotides. Another kind of studies was also determined; the intramolecular interactions of DNA. A homopolymer was covalently and simultaneously linked to the surface and probe. By elongating the sample, it was found a constant rupture force and distance. The force was assigned to changes in the chain conformation. Meanwhile, the distance was attributed to the polymer length. This experimentation approach has been extended to proteins to study the denaturation of the Fe-active center.[125-126] Mathematical models, like the worm-like chain model, explain differences in the elastic behavior of molecules.

The first experiments with carbohydrates were performed by Misevic.[127-128] Their surface and probe were functionalized with proteoglycans. The adhesion force between two of these proteoglycans was found as well as their dependence on calcium (II). Harada[129] has studied antibody interactions attaching them to the probe and the antigen to the surface. It was seen while unloading a stepwise profile of the multiple unbinding/disconnection events. The force range distribution was broad, from 25 to 450 pN. A Fourier transformation revealed a 63 pN period, later attributed to singular unbinding events. This result was unsuccessfully correlated with calorimetric measurements.

Host-guest supramolecular interactions can also be studied with AFM. Schönherr et al.[130] have functionalized a gold-coated tip with ferrocene moieties in order to face a functionalized gold surface with b-cyclodextrin heptasulfide receptors. The founded rupture force was of 56 ± 10 pN. They also found on the gold surface a highly ordered monolayer of the receptors because of their seven sulfide units.

1.3.2 Soft Colloidal Probe Adhesion

By means of soft colloidal probes adhesion (SCP-adhesion) the interacting energy between two surfaces can be determined. This approach was firstly established by Pussak et al.[97] to determine the interaction energy of carbohydrate-protein specific binding.

The soft colloidal probes (SCPs) are elastic entities and will result in contact areas upon precipitation on the surfaces that can be directly measured via Reflection Interference Contrast Microscopy (RICM). The resulting adhesion area depends on the interfacial forces, such as the ligand-receptor or electrostatic forces. The greater the attractive forces, the larger area results, Figure 8.

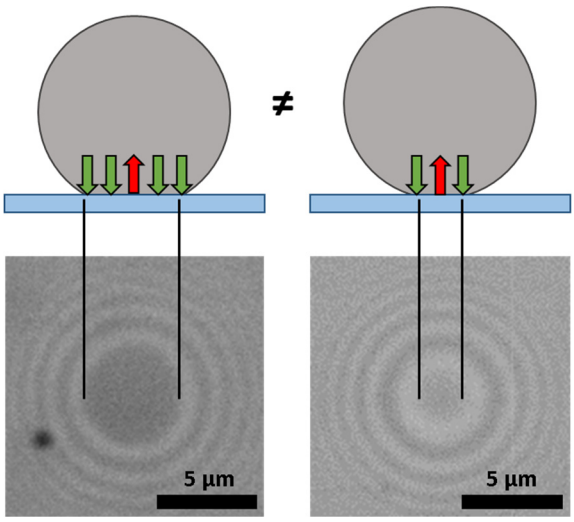

Figure 8- RICM images representing the adhesion area between the SCPs on a surface. The adhesion area depends on the overall surface forces exerted by the surface functional groups. Adhesive forces such as electrostatic attractive and specific ligand-receptor interactions develop greater areas. The presence of non-adhesive forces like electrostatic repulsive and inhibition of specific ligand-receptor interactions decrease the adhesion area until possibly fade it. Green/red arrows represent adhesive/non-adhesive forces.

The technique is based on the theory of Johnson, Kendall and Roberts (JKR) that allows determining the adhesion energy from the induced mechanical deformation of the SCP.[131] The JKR theory is valid when describing large adhesion areas and soft samples, which is the case in the present work. In brief, JKR theory states that the surface energy and strength of adhesion between elastic bodies are related through the action of surface forces, but in a way that is not always obvious. In order to separate bodies lying in intimate contact, mechanical work must be expended to overcome the adhesive forces; the free surface energy of the solid. This is work to create the "new" surface. The spreading or contracting of one liquid surface over another liquid or solid surface to reach an equilibrium state is dominated by the minimization of surface energy. Between two smooth solid surfaces, the equilibrium largely depends upon the distribution of elastic forces in the contacting bodies, despite the separation of the elastic bodies is independent of their elastic modulus. Derjaguin[132] approximated that the interaction force F between a flat surface and a sphere with radius R is related to the surface interaction energy W(d) per unit area:

$$F(d) = W(d)2\pi R \quad (4)$$

where d is the distance between the two surfaces. Elastic SCPs will then exhibit different contact areas:

$$a^3 = 6\pi \frac{W}{E_{eff}} R^2 \quad (5)$$

where *a* is the radius of contact, *W* the surface energy and $E_{eff}=[4E/3(1-v^2)]$ its effective elastic modulus, with v the Poisson ratio and E the elastic modulus. The contact area on the surface and the radius of the SCP can be calculated from the height profile reconstructed from the RICM images, Figure 13.

1.3.2.1 Reflection Interference Contrast Microscopy.

Reflection Interference Contrast Microscopy (RICM) is a very powerful technique that does not require sample labeling and can precisely study surface interactions and adhesions.[97, 133] It can be implemented with other microscopic techniques like fluorescence[134] and magnetic tweezers.[135] It was Adam Curtis in the 60s who first applied the principle of light interference to an optical microscope to determine the distance between the substrate and the lower side of a cell adhering on it; in an aqueous media.[136] The technique was called Interference Reflection Microscopy (IRM) and was firstly used to study living cells. This technique had an accuracy limitation due to the inhomogeneous refraction index of cells and slowly lost interest but for qualitative cell adhesion indicator. In the 80s, Sackmann and co-workers were the first to use the actual RICM to more homogeneous refractive index entities like unilamellar vesicles, membranes, lipid bilayers or colloidal beads.[137-138] RICM requires a planar transparent substrate to determine distances quantitatively. The registered image is a distribution of intensities that can mathematically be correlated to the real distances. Improvements made on RICM with simple objects have boosted the technique to quantitatively work with complex optical objects, like cells.[139] A major improvement is the use of multiple wavelength illumination to determine absolute heights.[140]

Equipment. RICM measurements are performed on an inverted microscope, Figure 9, where samples are deposited on the bottom of the substrates, usually as a product of precipitation or sedimentation. Samples are epi-illuminated with monochromatic light. Different devices can be used to ensure homogeneous and intense illumination, such as filters and diaphragms. The reflector cube includes a semi-reflecting mirror and two orthogonal polarizers. The antiflex objective presents a quarter wave plate (QWP). CCD cameras are preferred for detection due to display grey scale images, low integration times with appropriate signal-to-noise ratio and high frequencies to track kinetic processes. A primary calibration is needed in order to correlate the size.

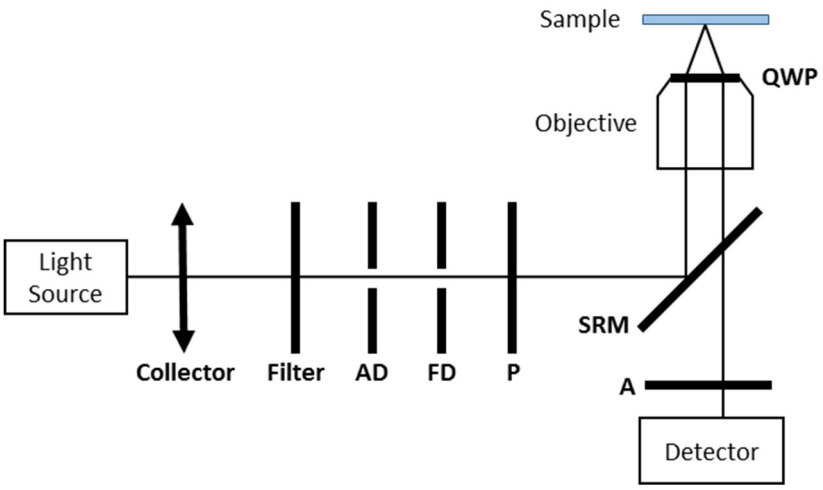

Figure 9- Scheme of a standard RIC microscope setup. AD: aperture diaphragm, FD: field diaphragm, P: polarizer, SRM: semi-reflecting mirror, QWP: quarter-wave plate, A: analyzer. Adapted from[139].

Samples. The samples are placed on a solid and transparent support. Common samples are spherical beads both inorganic and hydrogels, thin liquid or polymer films, vesicles including giant unilamellar ones, and cells. Some samples, like cells, should be within an aqueous media; either water or physiological buffers. Dissolved molecules such as carbohydrates and proteins raise the refraction index of the media; buffer.

Fundaments. The present theoretical description summarizes the basic features to understand the later application and not the vast area of the subjacent optics. In practice, many devices are illuminated with an incoherent source, not perfectly monochromatic, presenting a certain spatial extension. As well, some samples have internal vesicles complexing the final image and the corresponding theoretical and mathematical explanation. The theory of partial coherence, numerical-aperture illumination, multiple-monochromatic illumination and the effect of multiple interfaces are out of the scope for this work and can be found elsewhere.[141] So far, coherent monochromatic light and reflections from only two interfaces are considered.

Interferences and intensity. Light propagation is described in terms of rays by geometrical optics. Light is reflected on interfaces, refracted crossing towards different media and absorbed while crossing throw materials. Reflection arises from the interface between two materials with different refractive indexes (n_i with i=0,1,2) and undergoes simultaneously with refraction through the second media.

In RICM, interferences are produced with the superimposition of waves with the same trajectory, which in the present work arise from reflections on different surfaces. The monochromatic ray I_0 firstly reach the glass/medium interface, and it is partially reflected (ray I_1) and transmitted through the media. The transmitted ray interacts at the medium/sample interface resulting in

another reflection, which on its way back is newly refracted and reflected. Considering the transmission from the last event (ray I_2), the reflections from the two interfaces meet, Figure 10. The intensity of the interaction of rays I_1 and I_2 results in:

$$I = I_1 + I_2 + 2\sqrt{I_1 I_2}\cos[2kH(x,y) + \emptyset] \quad (6)$$

with $k=2\pi n_1/\lambda$, $\emptyset$ the phase shift and $H(x,y)$ the distance separating the object and the glass substrate at the lateral position (x,y). Subsequently, interference contrast images depend on the height of the sample interface and produce a fringe pattern, Figure 10.

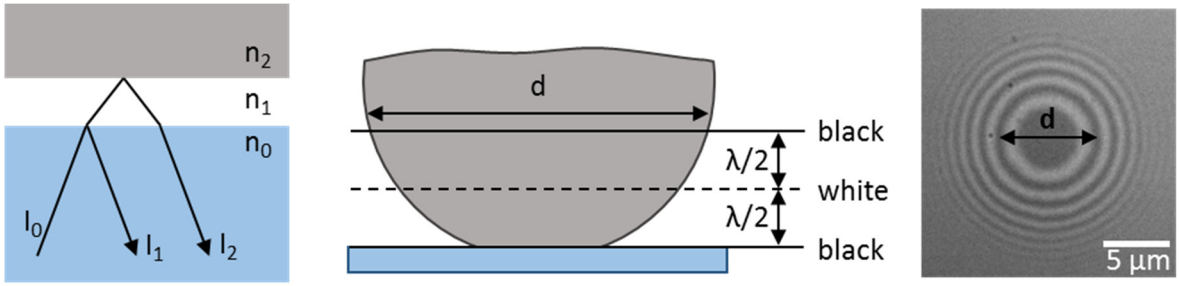

Figure 10- Left) Scheme of reflection on parallel surfaces from media with different refractive index. Notice that the reflected rays are parallel. Middle) scheme of the sample profile and alternation of the intensity as a function of interfaces distance. Note that the color spacing depends on the illumination wavelength. Right) fringe pattern of a deposited spherical sample. Notice the correspondence to the sample profile of the first black ring. Adapted from[139].

The intensities I_1 and I_2 depend on the incident I_0 as square power of the Fresnel reflection coefficient $r_{ij}=(n_i-n_j)/(n_i+n_j)$ (i,j=0,1,2). Their intensities are low if they are produced at interfaces with close refraction indexes media, precluding the signal to be discerned from stray reflections. That was solved by Ploem[142] with crossed polarizers and a quarter-wave plate; the antiflex method. Linear-polarized light is partially blocked at the semi-reflecting mirror and fully at the analyzer if it does not previously reach the sample, Figure 9. The light that reaches the sample becomes circular-polarized while crossing the quarter-wave plate, shifting the phase π/4, and newly turns linear polarized crossing the quarter-wave plate a second time. The returned light has a π/2 shift allowing crossing semi-reflector mirror and analyzer before reaching the detector, Figure 11.

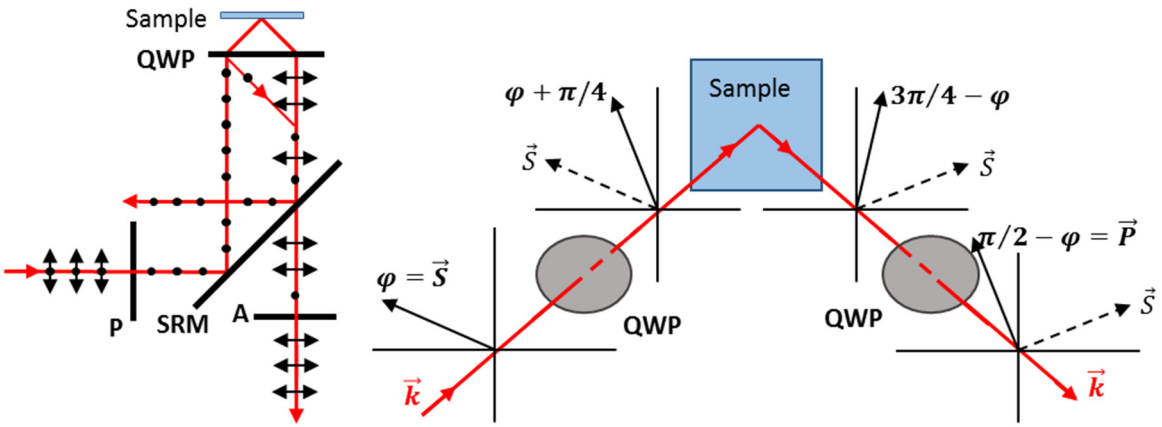

Figure 11- Left) Optical path and polarization of light in a RIC microscope. Note the presence of spurious reflection on the quarter-wave plate (s-polarized) that travels back and is blocked on the semi-reflecting mirror and analyzer. Right) representation of the π/2 shift of light (k) by crossing twice a quarter-wave plate, for any incident azimuth (ϕ). Angles are measured positive in a clockwise sense looking from the quarter-wave plate towards the sample. Note that a starting s-polarization results in p-polarization. Adapted from[143].

The interference contrast image displays the fringe pattern in grey scale; corresponding the brightest and darkest values to respectively the maximal and minimal intensities of the interferences.

Tilted and curved interfaces can be assumed as a succession of small flat and parallel surfaces, differing on the height/distance. However, the reflexion of light on planes that are not parallel is laterally shifted, Figure 12. Subsequently, to this shift and as a first approximation, the intensity decays with the plane slope increment. For a spherical object, the fringe pattern decreases the spacing and intensity while drifting from the central point; sphere base point. For a complete analysis, the contribution of every reflected ray to a given point should be considered.[144]

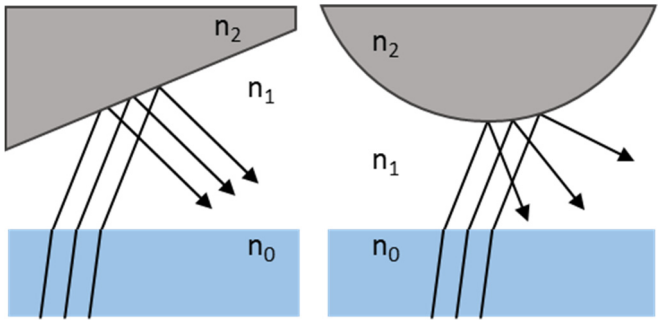

Figure 12- Scheme of lateral shift of light reflected on samples presenting inclined planes. Note that the greater the plane inclination, the greater lateral shift. Reflected rays from a single planar surface remain parallel among them, unlike from curved samples that are dispersed.

Height reconstruction and normalization of intensity are possible for known symmetric objects, despite some technical parameters that can hinder the information, such as inhomogeneous

illumination or intensity changes along time. It is possible to base the reconstruction on the maximal and minimal intensities, but precise knowledge of the refractive index is required for some applications. As well, the use of multiple-monochromatic illumination or calibration with known refractive index objects can determine absolute heights and intensities.

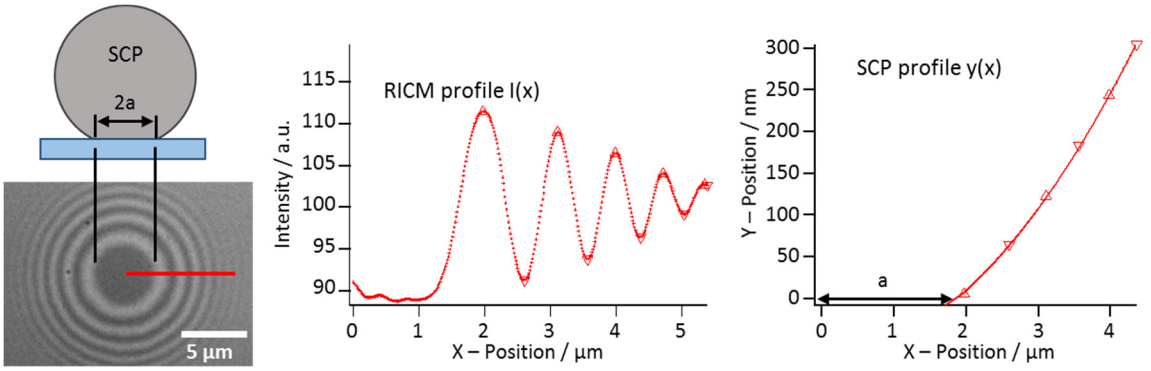

Figure 13- Left) Representation of an SCP adhesion on a surface with the corresponding RICM image. Middle) The integrated interference pattern over the complete circumference after determining the center. Right) From the RICM profile, the relative maxima are used to reconstruct the SCP profile. By extrapolating the SCP profile, the radius of the adhesion area (a) is determined at zero height.

2 AIMS AND OUTLINE

Ligand-receptor interactions enable many cellular processes like signaling, sensing, communication and viral or bacterial invasion. Molecular forces comprised of Van der Waals, electrostatic, hydrogen bonding and hydrophobic interactions are the basis for these interactions. These forces, however, are present at any biological surface, which gives rise to so-called non-specific interactions. In order to control the surface interaction of cells, i.e., in the context of adhesion processes, so-called specific interactions are formed by ligands and receptors that are usually larger compared to non-specific interactions and require structurally matching binding partners (lock-key principle). Carbohydrate ligands play a ubiquitous and highly important role in specific interactions at the cell level by triggering numerous processes and responses. Indeed, there is increasing evidence pointing towards the fact that the carbohydrates in the cells glycocalyx do not only present a physical barrier, but also help towards cell-cell recognition, communication, and intercellular adhesion.

Protein receptors or more specifically lectins are the binding partners for cell carbohydrate ligands; however, the interaction is generally weak. In order to overcome their low affinity, nature applies multivalency to bring about relevant binding in natural carbohydrate recognition events. Both, natural and synthetic interfaces with monovalent ligands or receptors are able to act as multivalent systems due to the immobilization of many monovalent ligands on the surface. Therefore, carbohydrate-mediated binding phenomena are not solely dependent on the affinity of individual molecules but also on the total number of interactions, as well as on their ability to act simultaneously. Specific interactions of carbohydrates are mediated by physicochemical properties of biointerfaces, e.g. the size of the interacting area as well as mechanical and structural properties. For instance, the inhibition efficiency of multivalent ligands follow the trend of the contact area with a larger magnitude than expected[7], being the size-dependent steric shielding and multivalency effects the main reason for the contribution[4]; remaining inaccurate the quantification of their contributions[7]. Besides, the mechanisms used for binding in such multivalent interfacial adhesion processes are not fully understood. Many of these studies report activity enhancements of multivalent ligands but few while controlling more than the valence or degree of functionalization.

This thesis aims to analyze carbohydrate-receptor interactions in respect to multivalent presentation of sugar units as well as the overall size of the interacting surfaces. More specifically, methods to study the carbohydrate interactions at different scales should be established with the aim to reveal the contribution of multivalent binding modes. The challenge of this task lies in the

fact that carbohydrates present low affinities to their receptors what can lead to greater non-specific interactions. Therefore, a major aim of the present thesis and the first part of it is to establish suitable methods capable of analyzing specific carbohydrates binding with adequate sensitivity and selectivity. Here, the developed methods cover the molecular scale analyzing the interaction of single carbohydrate molecules, the mesoscale by studying carbohydrate functionalized proteins, the cellular scale probing functionalized micrometer size hydrogels and macroscopic scale by functionalizing glass coverslips.

1) At the molecular scale, the binding mode between the ligands on a molecule scaffold and a receptor functionalized surface were performed by means of single-molecule atomic force microscopy (SM-AFM).
2) Regarding the mesoscale analysis, the specific binding and clustering rate of a sugar functionalized protein scaffold (neoglycoproteins, NGPs) are respectively tracked by fluorescence microscopy and turbidity. Besides that, mesoscale products are later used within cellular scale studies to test their inhibitory potential.
3) For the cellular and macroscopic scales, the adhesion energy between ligand-receptor functionalized micrometer-sized soft colloidal probes (SCPs) and a surface are investigated by reflection interference contrast microscopy (RICM).

In the second part of the thesis, a set of well-defined multivalent glycomacromolecules was produced by making use of multivalent sequence-defined glycooligomers and glycopolymers and then investigated with the established assays.

1) Using single molecule AFM the multivalent binding of carbohydrates on a polymer chain and their potential receptor chelate and cluster can be analyzed.
2) With optical techniques, the clustering rate can be studied for multivalent carbohydrate ligands presented as free oligomers and loaded on protein scaffolds.
3) By means of SCP-adhesion, the potential surface binding on larger scale constructs can be analyzed studying the adhesion area between multivalent cellular scale receptors and the multivalent surface ligand presentations. The steric repulsion can be quantified by inhibitory assays with multivalent free oligomers and mesoscale ligands.

3 RESULTS AND DISCUSSION

The unique features of multivalent carbohydrate ligands are based on the ability to cluster surface receptors and to occupy multiple receptor binding sites.[51, 145] Monovalent ligands can only bind to single sites, whereas higher-valent ligands can chelate, bind to subsites, sterically stabilize, statistically recombine or cluster receptors. Typically, only with the occurrence of these features, the required cellular functions are triggered.

In order to prepare synthetic mimicries, covalent coupling of carbohydrates can be performed on different carriers such as a linear polymer, proteins, microgels and glass coverslips. This kind of carbohydrate presentation roughly mimics natural recognition events at different size-scale. The reduced complexity of such artificial systems allows studying the molecular mechanism of carbohydrate binding.

Here, a series of techniques are established to analyze multivalent properties for four size range multivalent ligands. At the nanoscale range, the analysis (binding mode) is performed by single molecule force microscopy (SM-AFM). The mesoscale range is investigated (specificity and kinetics) using fluorescence and turbidity measurement with protein scaffolds. Cellular and macroscopic ranges were studied (surface characterization and steric shielding) by determining the adhesion energy between soft colloidal probes and planar surfaces by SCP-adhesion; making use of reflection interference contrast microscopy (RICM).

As a model for carbohydrate ligand and protein receptor, respectively, mannose bearing entities and Con A lectin were used. Con A is a tetrameric lectin from the kingdom of plants that binds to sugars, glycoproteins, and glycolipids, containing internal and non-reducing terminal α-D-mannosyl or α-D-glucopyranoside groups. The carbohydrate-lectin interaction of Con A and α-D-mannose (Man) as binding partners is a very well-known system.

Sequence-defined multivalent oligomers and sequence-controlled polymers were synthesized as nanometer-scale ligands varying the valence, density, and spacing of epitopes. First, they were analyzed in terms of single-molecule AFM measurements on receptor surfaces. Then, neoglycoproteins (NGPs) were synthesized as mesoscale ligands by functionalizing a protein scaffold with a fluorescent label and monovalent Man or the multivalent oligomer ligands bearing two and five Man moieties through different linker lengths to control the valence, epitope density, and flexibility. Mesoscale ligands were analyzed in terms of fluorescence and turbidity. Cellular scale ligands were produced by functionalizing hydrogel nanoparticles, also known as soft colloidal probes (SCPs). Macroscopic ligands were synthesized tethering multivalent oligomers on

a glass surface. Cellular and macroscopic scale ligands were analyzed regarding adhesion energy of SCPs by RICM (SCP-adhesion).

3.1 METHOD DEVELOPMENT

The scaffold on which multiple receptor-binding motifs are loaded controls the size, shape, density, flexibility, and multivalency of the final ligand. All these material parameters may affect the multivalent interaction of ligands. In the present section, techniques to track multivalent ligand properties at the different size ranges are described and validated.

3.1.1 Single Molecule AFM (SM-AFM)

In order to study how different physicochemical parameters of multivalent carbohydrate ligands affect the receptor binding at single molecule range, the studied system is reduced to the very molecular/primary level in which the multivalency of a single molecular scaffold is tested. The analysis of single molecules is performed by AFM because it allows observing interactions from van der Waals forces in the nN scale range down to single hydrogen bonding of a few pN and so it is possible to track the interaction between a multivalent ligand molecule and a receptor surface. To that purpose, the single multivalent molecule is tethered on the apex of an AFM cantilever tip and retracted from a receptor-functionalized surface. The linker molecule will help to differentiate the non-specific interactions between the tip and the substrate by distancing the specific ligand-receptor rupture events.[146]

SM-AFM provides information of the surface forces of the sample, i.e., attraction and repulsion interactions, from measuring the deflection of a micro-cantilever equipped with a nanometer-sized tip that is modified with the molecules of interest. The specific ligand-receptor interactions can be determined by monitoring the bending of the cantilever upon retracting its tip from a surface as a result of the ligand-receptor interactions between tip and surface. Rupture events occur upon matching the load-force with the dissociation force of ligand-receptor bonds. The rupture events correspond to the jumps in force in the force-retraction curve, see Figure 14. Calibration transcripts the cantilever bending into a force/speed-distance/time chart from where the ligand-receptor rupture events can be studied.

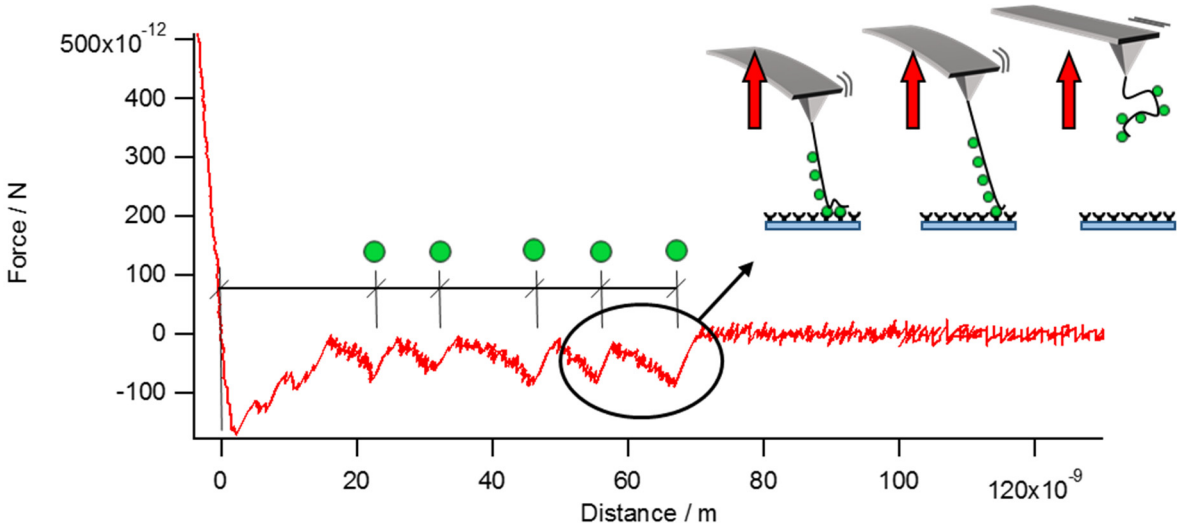

Figure 14- Force-distance curve with five dissociation steps of a retracting cantilever bearing a pentavalent ligand from a receptor surface. Surrounded and top-right represented are the fourth and fifth disconnection steps. The spacing among the steps can be resolved in the curve. The breaking force corresponds to the force difference before and after the event.

In order to establish SM-AFM, firstly the cantilever tip needs to be functionalized with the respective carbohydrate ligand, and secondly, the planar surface needs to be coated with active lectins. In order to improve the fidelity of force measurements, the carbohydrate will be tethered through a long spacer molecule.

3.1.1.1 AFM tip modification

Through the AFM tip functionalization with the respective carbohydrate ligand, two problems must be considered. The first one is to minimize the influence of non-specific interactions by tethering the ligands far from the tip since non-specific interactions among the tip, ligands, and substrate are reported to appear at closer distances in the force-distance curves.[146] The second one is to ensure a true single-molecule regime avoiding simultaneous binding from multiple ligands. Therefore, the functionalization of the AFM tip is performed through a long spacer molecule of polyethylene glycol (MW 10000 Da) with a contour length of ~80 nm[147], which separates the carbohydrate ligand from the cantilever tip. The end-functionalization of the spacer with a mixture containing the carbohydrate ligand and a molecule that does not show specific binding to lectins decreases the number of ligands favoring the single molecule regime.

Silicon cantilevers were used for carbohydrate ligand functionalization. Firstly the AFM tips were cleaned from interfering organic pollutants by oxidation in a UV ozone-chamber. That also oxidizes the surface providing a higher amount of surface silanol groups for coupling. Then, the AFM tips were coated with (3-aminopropyl)triethoxysilane (APTES) introducing primary amine groups to which a heterobifunctional PEG linker containing a reactive *N*-hydroxysuccinimide (NHS) ester can be coupled subsequently. Besides the NHS ester, the used PEG linker contains a terminal

maleimide group, which can be used for functionalization with thiols. Carbohydrate bearing ligands were synthesized with terminal thiol groups allowing for a straightforward functionalization of the maleimide presenting AFM tip, Figure 15. Possible oxidation of thiols forming ligand dimers is not hindered by reduction with phosphines, i.e., tris(2-carboxyethyl)phosphine (TCEP) since TCEP is reported to react with maleimide groups.[148]

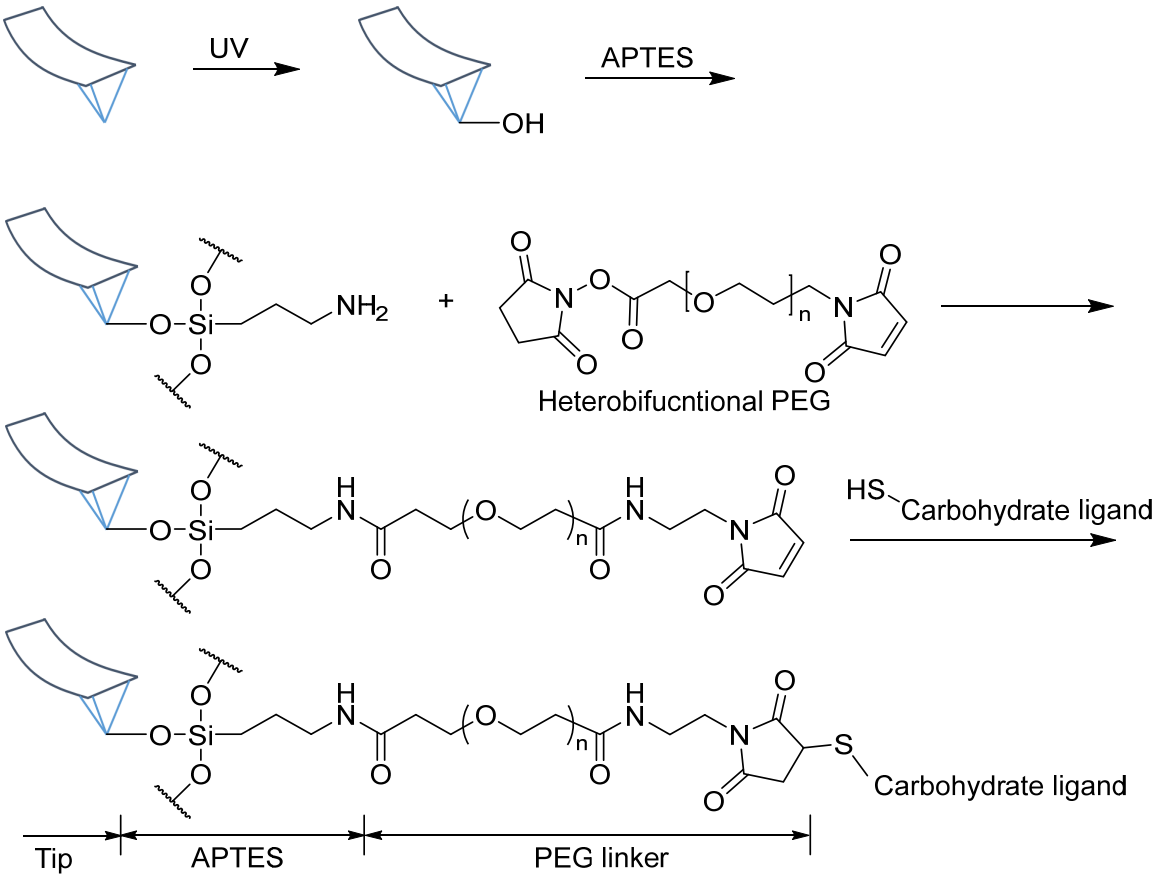

Figure 15- Scheme of the chemically modified cantilever tips. On the first step, UV light is used to activate the surface silanol groups, on where to react the amino functionalized silane (APTES). In the following step, the heterobifunctional PEG spacer is linked through its succinimide end group, serving the maleimide end group to later couple the thiol glycomolecule.

The molecular density regime to perform single molecule studies was achieved by dilution. There are two possible dilution options to decrease the number of ligand molecules on the AFM tip. The first one is to dilute the linker solution while reacting on the APTES layer, which can later react to pure ligand solution. The second possible dilution can be performed while reacting the ligand. The second approach was selected due to the straightforward analysis by XPS. There is not clear reported protocol on the diluting ratios while functionalizing the AFM cantilevers, but justifications through the hydrodynamic radius of the reactants.[149] The calculated hydrodynamic radius of the PEG linker (Mw 10000) is ~3.3 nm[150], which regarding geometry reduces the functional spots on where carbohydrate ligands are presented (Figure 16). In order to further

minimize the chances of multiple sugar presentation, the carbohydrate ligand reacting solution was diluted in a 1:4 ratio with 2,2'-(ethylenedioxy)diethanethiol. It presents two thiol groups and does not specifically interact with lectins. It is expected to diffuse easily and react faster capping the linkers. Therefore, making unlikely to have two exposed glycomolecules to interact simultaneously on the Con A surface. Nevertheless, the final discrimination is modeled in distance and energy and validated comparing with reported values.

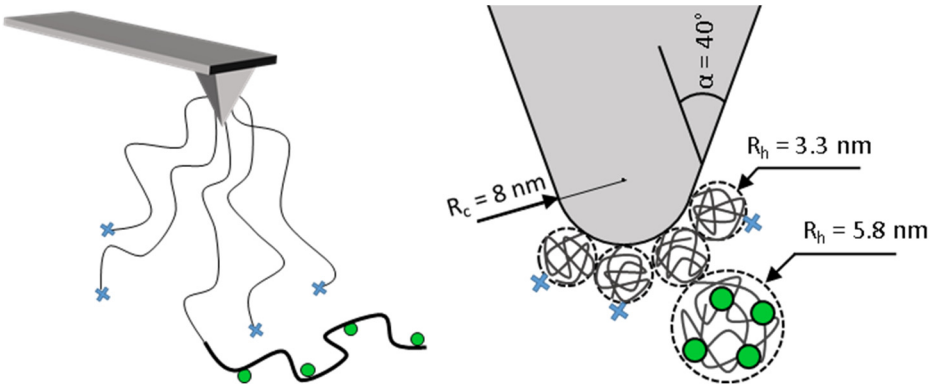

Figure 16- Left) Schematic representation of cantilever functionalization. Right) Real scale representation of the cantilever tip and the hydrodynamic radius of heterobifunctional PEG crosslinker and multivalent sugar bearing polymer. Notice the few linker molecules deposited on the tip and the single-molecule regime achieved by dilution. Green dots represent the carbohydrate moieties carried on a polymer; blue crosses represent 2,2'-(ethylenedioxy)diethanethiol molecules used for capping and dilute.

3.1.1.2 Immobilization of Con A on a planar surface for SM-AFM

Glass surfaces were functionalized with concanavalin A (Con A) lectin receptors on where to face the multivalent ligands. First, the glass coverslips were cleaned with a mixture of ammonia and hydrogen peroxide (RCA solution) to remove by oxidation any kind the adhered organic molecules. Then, glass surfaces were coated and annealed with (3-glycidyloxypropyl)trimethoxysilane (GLYMO) polymer introducing epoxy groups on where the lectins were covalently linked through some of their nucleophilic groups, Figure 17.

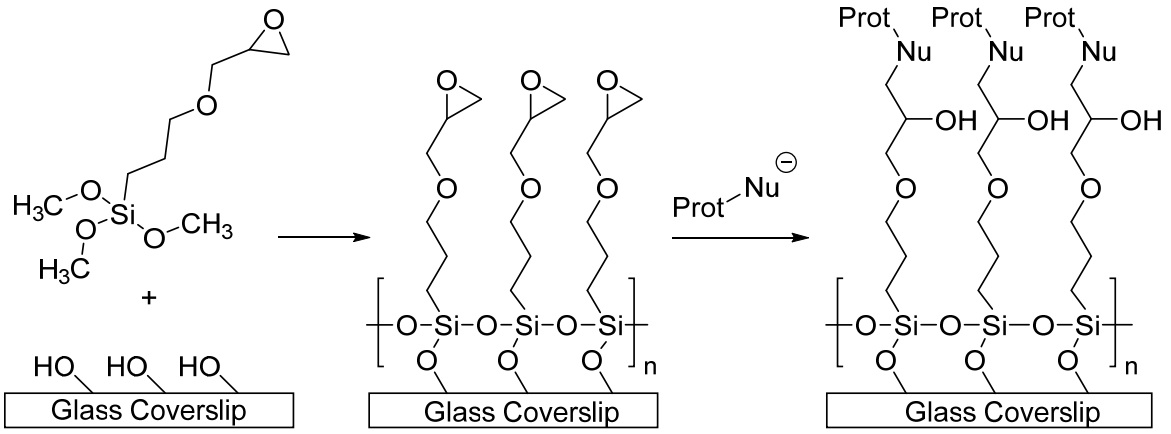

Figure 17- Protein functionalization of glass coverslips. Clean glass coverslips are coated with GLYMO polymer to introduce epoxy groups on where proteins are linked. The covalent linkage is formed as the result of the epoxy ring aperture by a nucleophilic group of the protein.

It is expected a full surface functionalization with a random but homogeneous density distribution of Con A. The tethering and following steps, including force measurements, are performed in pH 7.4 buffered solutions at which Con A lectins present a homotetrameric conformation. The random orientation of the immobilized Con A is supposed not to be critical for the force assay assuming that there are always Con A binding sites facing into the solution.

3.1.1.3 Characterization of ligand-functionalized tip and lectin functionalized surface

The surface chemistries for carbohydrate-tip and lectin-coverslip functionalization were tested using SCP-adhesion and x-ray photoelectron spectroscopy (XPS). Lectin surfaces were directly tested, the tip functionalization, due to its small size, was indirectly tested on glass surfaces that were equally treated with the same solutions and under identical reaction conditions.

Soft Colloidal Probe – adhesion. Intermediate steps of tip functionalization chemistry were tested by means of SCP-adhesion. Anionic crotonic acid functionalized SCPs (CA-SCPs) were used to determine the correct reaction of APTES and linker on the surface. The different adhesion of CA-SCPs on these intermediate surfaces shows the variation of surface groups and indicates the success of reacting the linker. The SCP-adhesion experiments were performed in lectin binding buffer (LBB) pH 7.4. The adhesion energy of CA-SCPs onto the intermediate functionalizing step surfaces show significant variation between ATPES functionalized glass coverslips and the PEG-linker functionalization, Figure 18. The main differences for the PEG-linker surface are the sterical repulsion and absence of attractive electrostatic interactions as was the case for APTES, both affecting parameters to the adhesion of the SCPs. The chemical composition of PEG linker does not present pH susceptible groups for electrostatic binding to the deprotonated CA groups

(pKa 4.69) to explain the adhesion energy difference, meanwhile immobilized APTES does (pKa 7.6[151]).

The protein activity can be reduced or even lost after surface deposition, which could be due to protein denaturation, conformational re-orientations or by active sites orientation.[152] The appropriate activity of surface Con A lectins was tested with Man-functionalized SCPs (Man-SCPs) since the adhesion between Man-SCPs and Con A surface is influenced by the specific sugar-lectin interaction. To that interaction happening, the Con A surface must, therefore, be active. The assays were performed in LBB pH 7.4 with a gradual inhibiting media increment. Smaller adhesion energies were developed while specifically inhibiting Con A surfaces by competition with free methyl α-D-mannose (MeMan), proving their activity and successful surface functionalization, Figure 18.

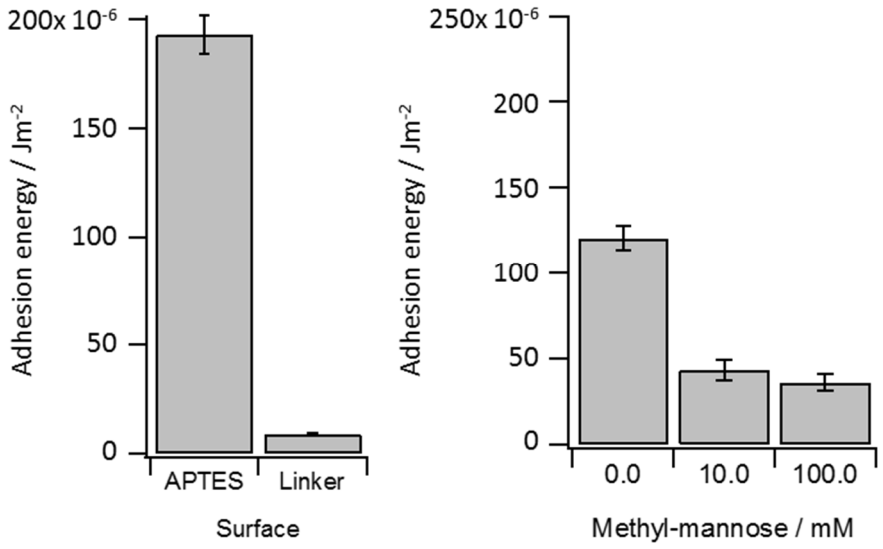

Figure 18- Left) Adhesion energy of CA-SCPs at sugar-functionalized surface steps; elastic modulus 30 KPa. Right) Adhesion energy of Man-SCPs on GLYMO-Con A functionalized surface under inhibitory conditions; elastic modulus 113 KPa.

X-ray Photoelectron Spectroscopy. The surface composition of glass coverslips functionalized by the same procedure as for the mannose thiol (ManSH) functionalized AFM tip (Figure 15) was analyzed using XPS. XPS is a technique that determines the atomic composition of the upper layers of surfaces.[153] It is assumed that the AFM tip functionalization procedure on glass results in similar surface chemistry as compared to the AFM tips. The target atom for the XPS analysis to prove an adequate functionalization is sulfur, which can be assigned to the carbohydrate ligand.

In addition, the Con A surface deposition on glass coverslips was corroborated by XPS pursuing nitrogen signal, which can be assigned to the protein since it is only nitrogen source on the

surface. Tested lectin-coverslips for XPS were discarded for further experiments due to protein denaturation by the required high vacuum conditions for XPS.

The presence of nitrogen and sulfur are, respectively, the confirmation for adequate surface functionalization, Figure 19 and Table 1. The ratio of the atomic composition cannot be used to correlate the surface thickness due to the non-quantitative profile depth of the technique. The high presence of oxygen and carbon was expected due to the high content of the linked organic molecules, as well as, being the most common surface pollutants. Pollution can be removed, i.e., by sputtering, which can also damage or remove the organic part of the sample. Due to the qualitative interest of the analysis, no dust removal process was undertaken. No further signals were found.

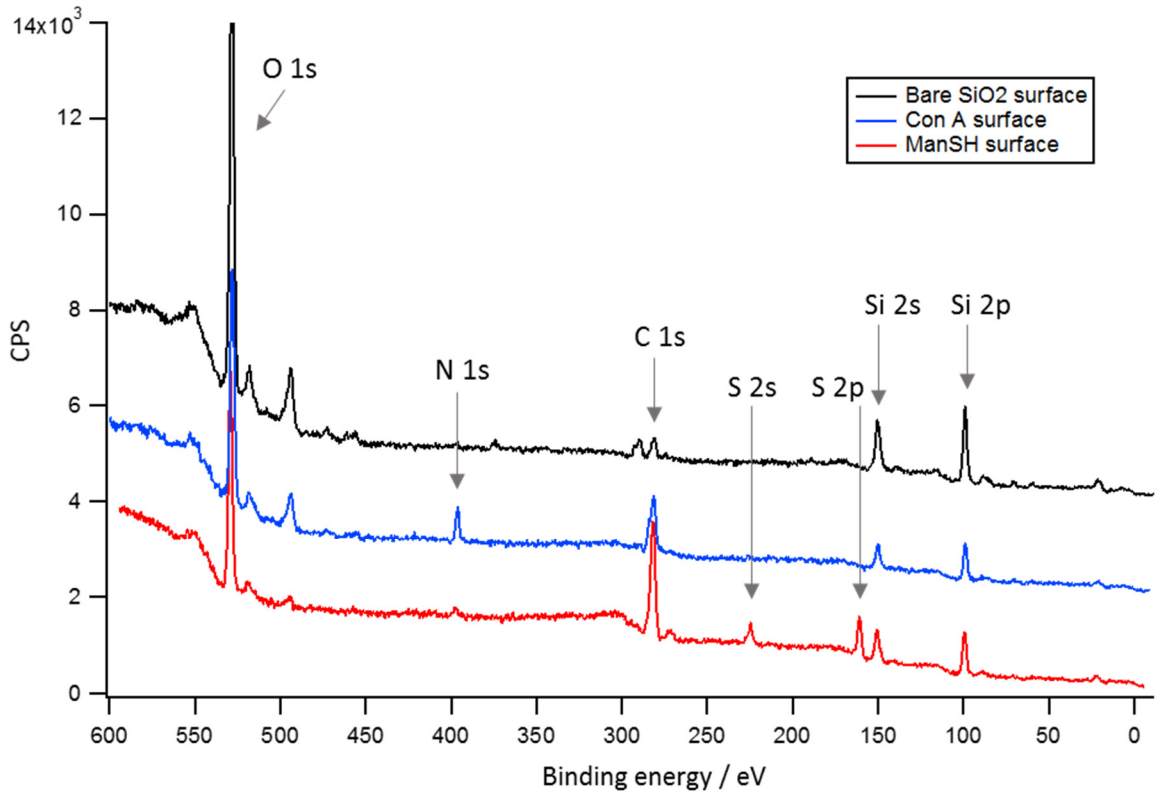

Figure 19- XPS spectrum for glass surfaces differently functionalized. For sugar functionalization (red), a glass surface was firstly coated with APTES that upon annealing was reacted with the heterobifunctional PEG linker. The surface was later reacted with a 1.25 M solution of mannose thiol in PBS pH 7.4. The S (2s and 2p) signal proved the covalent linkage of sugar macromolecules. For lectin functionalization (blue), glass surface was firstly coated with GLYMO that upon annealing was reacted with 0.05 mg/mL Con A in PBS pH 7.4. The N 1s signal proved the presence of linked lectins on the surface. A reference bare glass (black) is also shown for comparison. Note that the spectrum for bare glass and lectin functionalized surfaces have been rescaled in the y-axis (+2000 and +4000 CPS respectively)

The semi-quantitative approach and the low lateral resolution of the technique do not allow using atomic references neither determine the degree of functionalization regarding the area. It is

supposed to be complete and homogeneous due to the isotropic properties of every used material. Nevertheless, XPS spectra indicate successful surface functionalization.

Table 1- Atomic composition of silicon surfaces with chemically linked thiol molecules. For comparison, the precentral ratio of the most sensitive orbitals are considered; being those with the greater electronic population.

	ManSH surface		Con A surface		Bare glass	
Signal	Position / eV	Area%	Position / eV	Area%	Position / eV	Area%
Si 2p	99.49	23.38	98.86	9.55	99.02	32.92
S 2p	160.99	9.77	-	-	-	-
C 1s	281.99	41.54	281.43	59.94	281.08	7.72
N 1s	-	-	395.97	4.94	-	-
O 1s	529.49	24.38	528.52	25.57	528.67	58.65

3.1.1.4 Validation of SM-AFM approach for multivalent ligands

Generally, by means of AFM, interactions between the tip and the substrate can be detected. The overall goal is to establish SM-AFM studies to determine the binding strength of receptor and ligands, respectively Con A and Man-presenting scaffolds. Establishing the SM-method requires the ability to discriminate between specific and non-specific interactions, as well as techniques that identify and exclude non-specific binding events during data analysis.

Force-curve characteristics assigned to binding specificity. The characteristics of force curves can be assigned to specific and nonspecific binding. The validation of the method was performed functionalized cantilever tips with a Man-bearing polymer ligand **P5**, Figure 20 (see synthesis in section 3.2.1).

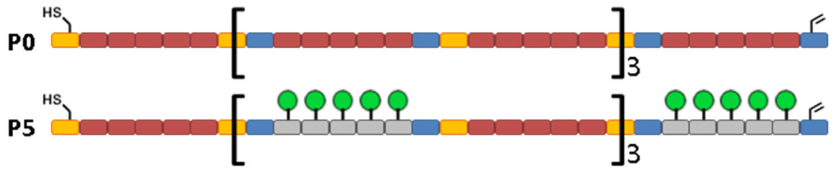

*Figure 20- Polymer ligands used for validation. The carbohydrate content difference between the mannose-free (**P0**) and the mannose-bearing (**P5**) polymers was used to determine the specific interactions between the carbohydrates and the lectin surface. Green circles represent the mannose moieties. For synthesis and specification see section **3.2.1**.*

A blank control was performed with a tip tethering a Man-free polymer **P0**, Figure 20. As receptor surface, a coverslip was functionalized with Con A. A carbohydrate-free ligand and the one

bearing Man were reacted on each cantilever tip following the chemical procedure mentioned above and faced (n=1024) to a Con A functionalized surface in LBB pH 7.4.

The vast majority of force-distance curves presented multiple signals at different distances while retracting the tip from the surface. Three signal kinds can be classified according to their specificity and source: 1) the non-specific interactions between the tip and the substrate that appear at the starting distances of the retraction, 2) the non-specific interactions between the linker and the substrate, and 3) the specific interactions between the ligand and the substrate; these last two appearing at greater distances, Figure 21. As well, a minor group of force-distance curves did not present any interaction (Flat curves) over 50 pN, which is the lowest reported value for monovalent Man-Con A interaction (49 ± 7 pN).[146]

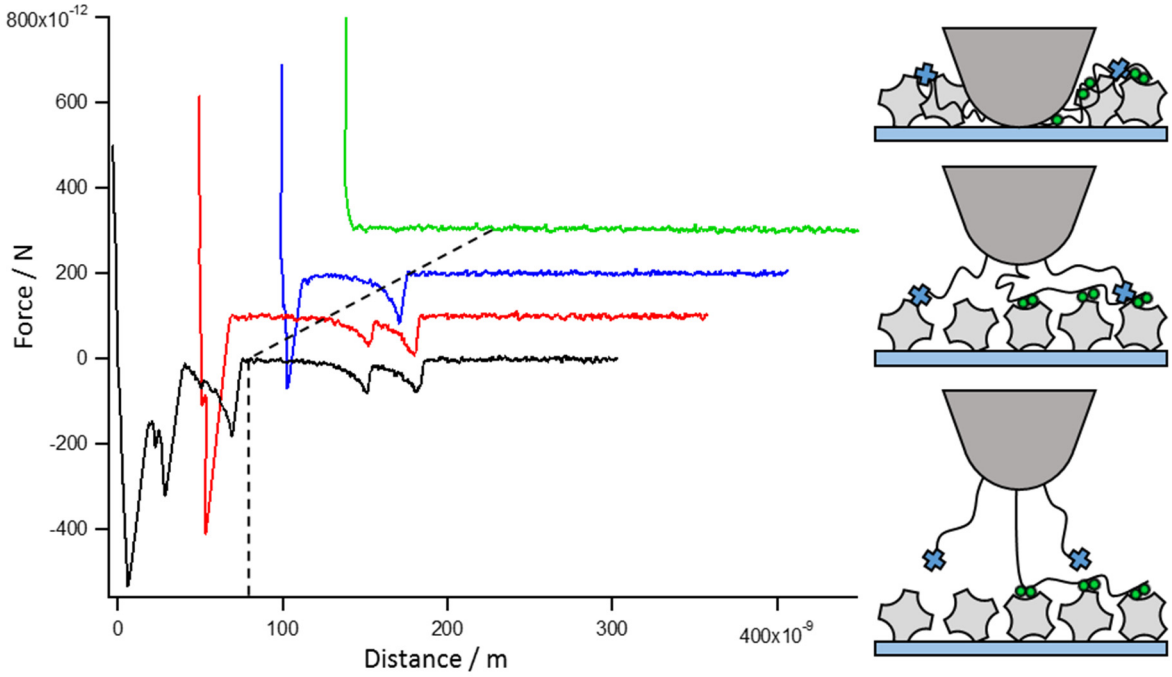

Figure 21- Left) Frequently recorded force-distance curves. The green curve shows the absence of interactions (flat curve). The blue curve shows the non-specific interactions: tip-substrate at starting distances and linker-substrate at further ones. The red curve shows the tip-substrate non-specific interaction together with specific interactions between multivalent ligand and substrate. Black curve simultaneously displays the three interaction kinds. Notice that non-specific interactions appear at smaller distances than the linker length represented with the dashed line at ~80 nm. Force curves are represented in perspective. Right) Representation of interactions: upper, non-specific tip-substrate interaction at close distances, middle, non-specific linker-substrate interaction presented at the contour linker length, lower, specific ligand-receptor interactions.

The three kinds of interactions can be presented long the force-distance curves without a clear difference, frequently overlapped, demanding a protocol to discern among them unambiguously. The non-specific tip-substrate interactions can be avoided considering disruptive events that

appear in force-distance curves after firstly reaching the baseline. Then, a comparison between the carbohydrate-free and carbohydrate bearing polymers was used to discriminate between the substrate interactions with the linker (non-specific) and the ligand (specific). All the disruptive events presented after reaching the baseline were represented in distance histograms for both samples. Carbohydrate-free polymer, **P0**, presents a defined distribution of events at smaller distances than 50 nm. Meanwhile, carbohydrate bearing polymer, **P5**, presents two distributions delimited at 70 nm, Figure 22. These distances correlate with the contour linker length (~80 nm) assuming height shifts while reacting the ligands on the tip. These height differences will be transcript as distance shifts in force-distance curves. The distance threshold can be therefore used as a reference from where to consider the specificity of ligand-substrate interaction.

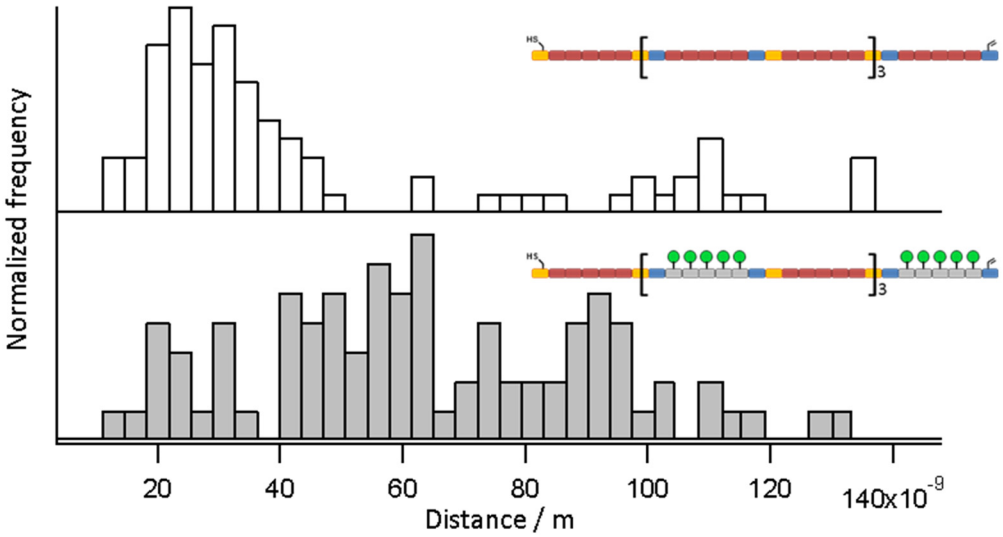

Figure 22- Normalized distance histograms for disconnection events of mannose-free and mannose-bearing polymer ligands. The presented events at lower distances than 50 nm for mannose-free ligand and 70 nm for mannose-bearing ligand are correlated to the non-specific linker-substrate interaction. Events presented at longer distances are correlated to the non-specific interactions polymer backbone-substrate (mannose-free ligand) and specific ligand-substrate interaction (mannose-bearing ligand).

Specific Con A-Man interaction confirmed by inhibition. As confirmation of the specificity of linker and ligand interactions, the carbohydrate (**P5**) functionalized tip was brought into contact (n=512) with a ligand surface at varying concentrations of methyl mannose (MeMan) as an inhibitor. MeMan in the solution competes for Con A binding sites and should overall reduce the frequency of specific interactions between tip and surface. The inhibitory conditions were achieved with 10 mM and 100 mM MeMan. As expected, the frequency of events surrounding the threshold distance was reduced while inhibiting, Figure 23. The event frequencies at higher distances than 70 nm were decreased, remaining almost constant at lower distances.

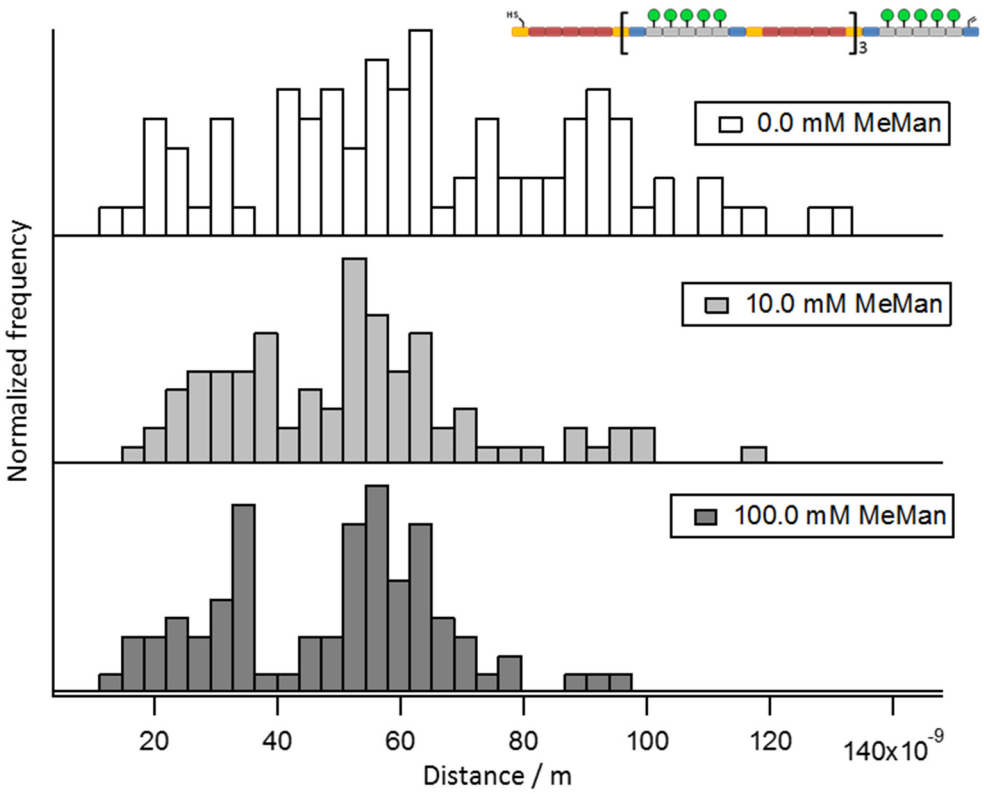

*Figure 23- Normalized distance histograms for disconnection events of carbohydrate bearing ligand **P5** after reaching the baseline at different inhibiting concentrations. Note the event frequency reduction at higher distances than 70 nm while inhibiting. The distance matches the linker contour length delimiting from where disconnection events can be correlated to the specific rupture of Man-Con A interaction.*

Closer data analysis supports the specificity of the SM-AFM rupture events. The threshold distance to consider the interactions was decreased from 70 to 50 nm in order to include more rupture events. The percentage of force curves presenting specific Man-Con A rupture events (Single Molecule curves) gradually dropped from 39% to 22% and 16% while increasing the inhibitory concentration, Figure 24. Subsequently, the total number of these events (Specific Interaction) also decreased, from 228 to 118 and 93. Simultaneously to the rise in inhibition, the percentage of force-curves not showing any interaction grew (Flat curves) from 8% to 27% and 17%. As well, the average rupture-force decreased (Step Force) from 136 to 81 and 83 pN.

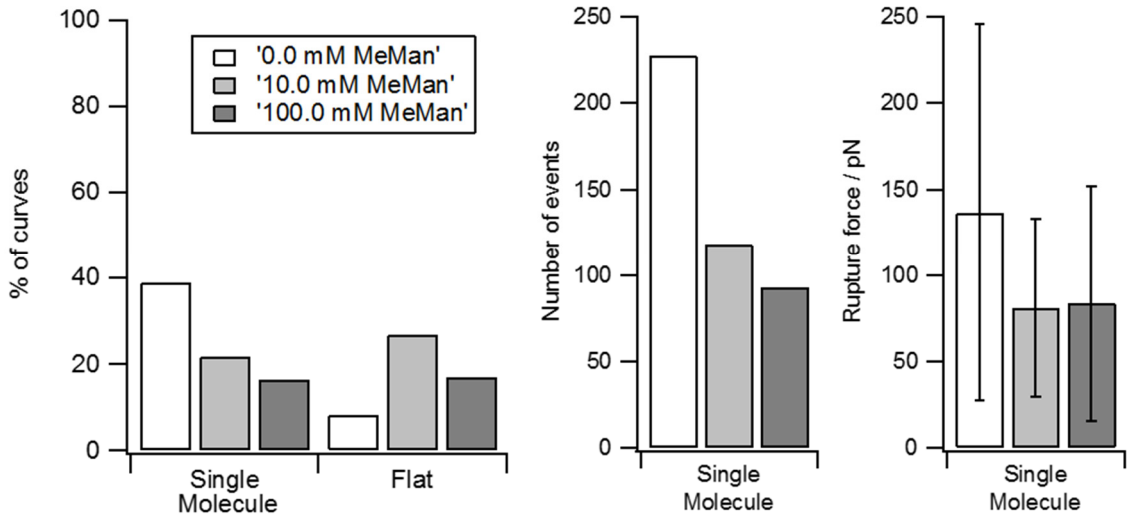

Figure 24- Force-distance curves while increasing the inhibiting media conditions with MeMan. Left) Percentages of retraction curves (n=512) presenting specific rupture events over 50 nm (Single Molecule) and not showing any interaction (Flat). Middle) Number of specific Man-Con A disruptive events within the single molecule curves. Right) Mean ± std. deviation of rupture force for the specific Man-Con A events determined in single molecule curves.

Under 10 mM MeMan the observed rupture force suffers a drastic reduction to almost half of the force, remaining constant at 100 mM MeMan. Both values are found within the reported rupture forces of monovalent ligands (96 ± 55 pN[154] and 49 ± 7 pN[146]) despite the different ligand structure and variations on the experimental settings. The greater force value in the absence of inhibitor could be correlated to the multivalent presentation, while, the smaller rupture force under inhibition correlates with the reported unbinding of monovalent Man. This suggests that the inhibiting media predominantly hampers multivalent binding but did not hinder specific binding completely.

Applying the stated validation procedure, it is assumed that the observed rupture events predominantly occur from specific interactions of the Man residues of the molecule attached to the AFM tip with the Con A on the opposed surface. Therefore, multivalent carbohydrate binding can be studied on the molecular level with the presented approach.

3.1.2 Mesoscale – Protein scaffold for sugar presentation

In mesoscale range, not single molecules are studied but assemblies of several molecules in a size range of several tenths of a nanometer. This can be achieved by tethering multiple sugar molecules on a protein scaffold to form so-called Neoglycoproteins (NGPs). Previous studies with NGPs have devoted attention on the methodology to load great amount of sugar moieties[85], but studies reporting on the effect of the ligand flexibility/length influence to the specific interaction rate and mechanism are scarce.

The following section describes a method in which various monovalent sugars and a fluorescent label are bound covalently to a carrier protein. Albumin as a carrier protein has been reported to show low non-specific binding to lectins, a key feature of the scaffold.[89] Here, the complete synthesis of NGPs was performed in a single-pot reaction under mild conditions to prevent the BSA from denaturation and preserve the pyranose form of the sugar; the one that can specifically interact with lectins.[80] Two heterobifunctional crosslinkers with varying in length were used to tether the sugar molecules providing different flexibilities in order to study their influence in multivalency. The analysis of NGPs was performed by fluorescence and turbidity assays pursuing the direct specific binding interaction to the respective lectin binding partner and determining the effect of linker flexibility. In this section, the development of the method and the feasibility to determine specific interactions are shown.

3.1.2.1 Synthesis of Neoglycoproteins

The synthesis of NGPs was performed using albumin (bovine serum albumin, BSA) as the carrier protein. The complete synthesis of NGPs was performed in a single-pot reaction under mild conditions to prevent the BSA from denaturation and preserve the pyranose form of the sugar, the one that can specifically interact with lectins.[80] As well, single-pot reaction minimizes the introduction of impurities, which are critical for surface experiments/chemistry, also avoiding time consumption and sample loss by cleaning and purification steps. SMCC and PEG heterobifunctional crosslinkers (Mw 334 and 10000 respectively) were used to tether the sugar molecules and vary the linker length, Figure 25. Firstly, to a starting solution of BSA in LBB buffer pH 7.4, a 30-fold excess of the linker was added and mixed. SMCC is not soluble in water and was reacted in dimethyl sulfoxide (DMSO), not exceeding a final concentration of 10vol%. PEG linker was reacted in LBB. The succinimide end-group of the linkers bind to amine groups of the BSA protein; the maleimide end-group then remains exposed on BSA. Simultaneously, a 300-fold excess of mannose thiol (ManSH, 10-fold excess in respect to the cross inker) was added and mixed. The thiol groups specifically and covalently bind on the maleimide group of the linkers.

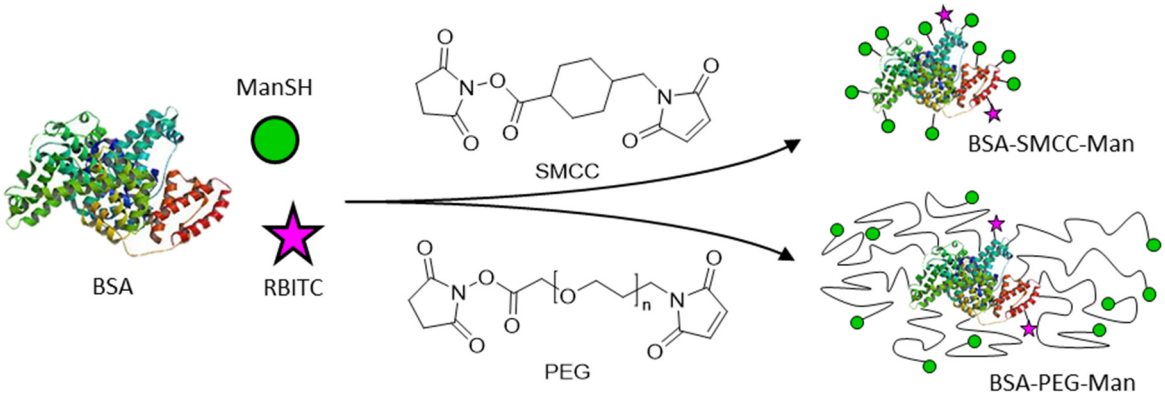

Figure 25- Schematic synthesis of NGPs with BSA protein as a scaffold on where to load sugar moieties. The functionalization takes place through heterobifunctional linkers of different lengths to provide despair ligand flexibilities. The reaction is produced in a single-pot approach with increasing excesses of linker and sugar. RBITC competes with the succinimide group of the linker to react on BSA primary amines and therefore was added with a delay to favor greater sugar functionalization degrees. BSA image from.[28-29, 155]

The fluorescent labeling was done with Rhodamine B dye in its isotiocianate form (RBITC), and it was added from DMSO stock solution. The isotiocianate group directly reacts on the nucleophilic side groups of the protein, such as amino groups, competing with the crosslinker. Only a few molecules are necessary for the fluorescent NGP detection. Therefore the addition into the single-pot was done with a delay in respect to the linker addition. The final NGP solutions were purified either by size exclusion columns or dialysis. After removing all the unreacted molecules from the media, the final composition of NGP solutions was determined.

3.1.2.2 Neoglycoproteins degree of functionalization by UV-Vis and NMR spectroscopy

UV-Vis spectroscopy. The composition of NGP solutions was quantified by UV-Vis spectroscopy regarding protein, sugar and fluorescent concentrations. The simultaneous presence of the three components was the first confirmation for an adequate synthesis. Values are summarized in Table 2. The fluorescent labeling degree was determined by direct quantification of BSA and Rhodamine B (RhodB) with the stock NGP solutions. The sugar composition was determined by colorimetry using the reaction products of added sulfuric acid and phenol with the sugars. Aliquots of the NGP solutions were therefore reacted, and the absorption of the products was correlated to a calibration line prepared by digesting ManSH.

The presence of Man in both linker NGP samples indicates the desired functionalization of BSA with ManSH. The presence of sugar for unfunctionalized samples (BSA and BSA-RhodB) is attributed to the error of the colorimetric assay and possible glycosylation of BSA according to manufacturer provided product description. Also, the reaction with the fluorescent label results in interferences as it can be seen from BSA-RhodB value, Table 2. The corrected Man

functionalization degree was calculated subtracting the Man degree of BSA and the proportional interference of RBITC calculated from BSA-RhodB. Regardless of their linker length and after correction, the products expose in average five sugar moieties per BSA achieving the pursued multivalency. There is no characterization determining the amount of unlabeled or non-functionalized proteins.

In comparison to similar studies that report the same functionalization degrees, it was expected that all proteins in the mixture react to sugar and label to some extent.[85] As well, the resulting final functionalization degree of BSA scaffolds for all the presented samples, which results from adding the ratio of Man/BSA and the ratio fluorescent dye/BSA, is smaller than the total amount of amino acids contain a free amine group on where the BSA is susceptible for functionalization, such as lysine (60), asparagine (14) or glutamine (20); in brackets is the present amount of each amino acid within a single BSA protein. Subsequently, the complete functionalization of BSA correlates with the number of reacting groups.

Table 2- Characterization of BSA scaffolds after sugar functionalization with two linker lengths and fluorescent labeling. Protein and sugar determination was done with the stock solutions. Meanwhile, sugar content was correlated through a calibration line. The concentration of solutions is determined by the mass of present BSA indifferently of its functionalization, including the short (SMCC) and long (PEG) linker length derivates. The degree of Rhodamine B (RhodB) and Mannose (Man) functionalization are expressed in a molar ratio to the BSA. Mannose correction corresponds to the Man functionalization degree after deducing the contribution of BSA and the proportional of the fluorescent label.

	BSA mg/ml	RhodB mol/mol BSA	Man mol/mol BSA	Correction Man mol/mol BSA
BSA	0.80	0.00_1	2.28	0.00
BSA-RhodB	0.75	0.22_5	7.27	0.00
BSA-SMCC-Man	0.46	0.16	9.25	3.42
BSA-PEG-Man	1.03	0.10	8.98	4.48

The fluorescent labeling shows an expected, two- and threefold, higher functionalization degree for sugar-free BSA than for the respectively short and long linked Man to BSA (BSM and BPM). The different labeling degree is assumed to be due to the consumption of reactive groups in the protein as well as hindrance of fluorescent label exerted by the linkers, showing greater hindrance for the bigger PEG than for the shorter SMCC.

NMR spectroscopy. The chemical procedure to obtain neoglycoproteins was tested using NMR. A ^{1}H-NMR spectrum was performed either to the bare starting BSA protein and the final NGP synthetized lacking the fluorescent marker. For that, the neoglycoprotein BSA-SMCC-O2 was synthesized with the multivalent glycooligomer **O2** (see section 3.2.1) and the short SMCC linker

(BSA-SMCC-O2 sample, see section 3.2.3) through the method mentioned above and freeze-dried after the synthesis. The BSA-SMCC-O2 sample for ^{1}H nmR was dialyzed and re-dissolved in deuterated water (D_2O). The linked multivalent glycooligomer **O2** presents two Man moieties grafted to the backbone through Copper(I)-catalyzed azide-alkyne cycloaddition (CuAAC). The comparison of spectra unambiguously reveals the triazole proton signal for BSD sample (δ=7.86 ppm), which is the result of the CuAAC reaction proving the unambiguous synthesis of NGP, Figure 26.

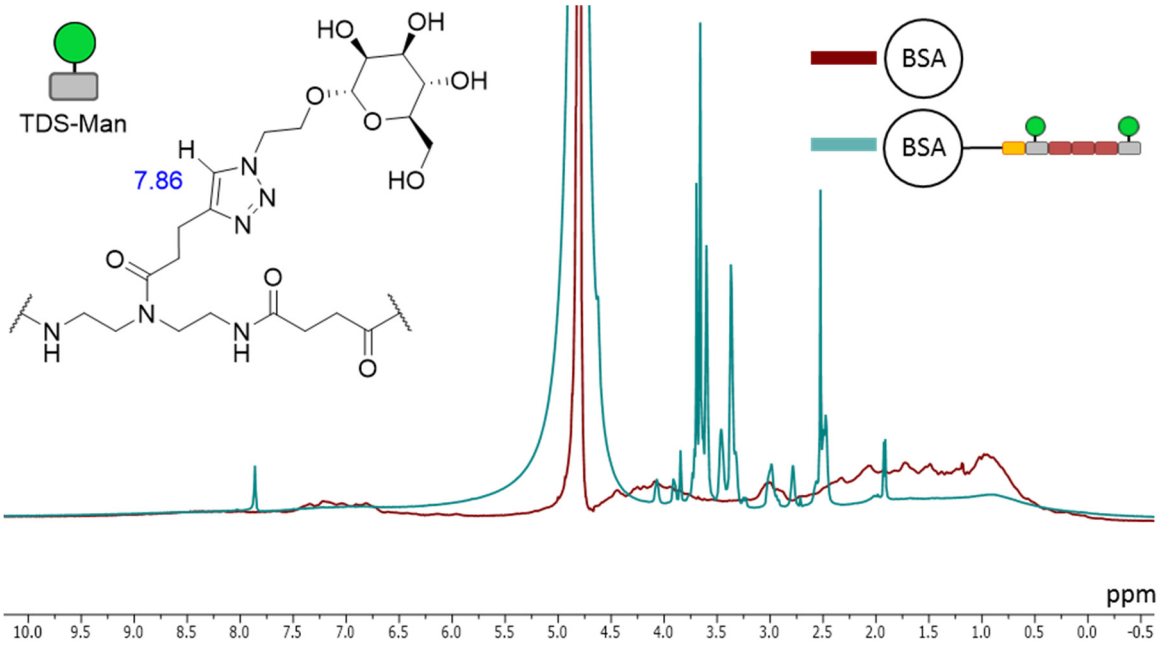

Figure 26- Superposition of 1H-NMRfor reference BSA (brown) and the neoglycoprotein BSA-SMCC-O2 (green). Note the resolved singlet signal of the imidazole proton resulting from the CuAAC reaction at δ=7.86 ppm. Spectra recorded in D_2O (δ=4.79 ppm) with a 600 MHz device.

The NMR spectra show a great degree of complexity and are not resolved for any of the chemical shifts but the singlet of the triazole group in the BSD spectrum. Further resolution of the spectrum is out of the scope of the present thesis.

3.1.2.3 Validation of NGPs to study linker effect to multivalent ligands

In order to validate NGPs as a tool to study the effect of the ligand flexibility to multivalent recognition, the affinity of the synthesized NGP ligands should increase for an increased number of presented Man-units, the binding should be specific, and flexibility of the linker should affect binding. In the following two assays, turbidity and fluorescence microscopy, are presented to test the specific binding of Man-functionalized NGPs and Con A.

Turbidity assay. UV-Vis and NMR previously showed the chemical composition and multivalent Man presentation of the NGPs. Here, the NGP binding activity as a function of ligand flexibility

(linker length) is tested by a turbidity assay with Con A. Con A is a lectin that presents a tetrameric conformation under neutral pH with four binding pockets.[156] The multiplicity of binding pockets allows to bind up to four ligands simultaneously. Therefore, ligands presenting multivalency can produce a network of Con A aggregates by simultaneously cross-linking to more than one Con A, Figure 27. The network density and rate of its formation can be determined through the light intensity decay as a result of scattering of light passing through the aggregate dispersion.

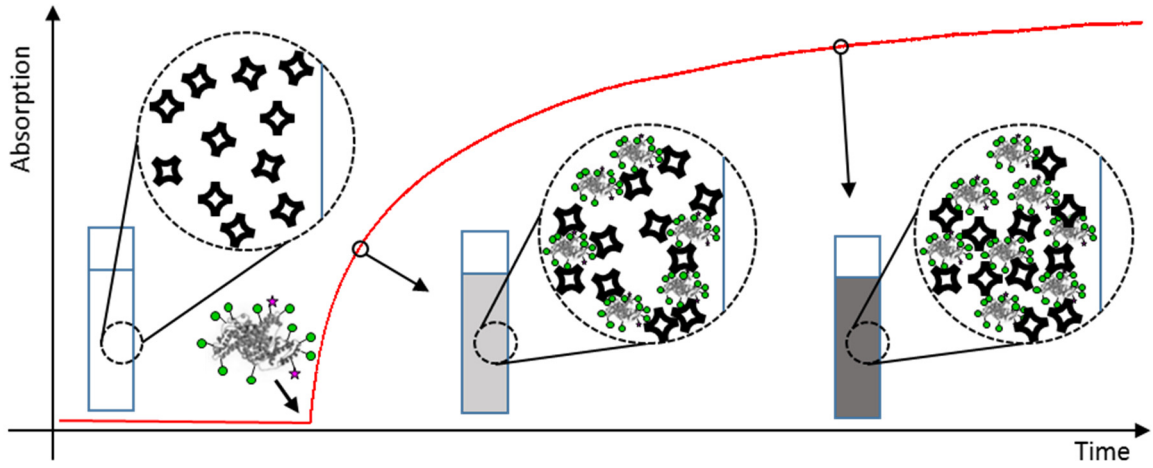

Figure 27- Schematic representation of a turbidity assay. To a starting lectin solution that does not absorb light (λ 420 nm) a multivalent NGP solution is added and mixed. A matrix is produced by crosslinking the lectin and NGP due to their respective multivalence and grows along time. The matrix disperses the light by scattering, which is determined as an absorption.

The transmitted light at 420 nm was detected while mixing a stock Con A solution in LBB (3.33 µM) with the NGPs (1.33 µM); what regarding Man concentration corresponds to 4.55 µM Man from BSA-SMCC-Man and 5.96 µM Man from BSA-PEG-Man. As a blank experiment, unfunctionalized BSA was mixed with Con A solution at the same concentrations to confirm its non-binding property. A control experiment was performed with the monovalent sugar solution (ManSH) used to synthesize the NGPs. It was expected not to develop turbidity in the Con A solution due to its monovalence, unlike the multivalent ligands.

The achieved multivalent binding activity is presented for the short linker Man functionalized BSA product (BSA-SMCC-Man), but not for the long linker one (BSA-PEG-Man), Figure 28. An extended discussion of the interaction of the linker length can be found in section 3.2.3.2. Here, evidence proving the influence of the linker length is provided.

The absorbance of BSA-PEG-Man in Con A remained unaffected together with the baseline and was similar to the blank test (BSA) and the monovalent ligand (ManSH), Figure 28. The

nonexistence binding activity of BSA is attributed to the lack of sugar moieties, meanwhile for ManSH to its monovalence.

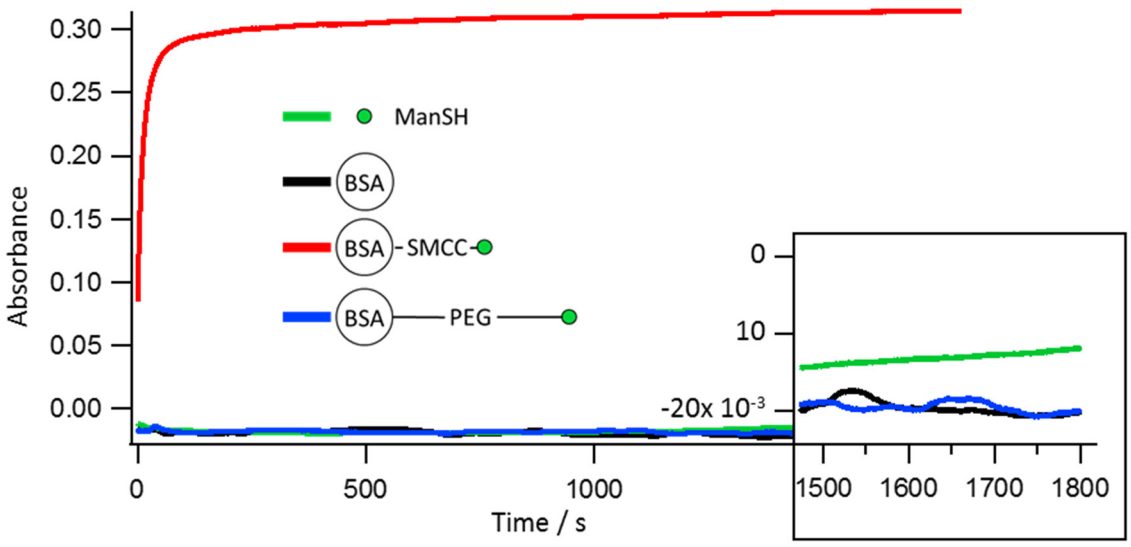

Figure 28- Turbidity assay. Transmission of 420 nm light in LBB of 3.33 µM Con A and 1.33 µM sugar ligands; 1.33 µM Man for ManSH, no Man present in BSA, 6.48 µM Man for BSA-SMCC-Man and 7.17 µM for BSA-PEG-Man. Note that only BSA-SMCC-Man flocculates the Con A solution while BSA-PEG-Man, unfunctionalized BSA, and the individual ManSH do not; all these curves remain together within the baseline. The small shift into negative values results from subtracting the average absorbance signal of the initial 600 s of 5 µM Con A solution in LBB used to test the signal stability.

BSA-PEG-Man has been proven to present multiple sugar residues. Therefore its missing activity is attributed to the final structure, where the linker length, and so the flexibility, play a key role. The PEG linker contour length (~80 nm[147]) is almost a hundred times larger than SMCC (~0.9 nm), which supports the hypothesis. The longer the linker is, the greater number of conformations and steric (entropic) repulsion it presents, which involves an increased thermodynamic cost for binding. Also, coiled conformations may involve slow kinetics demanding long times to uncoil and present the sugar moieties.

Fluorescent assays. The specificity of NGP ligands binding to their corresponding lectin receptor was tested by fluorescent assays. This method needs to be tested because the fluorescent label may affect the specific binding.[157]

Solutions of the synthesized NGPs were used to incubate Con A functionalized soft colloidal probes (Con A-SCPs) to bind on their Con A presenting PEG network specifically. The fluorescent label of NGPs allows quantification of the bound amount of BSA-SMCC-Man and BSA-PEG-Man on the SCPs, Figure 29. NGPs were also incubated with Con A-SCP dispersions under inhibitory conditions with α-methyl mannose (MeMan) aiming to track lower fluorescence in order to prove the specificity of NGPs.

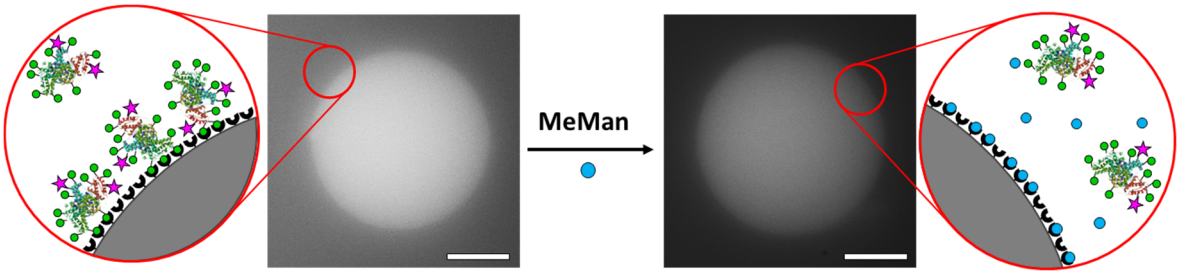

Figure 29- Schematic representation of the specific interaction of mannose functionalized BSA on Con A functionalized SCPs; not to scale. The fluorescent group (pink star) loaded on NGPs serves to detect their presence upon NGP binding on SCP surface. Inhibiting conditions with methyl mannose (MeMan, blue dot) is supposed to prevent the NGP interaction, and subsequently to decrease the fluorescence from SCP surface. Scale bars 10 µm.

As control experiments, labeled BSA was incubated with both crotonic acid and Con A functionalized SCPs (respectively CA-SCPs and Con A-SCPs). An increment in fluorescence was observed for control test that can be attributed to an increase of the hydrophilic behavior of the surfaces, Con A-SCPs, on where BSA adsorbs with higher interaction strength.[158] Meanwhile, a decrement in the values was found for the NGP samples under inhibiting conditions indicating for the NGPs specificity, Figure 30.

However, the first indication for the NGPs specificity was not confirmed with later repetitions of the assay, Figure 31. Several attempts of the experiments did not result in the fluorescence decrement under inhibitory conditions. Even or slightly higher fluorescent values whilst inhibiting were also found, resembling the control experiments. It could be argued that the high density of Con A on the SCPs induces non-specific receptor clustering binding to the BSA scaffold or less probable to

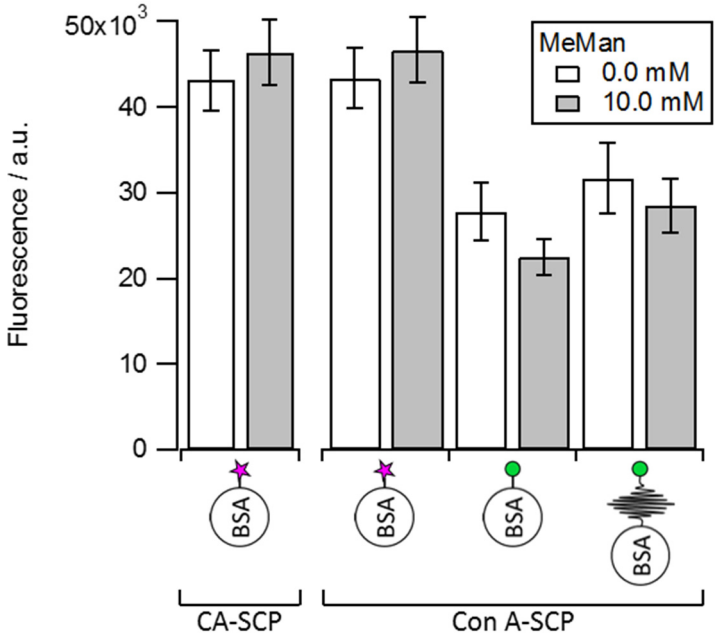

Figure 30- First results of surface fluorescence of SCPs incubated with NGPs. NGPs functionalized with the short SMCC and long PEG linkers, together with mannose-free BSA were incubated under different inhibiting conditions with bare crotonic acid-SCPs (CA-SCP) and Con A functionalized SCPs (Con A-SCP).

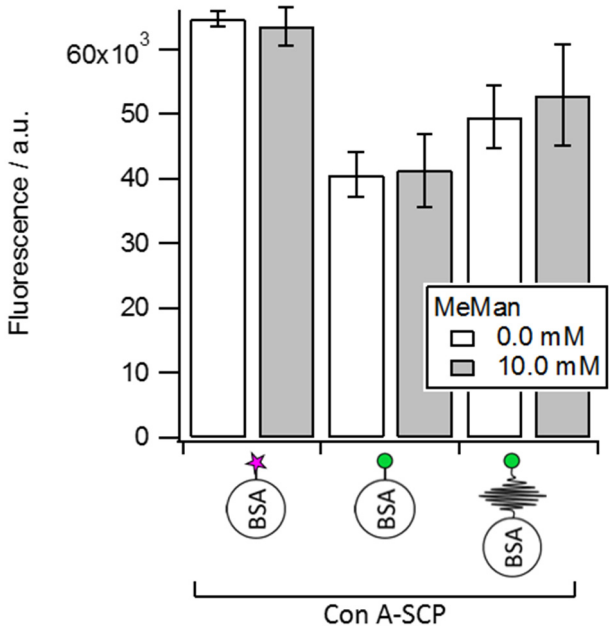

Figure 31- Example of repetition results of surface fluorescence of Con A-SCPs incubated with NGPs functionalized through the short SMCC and long PEG linkers. Mannose-free BSA was used as a reference. NGPs were incubated under different inhibiting conditions with Con A functionalized SCPs (Con A-SCP).

a low inhibition/competition concentration. Therefore, fluorescent tests did not resolve the specificity, neither proving the opposite. Many factors can interfere with the fluorescence capacity, and so, the presented fluorescent differences were not considered to be conclusive.

Overall, a successful synthesis and characterization of NGPs are achieved through different linker lengths. Although fluorescent assay does not confirm the specificity of the NGP interaction with Con A, the turbidity proves a mechanistic dependence on the linker length. Subsequently, the BSA based NGPs are a tool to study multivalency affecting parameters using turbidity assays, see section 3.2.3.2.

3.1.1 Cellular scale – Microparticle scaffold for sugar presentation

Microparticles are used in biological studies because they can be synthesized at the cellular scale objects. Their chemical composition varies (silica, gold, polymers), but hydrogel materials are of particular interest because they can mimic the material properties as well as the chemistry of cells and their surroundings. Therefore, they are often used for biological applications, i.e., sensing, drug delivery, and tissue regeneration among others.[91] In addition, some microgels respond to physicochemical stimuli[92] and others bind to determined targets after specific functionalization of the surface.[93-94]

Hydrophilic microgels are used in biological studies as they can be adjusted to the right mechanical properties, sizes and colloidal stabilities.[95] As well, with specific ligands tethered to the surface, they can mimic certain larger binding motives of the cell surfaces. A major application of microgels in biology is the separation of biomolecules like bacteria, proteins or DNA in aqueous solution[93, 96] but they can also be used as biosensors converting molecular binding events into a measurable and quantifiable signal.[97] The characterization of carbohydrate interactions at the cellular scale is of great interest, as carbohydrates cover the cell surfaces (glycocalyx) and so interact through larger areas.

The application of hydrogels as sensors for multivalent specific carbohydrate-ligand interactions can be established, varying the presented amount of carbohydrates, the density of them and the ligand flexibility. A complete understanding and controlling of their influence can lead to advanced biomaterials to be used as implants or tissue engineering scaffolds. In order to be used in the routinary analysis, it demands the characterization of the hydrogels. Although great contributions have been performed towards specific physical properties, the biological activity of functionalized hydrogels is neither fully understood nor controlled over several length scales.

In the present section, soft hydrogel particles so-called SCPs (soft colloidal probes) are synthesized as cellular scale multivalent ligand scaffolds. A colorimetric test is performed to determine the multiple functional groups that are subsequently functionalized with Man molecules (Man-SCPs). Using SCP-adhesion assays on Con A surfaces, the adhesion energy of Man-SCPs on receptor-functionalized surfaces confirms the multivalent behavior of cellular scale ligands, the robustness of differently prepared protein surfaces and the SCP stability.

3.1.1.1 Synthesis of SCPs and surface preparation

Synthesis of SCPs. The synthesis of SCPs is performed with the described protocol by Schmidt et al.[159] The macromonomer poly(ethylene glycol)-diacrylamide (PEG-dAAm) is added in a kosmotropic Na_2SO_4 solution and forms microscopic droplets under mechanical agitation,

Figure 32. Next, the dispersion is crosslinked by radical polymerization under UV-irradiation with the photoinitiator Irgacure® 2959. The synthesized colloidal hydrogels are transferred into ethanol, and then, crotonic acid was UV-grafted onto the colloids with benzophenone photoinitiator (CA-SCPs).

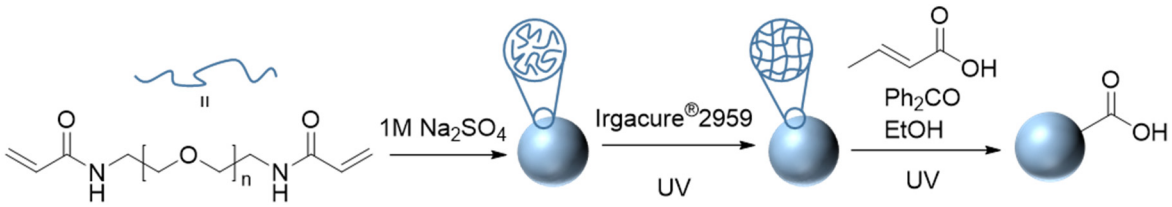

Figure 32- Schematic synthesis of CA-SCPs via free radical photopolymerization. PEG-dAAm is dispersed and crosslinked by UV in a kosmotropic saline solution. Then, crotonic acid is grafted in an alcoholic solution. Blue spheres represent the SCPs.

The final reaction of CA-SCPs toward Man functionalization was performed with amine functionalized Man (ManAm) presented in an acetylated protected form (Ac-ManAm), Figure 33**.** Firstly, CA-SCPs were dispersed in dimethylformamide (DMF). Then, the crotonic acid groups were activated with benzotriazol-1-yl-oxytripyrrolidinophosphonium hexafluorophosphate (PyBOP), hydroxybenzotriazole (HOBt) and *N*,*N*-diisopropylethylamine (DIPEA) and reacted with the protected amino derivate Man (Ac-ManAm). Finally, the Man functionalized SCP (Man-SCP) dispersion was washed, and the sugar moieties deprotected.

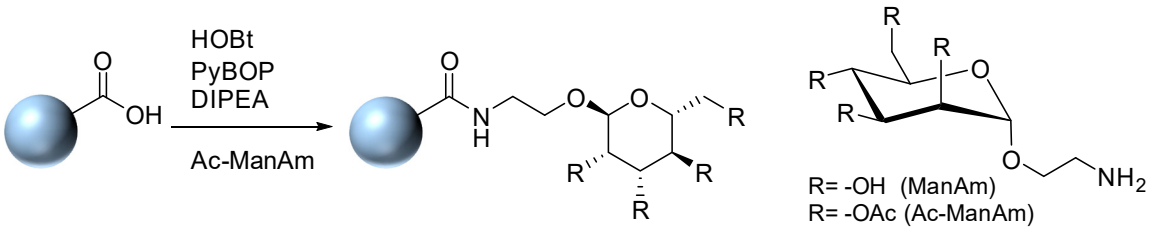

Figure 33- Schematic functionalization of Ca-SCPs with aminoethyl mannose derivate. The mannose is linked in a protected acetylated presentation.

Con A receptor surface. The functionalization of glass coverslips with lectins was performed through physical and chemical linking methods. Lectins were physically adsorbed by non-covalent bonds after a direct immersion of bare clean glass coverslips into a Con A solution in LBB pH 7.4 without using further reactions. Chemical linkage of lectins was achieved by undertaking the GLYMO approach through covalent bonds (see section 3.1.1.1).

3.1.1.2 Characterization of SCPs and lectin functionalized surfaces

The appropriate functionalization of CA-SCPs was confirmed by titration colorimetry with toluidine blue O test which measures the average amount of carboxylic groups in the SCPs. The

second functionalization step, the reaction of sugars with CA-SCPs was assumed complete[160] and not measured afterward. The elastic moduli of SCPs were determined by AFM force-indentation. The sugar presentation on SCPs was tested using SCP-adhesion of the Man-SCPs on Con A surfaces, which can be seen in section 3.1.1.3 while testing the lectin stability of surfaces with differed modes of Con A immobilization. The appropriate Con A surface functionalization was independently tested by XPS.

Toluidine Blue O colorimetry. The grafting of CA groups on the SCP surface was tested by a colorimetric titration assay conducted with toluidine blue O (TBO), Figure 34. A known mass of dried SCPs was incubated in TBO titration solution at pH 10.5. The TBO dye binds to carboxylic groups, by Coulomb interactions, reducing the concentration of free TBO in the media. The difference in TBO concentration respecting the initial dye solution is correlated to the amount of CA groups:

$$D_{cg} = M_{cg} + m_{SCP} \tag{7}$$

where D_{cg} is the carboxylic group functionalization degree of SCPs, M_{cg} is the mole amount of carboxylic group on measured SCPs, m_{SCP} is the dry mass of SCPs.

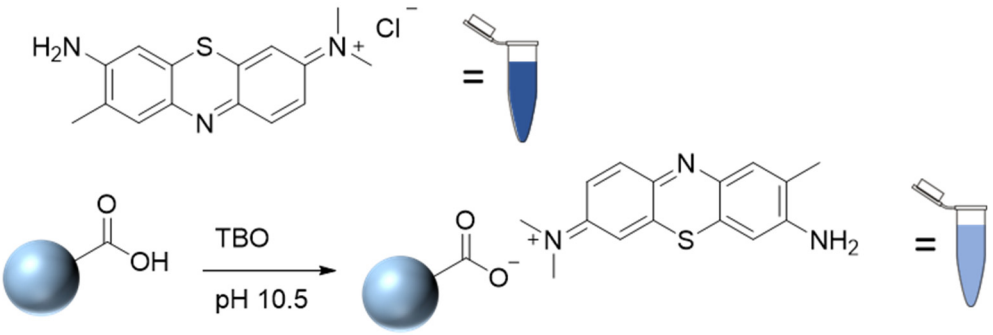

Figure 34- Schematic representation of the TBO test to determine the degree of functionalization of SCPs. The determination is based on the binding of TBO molecules to the carboxylic acid groups from crotonic acid grafting by Coulomb interactions, subsequently decreasing the blue solution coloring.

Elastic moduli determination via AFM. The elasticity of SCPs was measured through AFM indentation measurements, Figure 35. SCPs were swollen in LBB pH7.4 until equilibrium. A glass bead with a diameter of 4 - 5 µm was glued to a tipless AFM cantilever as indentation probe. The cantilever was approached and pressed onto the apex of the SCPs. Upon contact of the cantilever, the SCPs were mechanically deformed due to the applied force. The elastic moduli were calculated taking into account the cantilever spring constant and sensitivity through the Hertzian model.[161-162]

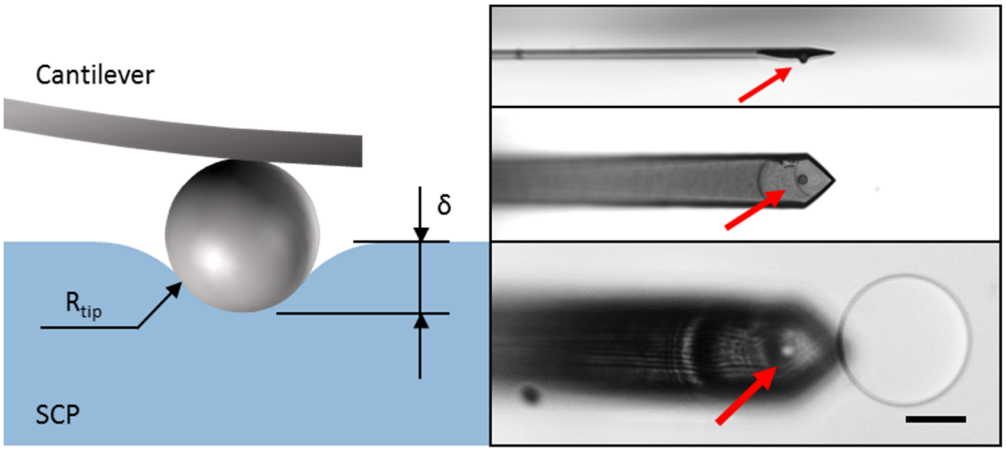

Figure 35- Principle of Young's modulus measurements via colloidal probe AFM indentation measurements with the Hertz model. The analysis is performed on crotonic acid functionalized PEG SCPs (CA-SCPs). Right) microscope images of the attached silica bead on a tipless cantilever (pointed with red arrows): side view (up), top view (middle) and top view focalizing on a close SCP (down). The scale bar is 25 µm and applies to all three images.

X-ray Photoelectron Spectroscopy analysis. The surface chemistry of the planar Con A surfaces on glass coverslips was tested means of XPS measurements. For physisorbed Con A, the successful functionalization with GLYMO is shown in section 3.1.1.3. The results for physical adsorption procedure can be seen in Figure 36. There was approximately 6% of nitrogen, which was introduced solely by lectins. This confirms the adequate surface functionalization by physical adsorption of Con A, Table 3. The ratio of the atomic composition cannot be used to correlate the surface thickness due to the non-quantitative profile depth of the technique. The high presence of oxygen and carbon was expected due to the physisorbed proteins, as well as, being the most common surface pollutants. The low lateral resolution does not allow using atomic references and determination of the degree of functionalization. Nevertheless, the XPS results so far indicate successful surface functionalization by physisorption.

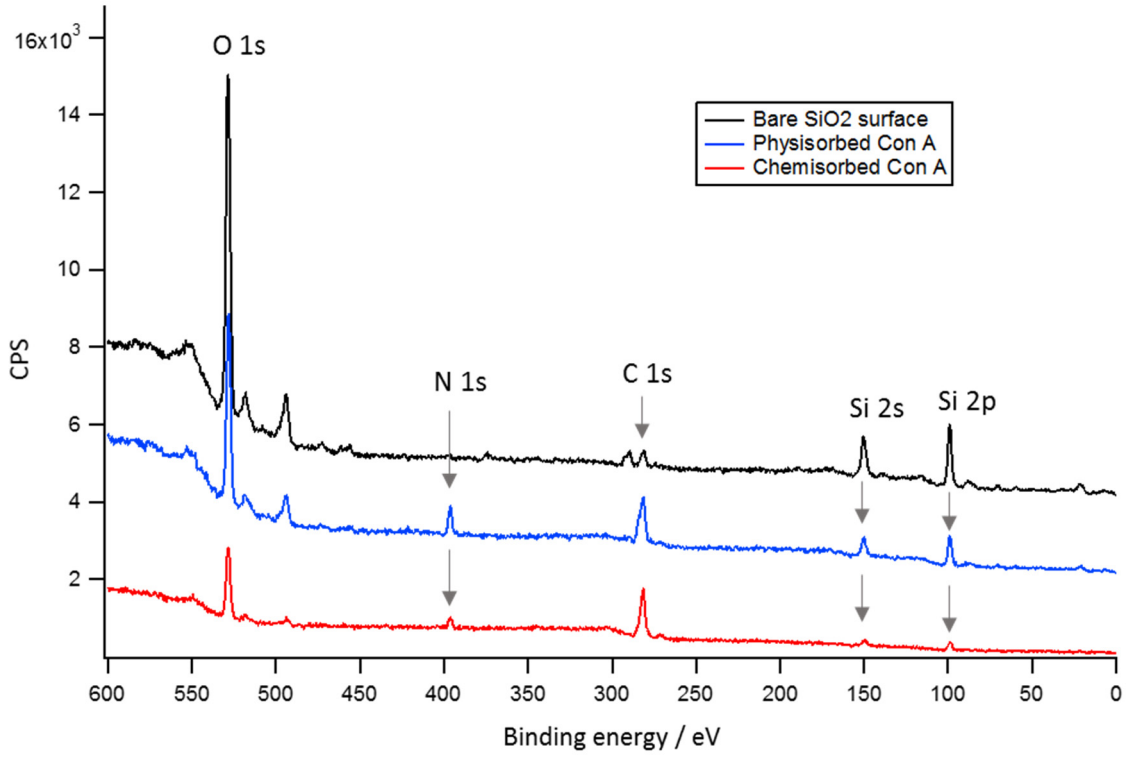

Figure 36- ESCA spectrum for Con A functionalized surface by physical adsorption (blue) and chemical adsorption (red). Glass surface was firstly immersed in a 0.05 mg/mL Con A solution in LBB pH 7.4. The N 1s signal proved the presence of linked lectins on the surface in comparison to a reference bare glass (black). Note that spectra have been rescaled in the y-axis bare physical adsorption +2000 CPS and bare glass surface +4000 CPS.

Table 3- Atomic composition of silicon surfaces with physically linked proteins. For comparison, the precentral ratio of the most sensitive orbitals are considered; being those with the greater electronic population

Signal	Position / eV	Area%
Si 2p	98.33	16.03
C 1s	280.39	44.45
N 1s	395.94	6.36
O 1s	527.48	33.15

The chemical linkage of Con A to GLYMO functionalized glass coverslips was already shown in sections 3.1.1.2 and 3.1.1.3 since similar Con A surfaces were used for AFM force spectroscopy. The XPS spectra of physisorbed and chemisorbed Con A appear similar as expected.

Testing the adhesive properties of Man-SCPs on unfunctionalized and Con A functionalized coverslips. Man-SCP adhesion was tested either on completely unfunctionalized glass surfaces as well as Con A functionalized surfaces to show specific binding successful surface preparation. Also, Man-SCP adhesion was studied in GLYMO functionalized surfaces to show the presence of

reactive groups. They upon contact on the flat surfaces the SCPs developed different contact areas depending on the surface chemistry. Overall, these variations proved the success of the subsequent surface chemistry reactions.

The SCP-adhesion experiments were performed with Man-SCPs of 139 µmoles/g and 79 KPa on IBIDI µ-well slides cleaned in an UV-ozone chamber in LBB pH 7.4. The Con A functionalized surfaces, both physically (P-ConA) and chemically (C-ConA) adsorbed, present greater values of adhesion energy than bare glass surfaces, due to the stronger binding through specific sugar-lectin interactions, Figure 37. On the other hand, this adhesion energy is smaller in comparison to the one on highly reactive GLYMO surfaces, which bind any nucleophile resulting in stronger covalent bonds. The adhesion energy variation between the two Con A functionalization kinds (P-ConA and C-ConA) could be due to different amounts of adsorbed protein as a result of a conformational re-organization[163] or an altered secondary structure[164] as well as to activity loss upon adsorption.[165-166]

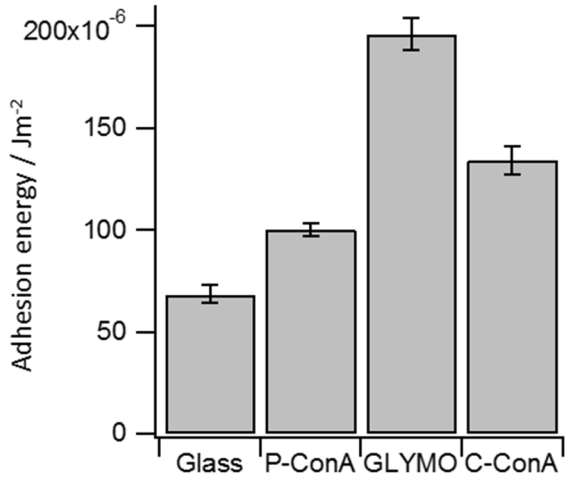

Figure 37- Adhesion energy of Man-SCPs on Con A-functionalized surface along different reaction steps. The smallest adhesion energy is presented for bare glass (Glass), which can bind Man-SCPs through hydrogen bonds, while bare GLYMO surface (GLYMO) can covalently link the probes resulting in the largest adhesion energies. The specific interaction that links the Man-SCPs on Con A functionalized surfaces is greater than H-bonds with bare glass but smaller than GLYMO covalent bonds. The adhesion energy difference between physisorbed (P-ConA) and chemisorbed (C-ConA) is presumably due to the different surface lectin density or activity.

The adequate activity of surface deposited Con A and Man-SCP specific binding. The activity of immobilized Con A lectins on coverslips was shown by the decrement in adhesion energy of Man-SCPs under inhibiting conditions. The inhibition of Con A coated surfaces, regarding adhesion energy decrement, simultaneously proves the correct functionalization of Man-SCPs. Previous results on chemically linked Con A on GLYMO surfaces can be seen in section 3.1.1.3, although a

complete study for physical and chemical Con A deposition approaches can be seen in terms of stability and activity in the upcoming section 3.1.1.3.

3.1.1.3 Lectin surface stability

The SCP-adhesion assay has already been introduced for determining the inhibitory potential of multivalent ligands.[97, 133] Here the SCP-adhesion is conducted with Man-SCPs of 45 µmoles/g and 136 KPa to characterize the robustness of the functionalized Con A glass surface, and overall, two handling procedures were analyzed to avoid hysteresis, surface damage and minimizing the sample expenses. The robustness of lectin surfaces directly affects the reproducibility of the method and the stability of surfaces to be repeatedly used.

The experiments to study the effect of buffer flushing steps to the adhesion energy on respectively physisorbed and chemisorbed approaches were performed on round 25 mm diameter glass coverslips in LBB pH 7.4, Figure 38. After the surface functionalization, the unreacted lectins were removed by brisk flushing with PBS and HEPES, both at pH7.4, and then adhered lectins were stabilized in the experimental LBB buffer prior the Man-SCP addition. The flushing step removing unreacted proteins was considered critical since adhered proteins could be either removed or denaturized on the surface. In order to demonstrate the possible flushing damage, surfaces were functionalized with Con A, and the adhesion energy to Man-SCPs determined. Then, a slightly aggressive LBB flushing step with a wash bottle followed by equilibration was performed before newly determine the adhesion energy. Series of this flushing procedure were steadily performed and the adhesion energy determined. In the very last step, a MeMan solution in LBB was used to equilibrate and inhibit by competition the Con A lectins to check whether their activity remained unaffected.

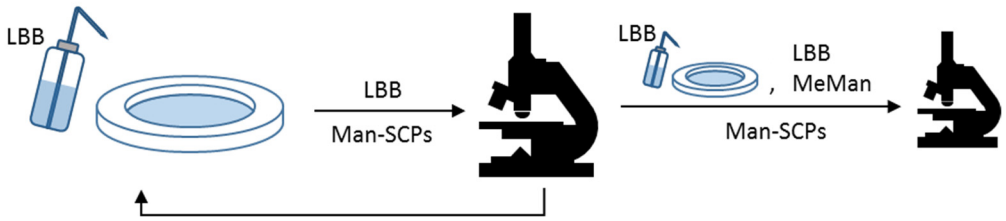

Figure 38- Representation of lectin surface robustness tests. Cyclic determination of adhesion energy in LBB after intense surface flushing with LBB before a final adhesion energy measurement under inhibiting conditions with MeMan.

On the physisorbed lectin surface, the adhesion energy with Man-SCPs decreases after each flushing event until achieving a plateau on where the adhesion energy remained constant, Figure 39. The Con A immobilized GLYMO surface shows constant adhesion energy since the first analysis, Figure 39. It should be noticed that the achieved final energy for physisorption equals

the initially expressed through the GLYMO protocol. This effect suggests the formation of a weak lectin multilayer for the physisorption method, which during the SCP incubation diffuses to the SCP contact edges enhancing the area, rendering greater adhesion energies. It is reported that proteins loosely bind at early stages increasing their affinity through time, affecting the desorption kinetics.[152]

Both physisorbed and chemisorbed surfaces showed an energy decrement while being fully inhibited for the final adhesion measurement, consequently proving their specific activity. In comparison to GLYMO protocol, the physical adsorption of Con A has a smaller decrement in adhesion energy for the inhibiting step. Since both experimental setups remained constant, the smaller adhesion energy is attributed to the flushing step, either removing or producing surface Con A denaturation. Strong flushing could stack proteins until their denaturation, exposing the hydrophobic internal groups[167], resulting in SCP smaller adhesions or even repulsion.

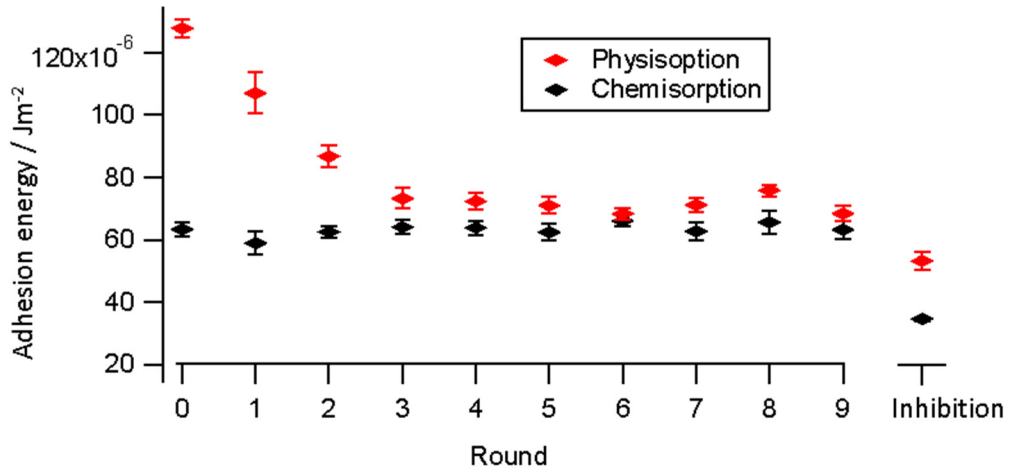

Figure 39- Effect of flushing steps in adhesion energy between Man-SCPs and Con A functionalized surfaces, both by physisorption and chemisorption. The inhibition is performed with 10 mM methyl-mannose.

Adhesion energy decrement under inhibitory conditions proves the lectin surface presence and adequate activity. The variations in adhesion energy of the SCPs while flushing the protein surface remarks the different robustness of the process. About section 3.1.1.3, the presence of GLYMO coating of glass is also proven.

3.1.1.4 SCP-adhesion handling

SCP handling is related to the technical requirements and availabilities of samples. Reducing sample quantity promotes SCP-adhesion to be included as routine analysis. An experimental approach to preserve SCPs is by decreasing the liquid volume. Also, SCPs could be reused to reduce their consumption, i.e., SCPs can be removed from the surface applying a shear force which can be exerted, for instance creating a parallel flow to the surface by pipetting. It will also

help to mix the media readjusting the conditions simultaneously when the inhibitor concentration is varied. It is then necessary to check the solidity of SCPs and their behavior while handling to respond fast and unequivocal to the new media conditions. On a first approach, SCPs can be *pushed* to the edges of the well, for fresh SCPs to be added, Figure 40. A second approach is *shaking* the SCPs, not directing them to the sides but the whole area, for them to newly precipitate, Figure 40. Both approaches were undertaken in LBB pH 7.4 with Man-SCP of 45 µmoles/g and 136 KPa and Con A functionalized surfaces with the physical (physisorption) and chemical (GLYMO) lectin adsorption protocols.

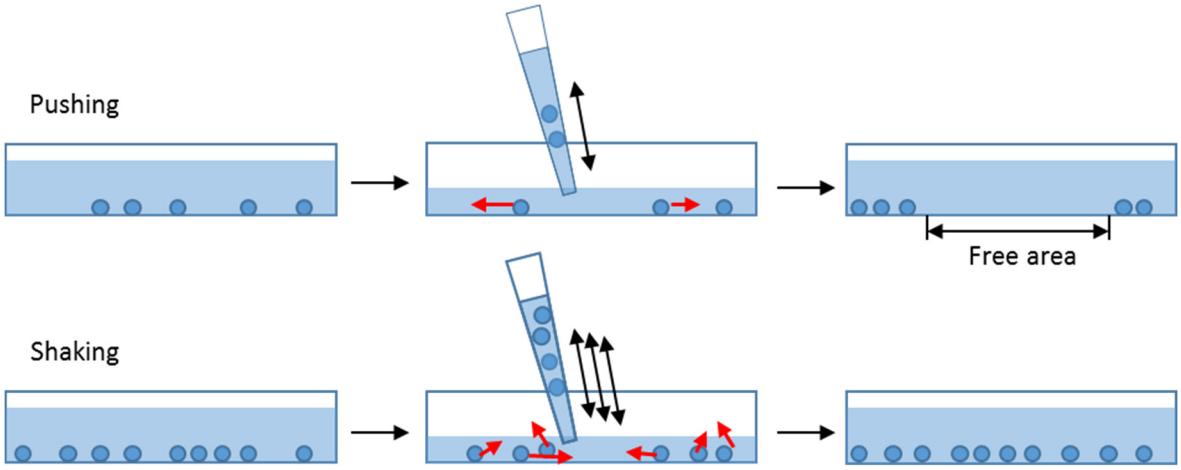

Figure 40- Schematic representation of proposed mechanisms to handle SCPs and reuse the surfaces. Through the "pushing" approach flow shear forces are applied with pippeting the media to bring the SCPs to the surface edge and have a free area for new SCPs to precipitate. The "shaking" approach removes the adhered SCPs through a more intense pippeting for them to re-precipitate over the whole surface; also reusing the SCPs.

Cyclic steps of *pushing* the SCPs away from the observed area simply reproduce the already described effect of surface flushing, Figure 41. Together, the additional drawback of slowly saturating the surface with SCPs, which will turn in hardening their identification, is presented. Thoroughly *shaking* the solution looking forward SCPs to respond to the new conditions before re-precipitation presents the negative effect of distorted adhesion areas for some SCPs, and so their adhesion energy, Figure 42. SCPs are elastic entities that may suffer from hysteresis. Enlarged contacts are attributed to the result of the exerted forces on the SCPs derived from the media shaken. Subsequently, shaken SCPs were compressed on the surface leading to enlarged contact areas. It was confirmed finding reproducible values while repeating the procedure under inhibiting conditions. The constant adhesion energies under inhibition media prevent compressed SCPs to develop larger contacts, from specific Man-Con A interaction. The shaking approach was only performed on lectin functionalized surfaces by physisorption presuming the same unreliable behavior on the covalently functionalized one.

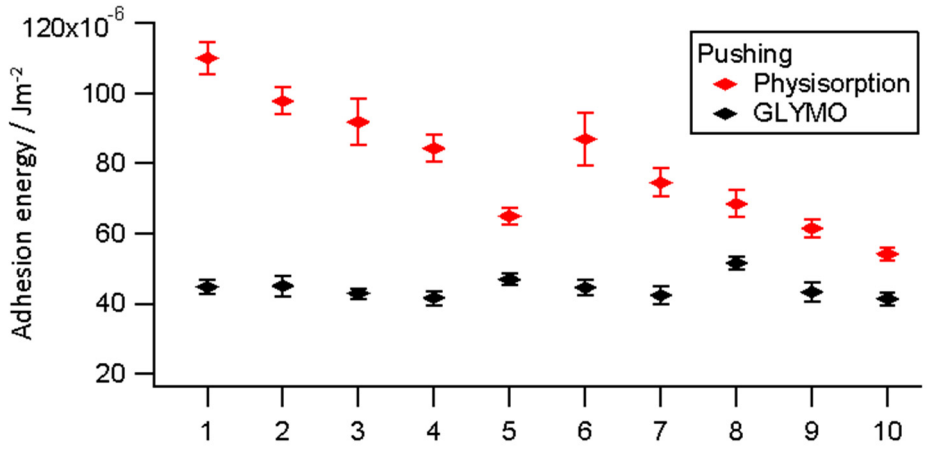

Figure 41- Effect of adhesion energy for fresh Man-SCPs on Con A functionalized surfaces after "pushing" previous SCPs away from the observed area.

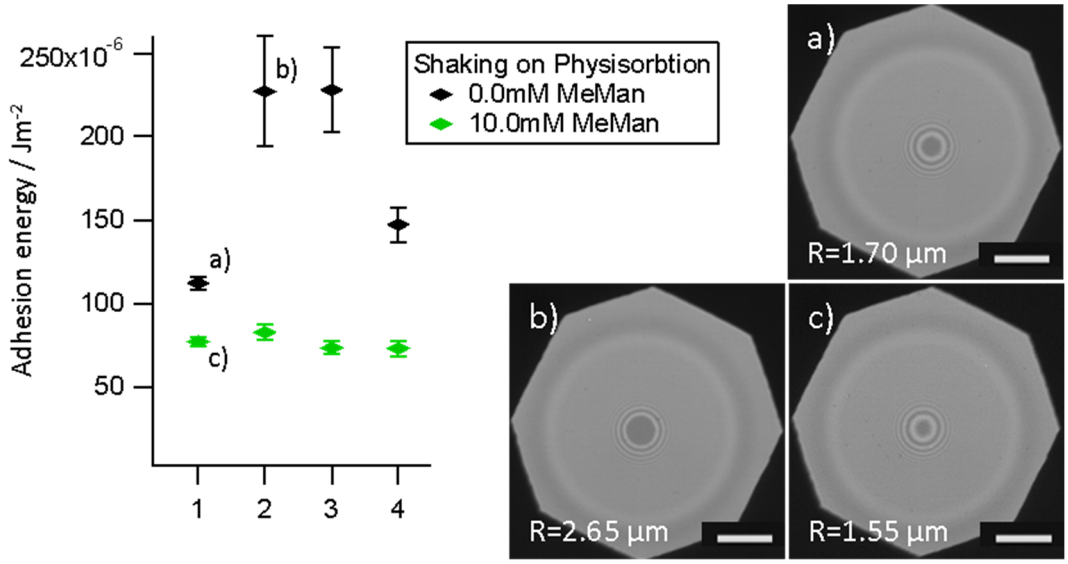

Figure 42- Effect of adhesion energy for thoroughly mixed and re-precipitated Man-SCPs on physisorbed Con A surfaces. Distorted adhesion energy appears in the first round. Confocal RICM images for non-inhibiting conditions round 1 (a) and round 2 (b), round 1 (c). For better comparison Images track SCPs of the same size. The adhesion area corresponds to the dark central spot, which radii are indicated. All three scale bars are 10 µm.

The elastic nature of SCPs and the fragility of protein-functionalized surfaces can lead to unreliable adhesion values. To this point, there is not an optimal procedure to reuse either SCPs or surfaces. as well, inhibiting conditions

Therefore the best approach to improve the yield of functionalizing molecules is by decreasing the size of wells. Concerning the surface functionalization, physical absorption of lectins presents weaker reliability than covalent functionalization.

3.1.2 Macroscopic scale – Coverslips for sugar presentation

Macroscopic scale functionalized objects in the context of this work could relate to tissues, organs, and implants but sugar surface functionalization finds much more applications with glycoarrays in the field of biology. With them, immobilized molecules can simultaneously and with high-performance be analyzed. In these arrays among other applications, glycans can be organized to form clustered saccharide patches (CSPs) in order to study their multivalent interaction to proteins.[168] The most common detection method of carbohydrate arrays relies on fluorescence despite their self-drawbacks like sensitivity to light[169] and the easy oxidative degradation.[170] Therefore carbohydrate functionalized surfaces could study the adhesion energies with receptor-functionalized SCPs. This approach presents two main advantages over the SCP-adhesion method introduced earlier where the carbohydrates were presented on the SCPs whereas the receptors were presented on the surface: 1) in the "inverted" SCP assays the lectins are presented on the SCPs which means, that the proteins are more mobile and in a highly hydrated surrounding, which ensures more biocompatible protein presentation. That will reduce the odds of protein conformational changes due to be supported on a more polar substrate with lower surface tension than the glass coverslips[171], subsequently preventing from activity lost.[152] 2) Functionalization of SCPs with proteins (the expensive component) is more profitable since less protein sample is consumed, resulting in a larger number of measurements when compared to functionalizing glass slides.

The altered presentation of carbohydrates to be on the glass surface may help to control some parameters like density and packing. Intuitively, flat planar surfaces can present greater number and packing of epitopes than convex curved surfaces such as SCPs. Therefore, a flat surface helps to control the monolayer density and study its affinity. It also allows faster synthesis and functionalization by decreasing the washing step timing; as solid phase synthesis does.

In the present section, carbohydrate functionalized glass coverslips are presented, and the effect of ligand density by "diluting" the surface with non-binding molecules is studied. The ligand flexibility is controlled tethering ligands through different length linkers. The resulting sugar coated surfaces are analyzed using SCP-adhesion, using Con A functionalized probes.

3.1.2.1 Synthesis and characterization of carbohydrate surfaces and Con A-SCPs

Carbohydrate surface functionalization. The chemical procedure to functionalize surfaces with sugar molecules is similar to the used approach for AFM tip and neoglycoproteins as it employs a heterobifunctional linker containing succinimide- and maleimide-terminal groups. Firstly, the glass bottom microplates were cleaned from interfering organic pollutants by oxidation in UV ozone-chamber. Then, the coverslips were coated and annealed with (3-aminopropyl) triethoxysilane

(APTES) introducing primary amine groups to which heterobifunctional linkers containing a reactive *N*-hydroxysuccinimide (NHS) ester can subsequently be coupled. To vary the flexibility of the ligand surface, SMCC and PEG heterobifunctional linkers (contour lengths ~0.9 nm and ~80 nm[147] respectively) were used. Besides the NHS ester group, the linkers contain a terminal maleimide group which can be used for functionalization with thiol molecules. Mannose thiol (ManSH) was used to functionalize the surfaces, and the surface density was controlled by adding other non-binding small thiol molecules, Dithiothreitol or 2-Mercaptoethanol, effectively diluting the ManSH density. See the schematic approach in section 3.1.1.1, Figure 15.

Carbohydrate surface characterization was performed using XPS and SCP-adhesion along the synthesis steps. XPS determined the presence of sulfur proving the linkage of carbohydrate moieties; meanwhile, SCP-adhesion determined the adhesive forces between the synthetic surface functionalization steps and SCPs, which, depending on the exposed surface functional groups, indicates the success of the reaction. Both techniques and their results were previously introduced in section 3.1.1.3 while characterizing ligand AFM tip functionalization and remain applicable in the present section.

SCP functionalization with Con A. Con A-SCPs of 47 µmoles/g and 30 KPa were obtained by functionalizing CA-SCPs and used to adhere on sugar-coated surfaces. The synthesis and characterization of CA-SCPs were previously described in sections 3.1.1.1 and 3.1.1.2. The functionalization of CA-SCPs with Con A firstly proceeded to activate the SCP crotonic acid groups in an MES pH 5.5 buffered solution containing *N*-Hydroxysuccinimide (NHS) and 1-Ethyl-3-(3-dimethylaminopropyl) carbodiimide (EDC). Then, the unreacted products were removed centrifuging, and the SCP pellet was reacted with an excess of Con A in phosphate buffer pH 8.0, Figure 43. The covalent linkage of Con A happens through nucleophilic groups such as amines, which are presented in lysine amino acids among others. The untethered proteins were carefully washed with PBS pH 7.4. SCPs were transferred into water, then HEPES (10 mM) pH 7.4 and finally LBB pH 7.4 to avoid precipitation of phosphate salts of calcium. An aliquot of SCPs was split to be dispersed in 10 mM MeMan in LBB for inhibition assays (inhibited SCPs).

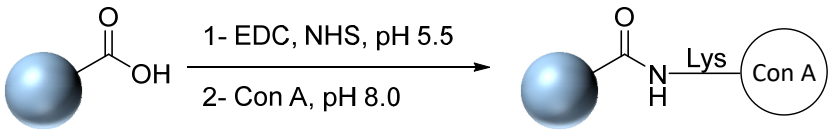

Figure 43- Scheme of SCP functionalization with Con A. The crotonic acid groups are activated at pH 5.5, meanwhile the reaction with Con A at pH 8. The reaction proceeds through nucleophiles, such as amines presented in lysine amino acids.

The adequate synthesis of Con A-SCPs was tested regarding adhesion energy on sugar surfaces. The activity of lectins was determined by observing the reduction in adhesion energy under lectin inhibitory conditions, i.e., the addition of MeMan. Both are seen in the following section.

3.1.2.2 Carbohydrate surface density

The ligand density on the surface is controlled by varying the ratio of ManSH and 2-mercaptoethanol. Four microplate wells were functionalized with 100%, 50%, 25% and 0% of ManSH through short SMCC and long PEG heterobifunctional linkers (see structures in Figure 25) and all wells filled with the same amount of LBB. Con A functionalized SCPs were added into the wells, and the adhesion energy was determined after equilibration. To measure the specificity of adhesion, the wells were then flushed with water and equilibrated in 10 mM MeMan in LBB as inhibiting media. Then, inhibited SCPs (dispersed in 10 mM MeMan in LBB) were added, and the adhesion energy was newly determined, Figure 44.

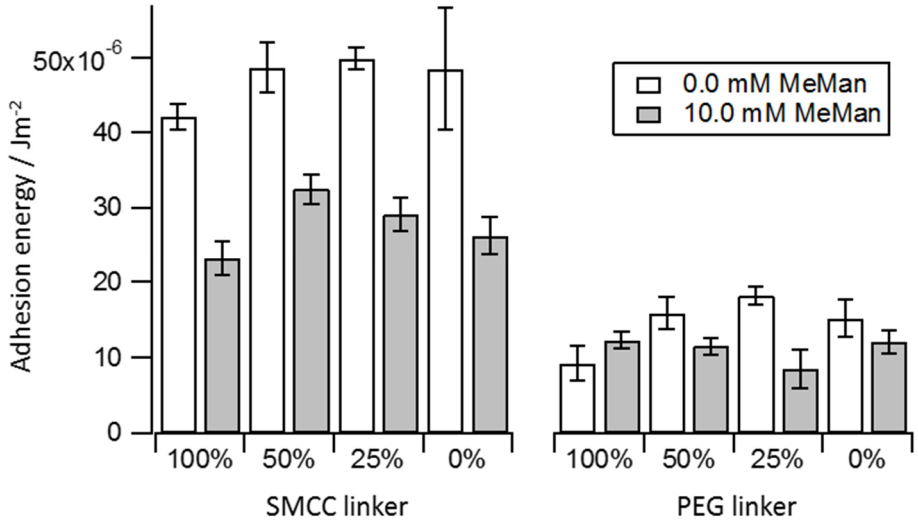

Figure 44- Adhesion energy of Con A functionalized SCPs on sugar functionalized surfaces with the indicated linker and density of mannose diluted with 2-mercaptoethanol.

The adhesion energy of Con A-SCPs on carbohydrate surfaces greatly depends on the linker length, Figure 44. The short SMCC linker presents greater adhesion energies than the long PEG linker, which is attributed to the steric repulsion and hydrophilicity of as well as self-hindrance of the bulky linker chains.

Independently of the used linker to tether the carbohydrate moieties on the surface, it can be seen that decrements in sugar density do not correspond to lower adhesions, but larger ones. It can be attributed to high sugar surface densities presenting closer packing of the ligands, subsequently hindering the SCPs to adhere. That will result in a threshold surface density at which

SCPs can exert the greatest adhesion. Ligand-free surfaces present higher adhesion energies in comparison to fully Man-presenting ones. Therefore, the adhesion of Con A functionalized SCPs could be attributed to non-specific interactions mainly compared to specific Man-Con A binding.

Inhibitory media decreases the adhesion energy of Con A-SCPs on Man-coated surfaces, except surfaces with 100% Man through PEG linker. Nevertheless, the activity of Con A functionalized SCPs is not fully proven since adhesion energy decrements are also present on Man-free surfaces. Although the adhesion between Con A-SCPs and Man-surfaces may not only be mediated by specific interactions, the addition of MeMan should not reduce the adhesion on sugar-free surfaces unless it affects, reducing, the non-specific interactions. This may happen whether Con A turns more hydrophilic upon MeMan binding, disfavoring surface adsorption.

3.1.2.3 Long-term binding kinetics

The final contribution of non-specific interactions can be thought to be dependent on the random conformation of the surface-bound sugars. Possibly a long-term kinetic study will help to reveal their effect on the adhesion energy. It is expected that the conformational character of surface-bound sugars is prone to long-term changes while binding to SCPs, subsequently adhering with greater energies.

Tracking the adhesion energy of Con A-SCPs over longer times on sugar functionalized glass surfaces with the short linker and varying the sugar density with Dithiothreitol revealed the time dependence of non-specific contributions, Figure 45. Images of the SCPs were tracked at 60, 120 and 600 min after SCP addition. Studies on sugar surfaces tethered through the long linker were assumed to follow the same trend presenting lower energies and slower kinetics.

Again, the adhesion energy of fully sugar-functionalized surface is the lowest. Interestingly, its adhesion energy remains constant in time. All the other surface functionalization densities shift in adhesion over time. This effect could be related to the stronger adhesion energy acting on the SCP. A stronger adhesion leads to a larger deformation of the SCPs, which could result in time-dependent changes of adhesion. Also, adhesion energy changes can presumably be a result from denaturation of Con A while facing a more hydrophobic surface. On the other hand, inhibiting conditions decreased the adhesion energy of SCPs on every surface, also showing changes along time, but for 50% sugar surface.

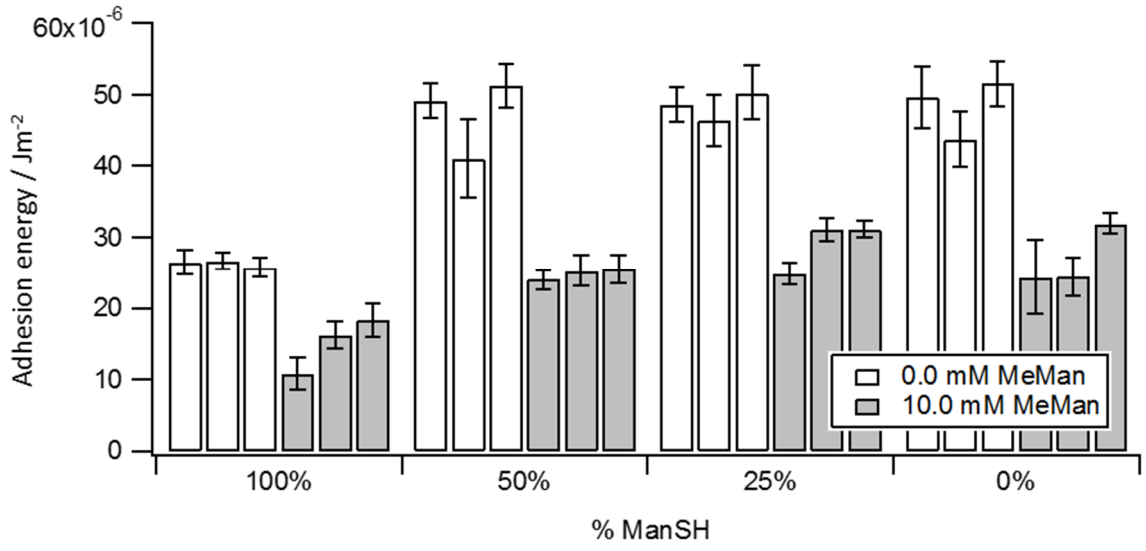

Figure 45- Adhesion energy of Con A-SCPs on sugar functionalized surfaces with the short linker (SMCC) in LBB. The indicated density of mannose is achieved by dilution with Dithiothreitol. Note that bars are grouped in three corresponding to the adhesion energy at 60, 120 and 600 min of the SCP addition.

The variation in adhesion energy under inhibition could be attributed to two processes. A first one presented in 100% sugar surfaces, in which the high density prevails to the starting inhibition. A second one observed for 25% and 0% sugar surfaces, in which non-specific interactions and protein denaturation lead to the adhesive process.

As a control to prove the non-specific contribution to the SCP adhesion energy, the sugar-lectin interaction was tested on the same surface kind after a sugar post modification. The surfaces tethering ligands through the short linker and varying the sugar density were incubated with acetic anhydride. Therefore, sugar hydroxyl groups were acetylated leading to a different structure, preventing the sugars to specifically bind to the lectin binding pockets; precluding the specificity of the binding. In addition, the surfaces become much more hydrophobic using acetylation. The result was that the adhesion energy grew over time for every surface and inhibiting media, which might indicate protein denaturation due to the increased adhesion, Figure 46.

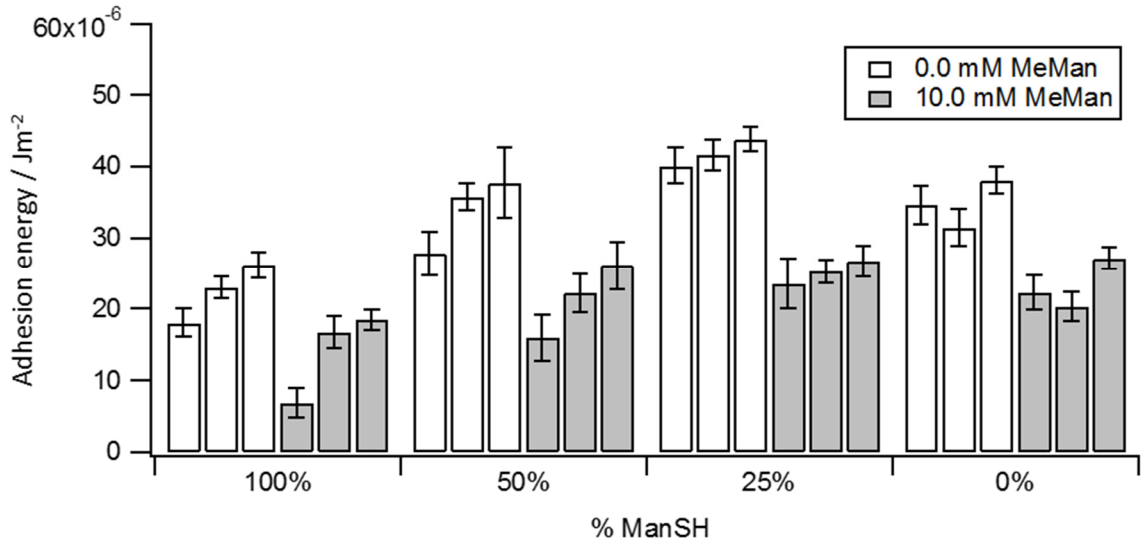

Figure 46- Adhesion energy of Con A-SCPs on sugar functionalized surfaces with the short linker (SMCC) in LBB. The indicated density of mannose is achieved by dilution with Dithiothreitol. Sugar surface residues are acetylated after tethering. Note that bars are grouped in three corresponding to the adhesion energy at 60, 120 and 600 min of the SCP addition.

For acetylated surfaces, the variation in adhesion energy under inhibition could be attributed to protein denaturation due to the hydrophobic of the surfaces. Since hydrophobicity is increased through the sugar moieties, greater densities lead to higher adhesion increments.

Overall the results suggest that Con A on the SCPs is prone to strong adhesion by non-specific interactions, which might be caused by proteins denaturation exposing cryptic binding sites that increase adhesion over time. Interestingly, the addition of carbohydrates renders the interaction lower, which could be a result of Con A stabilization upon sugar binding or sugars rendering the protein more hydrophilic and therefore reduce non-specific binding. In order to avoid the contribution of non-specific interactions, the glass surfaces must be fully functionalized with carbohydrate solutions. Therefore, the surface ligand density cannot be controlled to lower but greater densities, by coupling molecules containing greater amounts of sugar moieties. Further analysis and experimentation can be done towards determining the effect of non-specific interaction while inhibiting, but at this point, it is not conclusive.

3.2 MULTIVALENT ACTIVITY AS A FUNCTION OF SCALE DOMAIN AND ITS INFLUENCES

Techniques to study the specific interaction of carbohydrate ligands with lectins at different scales have been presented so far. It has been already seen that affinity depends on properties such as ligand flexibility but also other parameters such as quantity and density of epitopes. The objective of the present section is to study the multivalent binding mechanism along the four scale sizes while altering the carbohydrate density and valency as well as ligand flexibility. Man residues and a defined spacing between them are introduced in a series of precision oligomeric and polymeric scaffolds during respectively their sequence-defined and sequence-controlled synthesis.

3.2.1 Synthesis and structure of precision multivalent ligands – oligomers and polymers

Four so-called precision oligomers presenting Man units were investigated in this work, Figure 47. The synthesis of glycooligomers **O1**, **O2**, **O3** and **O5** with a defined amount of Man moieties (1, 2, 3 and 5) as well as a defined spacing between the carbohydrate ligands was achieved using solid phase synthesis (SPS). The approach of using SPS to synthesize sequence-defined glycomimetics was developed in the group of Prof. Hartmann[172] and is based on solid phase peptide synthesis firstly introduced by Merrifield in 1963.[56] Instead of amino acids, an iterative coupling of tailor-made building blocks with different chemical and physical properties is performed on a solid support. Similar to amino acids used in SPS, all building blocks contain a Fmoc-protected amine and a free carboxylic acid group. In brief, the alkyne group containing building block TDS is used to couple azide functionalized sugar moieties onto the oligomeric scaffold by copper-mediated azide-alkyne cycloaddition (CuAAC) and the hydrophilic building block EDS is used to achieve a specific spacing between the sugars moieties (Figure 47). Glycopolymers **P1**, **P2**, **P3** and **P5** are sequence-controlled multiblock copolymers with two strictly alternating blocks, one Man bearing binding block and one hydrophilic spacing block.[173] The binding block of a glycopolymer has the same sequence as its oligomeric macromonomer (**O1**, **O2**, **O3,** and **O5**) which is then incorporated four times in total within the polymer sequence. Their synthesis was achieved by generating macromonomers containing reactive end-groups using SPS which were subsequently copolymerized in a step-growth fashion using thiol-ene click chemistry.[173] Therefore, the glycomacromonomers, which later form the binding block in the polymer, were synthesized with two terminal alkene moieties introducing two DDS building blocks, whereas the spacing macromonomers were equipped with two terminal thiol groups by introducing the amino acid L-cysteine twice (Figure 47).

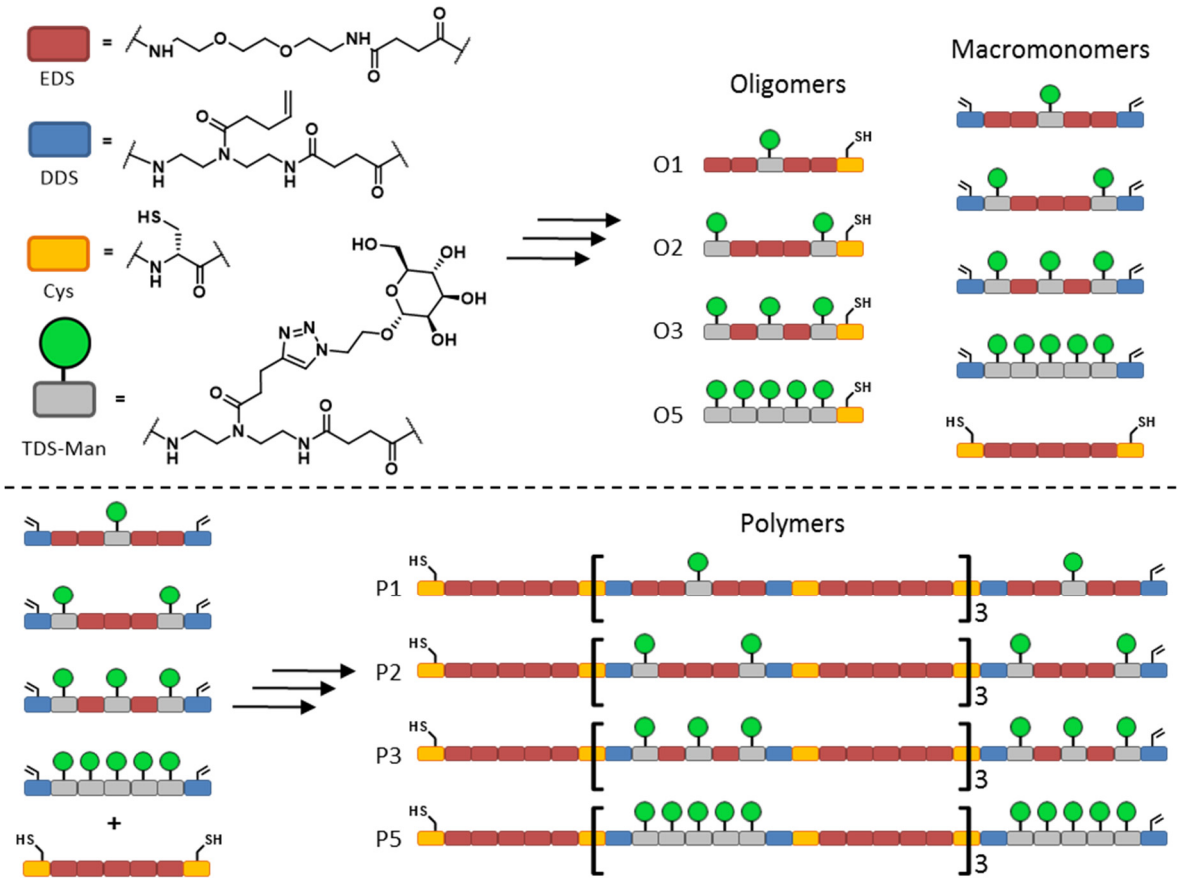

Figure 47- Sequence defined oligomers carrying 1, 2 3 and 5 mannose residues (respectively O1, O2, O3 and O5) and the corresponding polymers (respectively P1, P2, P3 and P5) made repeating 4 times the oligomers while spacing them.

3.2.1.1 Hydrodynamic radius of sequence controlled multivalent oligomer and polymer ligands

The sugar spacing within oligomers was achieved by altering the sugar carrying TDS with the spacing EDS building blocks during their synthesis. As well, TDS and EDS building blocks differ in their contour lengths producing shorter oligomers and polymers while increasing the sugar content, Figure 48. The contour length and the sugar spacing of ligands were theoretically calculated as described in literature[172], what for oligomers, unlike for polymers, were not enough to simultaneously bind two binding pockets of the same Con A (~72 Å).

The molecular conformation in solution was expected to be coiled due to the polyamide nature of the ligand backbones that can lead to intramolecular H-bonds holding a closed conformation. The hydrodynamic radius of the samples in solution was determined using dynamic light scattering (DLS), Table 4.

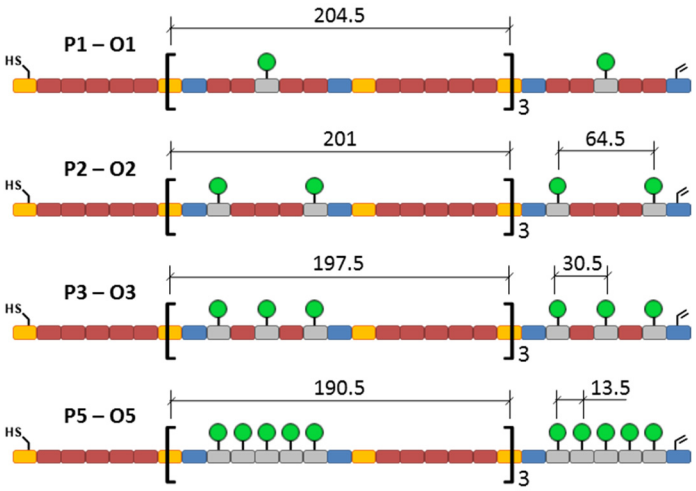

Figure 48-. Scheme of the primary structure and relative distances of oligomer and polymer samples. Note that the sugar spacing within oligomers is also found in polymer samples. The spacing between consecutive mannose moieties within oligomers was achieved during the sequence control synthesis and resulted in shorter polymer repeating units, and so polymer length while increasing the sugar amount. Scheme is not scaled. Distances are expressed in angstroms.

As expected, the contour length decrement for oligomers carrying a greater number of Man moieties resulted in smaller coiled structures, Table 4. On the other hand, the variations in contour length among the polymers are not presumed to significantly alter the hydrodynamic radii, but the number of Man moieties, which can hamper the intramolecular H-bonding, leading to less compacted coils while increasing the valency, Table 4.

*Table 4- Determined hydrodynamic radius (Rh) and polydispersity (PDI) of oligomer and polymer samples by DLS, together with the theoretical weight average (Mw) and number average (Mn) molecular weights, polydispersity (Mw/Mn), and contour length (CL). *The degree of polymerization for DLS measurements was 8 for all oligomer and polymer samples, but for P2 and P3 that was 7.*

Ligand	Rh / nm	PDI	Mw / Da	Mn / Da	Mw/Mn	CL / nm
O1	1.8	0.27	1598	1598	1.00	8.6
O2	1.7	0.23	1881	1881	1.00	8.3
O3	1.5	0.28	2166	2166	1.00	7.9
O5	1.4	0.28	2735	2735	1.00	7.3
P1	5.8	0.33	25000	13400	1.87	84.2
P2	7.0*	0.60*	27700/33900*	14800	1.87/2.4*	83.0
P3	5.8*	0.32*	29700/24700*	16600	1.80/1.9*	81.4
P5	7.0	0.5	30800	17500	1.76	79.0

3.2.2 Single molecule multivalent ligands – SM-AFM Rupture force

To study the multivalent binding of carbohydrate ligands by means of SM-AFM, the tips were functionalized with the multivalent oligomers and polymers through the thiol group. As previously

described in section 3.1.1.1, the tip surface was firstly coated with APTES introducing amino groups on where a heterobifunctional PEG linker reacts on its succinimide group. The incorporation of the ligands happened through the linker exposed maleimide end group on where the thiol functional group of the ligand reacts. In order to minimize the sample presentation and more easily reach the single-molecule range, the ligand solution was reacted in dilution with 2,2'-(ethylenedioxy)diethanethiol whose thiol groups compete for the maleimide groups of the linker. The SM-AFM analysis of multivalent carbohydrate samples was performed facing the functionalized cantilever tips to Con A functionalized flat coverslip (n=512 oligomers and 1024 polymers) in LBB pH 7.4. The experimental media, device settings, and data treatment remained constant for all the samples. The rupture events were solely evaluated from force-distance curves fulfilling the baseline and single-molecule criteria, as described in section 3.1.1.4. Subsequently, these events were correlated to the specific interaction on Con A of multivalent Man molecules, later confirmed by comparison with reported values in literature.

3.2.2.1 The frequency of binding events in approach-retract cycles

The obtained frequency of force-curves containing single molecule binding events is greater for the oligomers than for the polymer samples, Figure 49. This fact is attributed to the molecular weight and steric repulsion, which are greater for polymer ligands.

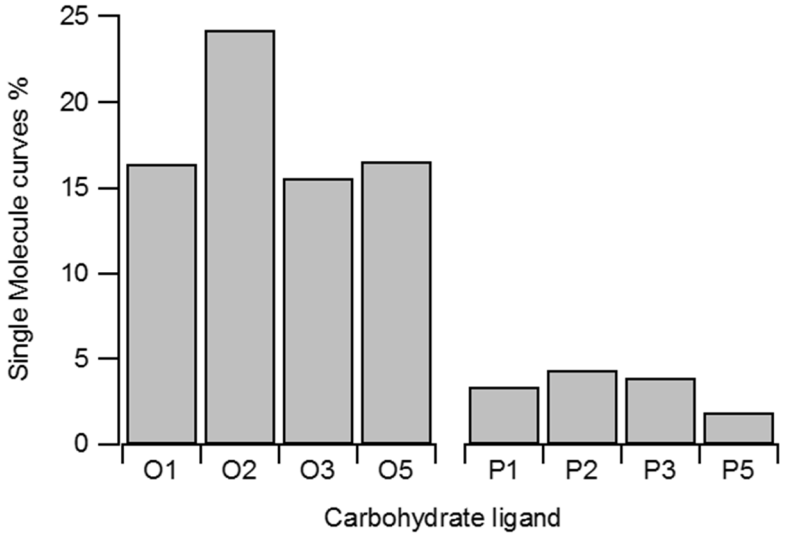

Figure 49- Frequency of "Single Molecule" curves expressed as a percentage for oligomers (n=512) and polymers (n=1024) Man ligands. The Single Molecule curves are those reaching the baseline before rupture events presented after 50 nm.

The bigger molecular weight of the polymers and the longer contour lengths result in bigger hydrodynamic radii; being these last supported by the DLS measurements, Table 4. Longer lengths result in greater steric repulsion preventing from binding. In addition, there are greater chances

for Man moieties to be buried inside bigger coiled structures precluding from binding, Figure 50. As well, oligomer ligands lack of the spacing macromonomers which are less hydrophilic, therefore, the sugar exposure is favored regarding size and hydrophobicity.

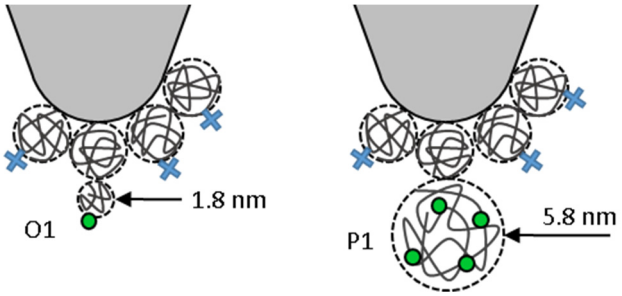

Figure 50- Scheme of the functionalized AFM tips displaying the hydrodynamic radius of the linker and ligand molecules: left) the oligomer O1, right) the polymer P1. The bigger hydrodynamic radius of polymers reduce the chances to expose the mannose moieties (green dots) to face the substrate (not represented) resulting in a less frequent Man-Con A binding events.

Every ligand, regardless of being polymeric or oligomeric, presents in average one or two rupture events per curve, Figure 51. This might be surprising given the large contour length of the polymeric ligands (~80 nm). Namely because the hydrodynamic radius of the polymers matches the spacing of two Con A binding sites making it unlikely that there are not more than two binding events in a single force curve. Electron spin resonance equipped ligand showed that they could stretch when contacting the receptor in order to bind to two binding sites simultaneously.[174] In this case, probably too short contact times of the tip on the receptor surface were used for the ligand to stretch to the binding sites.

On the other hand, a more plausible explanation arises from the ligand composition. The ligand sequences were grown by means of amide bonds, which can lead to intramolecular H-bonds within the polyamide coiled structures. Whether the polymer internal forces are great, the coiled configuration may be preferred over the spreading, subsequently resulting in the few tracked steps per curve.

The frequency of steps per curve for the monovalent oligomer **O1** differs from one, suggesting, at first sight, the presence of more than a single molecule appearing in the force curves. If that is the case and due to be a monovalent ligand, it does not constrain the analysis as will be seen in the following paragraphs.

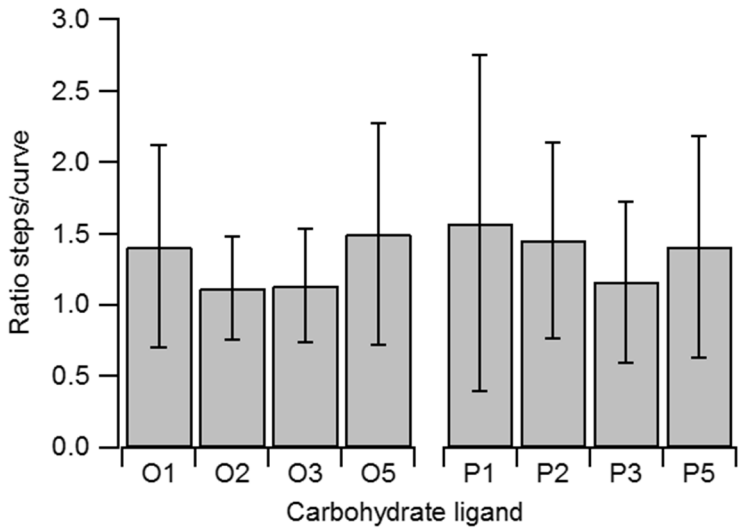

Figure 51- Frequency of rupture events in "Single Molecule" curves for oligomer and polymer carbohydrate ligands.

3.2.2.2 Rupture position histograms

In addition, the position of events and the rupture force were compiled in histograms for comparison. All the histograms present the main position contribution, encompassing the bulk of the rupture events, Figure 52, at small distances after the linker length (threshold point), which for both oligomers and polymers is comparable in length. The upper tail of the distribution (at greater distance positions) decays before the 100 nm, presenting very few rupture events above. This indicates that oligomers and polymers form compact coils that do not open upon forced detachment when retracting the cantilever. This is supported by DLS experiments, where it was shown that the ligand adopts a preferable coiled structure in solution, differing from the extended presentation during the rupture. Supposing that coils open, the ligand and linker are supposed to newly coil together after rupture resulting every time in a random configuration, which subsequently broads the distribution for rupture positions in the histograms. Therefore, the distance in force curves with more than one step, together with the low frequency of these, cannot be correlated to sample carbohydrate spacing.

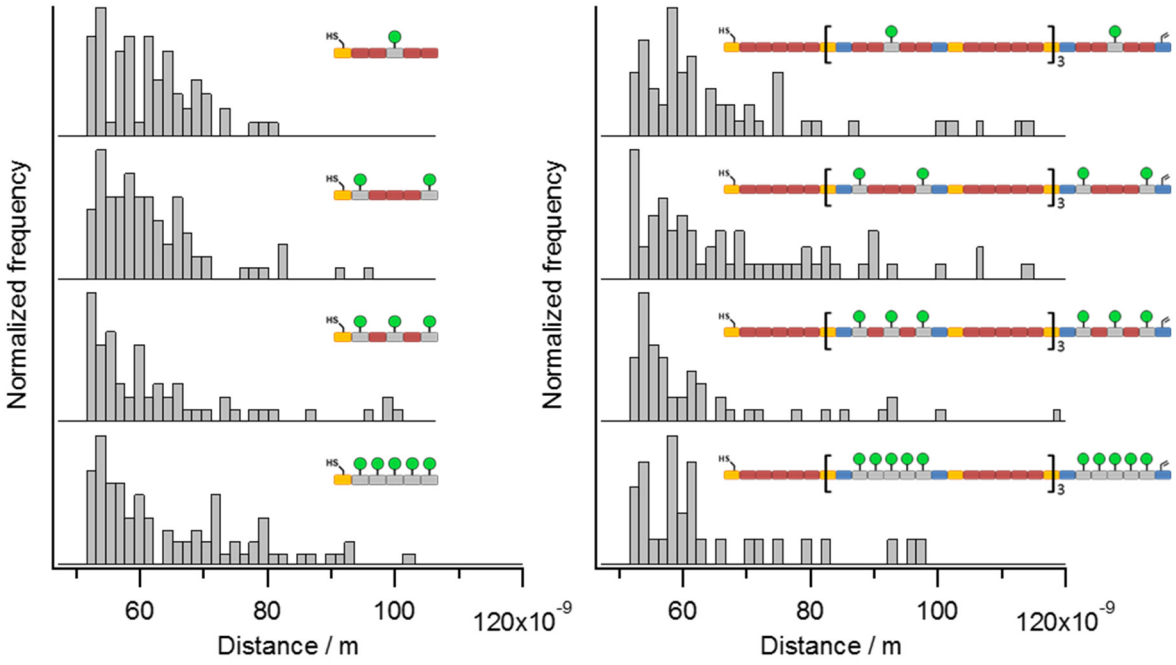

Figure 52- Histograms of the rupture event positions for the oligomer and polymer carbohydrate ligands. Bins 1.5 nm.

3.2.2.3 Rupture force histograms

The force histograms show a shift to higher energies while increasing the Man quantity, Figure 53. It can be seen through the modal bin of the histograms, and so the distribution, that gradually shifts to higher forces while increasing the sugar content of the ligand. For **O1** and **O2** the modal bin lies at ~50 pN, and meanwhile, the surrounding bins are almost equal in frequency for **O1**, for **O2** is more frequent the higher force one. The modal bin for **O3** and **O5** are greatly shifted. This is an indication of a secondary contribution to the ligand binding like the subsite binding and statistical rebinding; this last also called *bind and slide*.[50] Note that for all ligands, the contribution at ~50 pN remains with high frequency and it is attributed to the simple Man-Con A rupture. The shift in the rupture force can be correlated to the sugar quantity (valence) since all of the multivalent samples present a shift to higher forces in the distribution in comparison to **O1**. Therefore, the greater sugar amount, the higher shift. As well, it can be correlated to the sugar density (spacing) because the greater the valence is, the smaller sugar spacing. Therefore, the shift in force can be either attributed to the subsite binding and statistical recombination because intuitively both are affected by the quantity and spacing of sugar moieties. Subsite binding appears as a more plausible contribution considering the coiled configuration of the ligand and the experimental setup, in which the ligands are fast retracted from the surface making the statistical rebinding very unlikely.

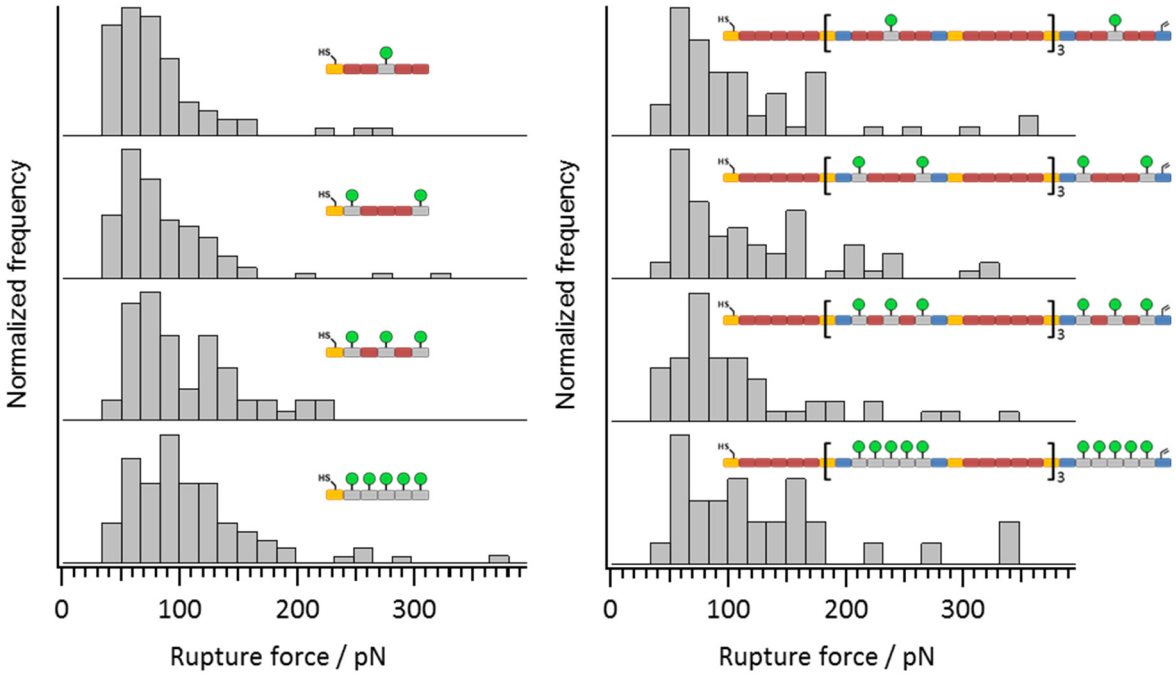

Figure 53- Histograms of the rupture event forces for oligomer and polymer ligands. Bins 16.5 pN.

A similar trend is presented for polymer ligands. The histograms show the same shift in rupture force to higher values, Figure 53. The histogram of **P2** presents a longer tail (up to 250 pN) than of **P1** (up to 200 pN); higher forces appear to be outliers. The modal bin for **P3** is shifted, unlike the mode of **P5** that is presented at ~50 pN. The shift in force for **P5** could be appreciated by estimating the second most frequent signal (at ~110 pN). Due to the greater valencies, the polymer histogram distributions could also be expected to be shifted to higher rupture forces in respect to the oligomer homologs, which cannot be seen.

Polymer histogram distribution for **P5**, and less clear for **P2** and **P1**, can be resolved with three contributions at 50, 100 and 150 pN that could be recognized as simultaneous rupture events of 1, 2 and 3 Man moieties. The distance of vicinal Con A binding pockets lies on the size of the coiled structures, meaning that simultaneous multivalent-rupture events should have happened, especially considering the internal polymer forces that may preserve the ligand in a closed or fixed conformation able to share the tension. Moreover, even though the polymer ligands could have spread on the receptor surface or uncoil while retracting, it has been reported for linear multivalent ligands a sequential and independent bond rupture[149]; newly supporting the close polymer conformation.

3.2.2.4 The average rupture value

The average rupture force grows with the number of Man moieties and the molecular weight of ligands, Figure 54. From the tracked single rupture steps, the binding modes are found to be

energetically influenced by subsite binding rising the average rupture force, especially for oligomers not being able to reach more than a single Con A binding pocket due to their size. The subsite binding may be enthalpically enhanced by the Man density, in which closer moieties may reduce the scaffold torsion raising the contribution from **O2** to **O5**. Polymers show rupture forces almost twice of a single Man-Con A. The shift in force between oligomers and polymers is correlated to the mass increment; more precisely to the size growth allowing sugars to reach more than a binding pocket.

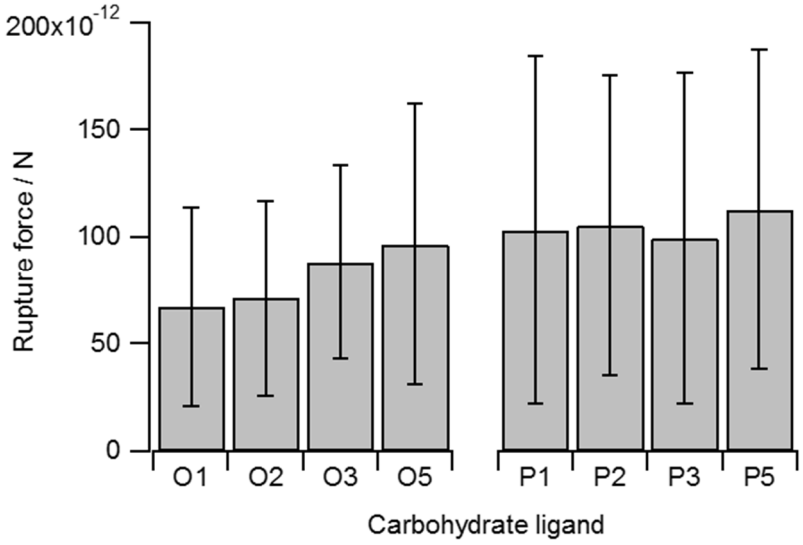

Figure 54- Average rupture force for the oligomer and polymer carbohydrate ligands (mean ± std. deviation).

3.2.2.5 Discussion of SM-AFM assay with multivalent studies

Overall, the valence is found for multivalent carbohydrate oligomer ligands as the most determinant factor for the binding force. The force enhancement is due to the specific subsite binding interaction, which is reported for Con A[49], and to the non-specific interactions of additional Man moieties. The chelate effect is not seen due to the ligand hydrodynamic radius, which for every sample is smaller than the spacing distance between Con A binding pockets (7.2 nm); despite it could not be discarded for polymers presenting coils of similar sizes. for multivalent carbohydrate polymer ligands are the size, i.e. the hydrodynamic radius, and the polyamide backbone the most contributive factors allowing Man moieties reach multiple binding pockets and to remain in a fixed conformation to share the tension during the simultaneous rupture events.

Multivalent assays performed by with SM-AFM for carbohydrate-lectin interaction scarce in the literature. Fortunately, few deals with the same Man-Con A system reporting similar breaking forces for the monovalent system (~47 pN[109, 146]) to the presented values, in which small differences are attributed to the loading rates. Ratto et al. tracked the simultaneous dissociation

of few Man units binding to a Con A due to their altered setup in which the Con A is presented on the cantilever tip.[109] Their presented dimer and trimer conformation rupture forces do not correlate to the values reported in this thesis, at first sight probably due to the experimental settings that affect the rupture forces and the also discussed non-additive multivalent rupture process.[109]

In this thesis, simultaneous multivalent-rupture of polymers is due to the polyamide-based scaffold that contributes to close presentation in which intramolecular H-binding do not open the ligand coil. Although the short persistence length of the PEG-linker can also contribute to a coiled arrangement, it has been shown that PEG backbone molecules can uncoil, reaching ligands the lectin binding pockets.[174] Analysis of a multivalent ligand attached on the tip, remaining the receptors on the surface, has been performed by Bano et al. tracking multiple rupture bonds within the same retraction force-curve.[149] It was achieved among CD44 receptors and hyaluronic acid (hyaluronan polymer) sample of comparable contour lengths but higher molecular weight than the polymeric samples used in this thesis. Hyaluronic acid is an anionic polymer which conformation can be tuned by the pH, being more randomly coiled whilst presenting fewer charges, i.e., it adopts more extended structures at the basic pH of 9.[175] They reported independent and sequential rupture events, what differs from the obtained in this work because their system precludes the simultaneous multivalent-rupture events despite of the ease and quantity of data collection. Han et al. also worked with HA polymer tracking multiple but not simultaneous, rupture events between biotin and streptavidin within the same retraction force-curve by making use of physisorption forces to simplify the effort of surface and tip functionalization; the fishhook approach.[175] Adapting their approach with sequence controlled multivalent polymer samples may result promising, and it will allow to fully stretching the polymers favoring the interactions with free lectins. Subsequently, it will be possible to perform a better study of the multivalent binding and rupturing modes while varying the local Man density along the polymer chains.

3.2.3 Mesoscale – NGPs functionalized with multivalent oligomers

Series of neoglycoproteins were produced as multivalent mesoscale ligands. The synthesis was performed using the described single-pot reacting procedure described in section 3.1.2.1. A short (SMCC) and a long (PEG) linkers were used to tether the sugar bearing molecules. Monovalent, divalent and pentavalent Man molecules were used for functionalization; corresponding respectively to ManSH, and the previously introduced multivalent oligomers **O2** and **O5**. Therefore, multivalent mesoscale ligands were synthesized varying the quantity and density of epitopes, together with the ligand flexibility, Figure 55.

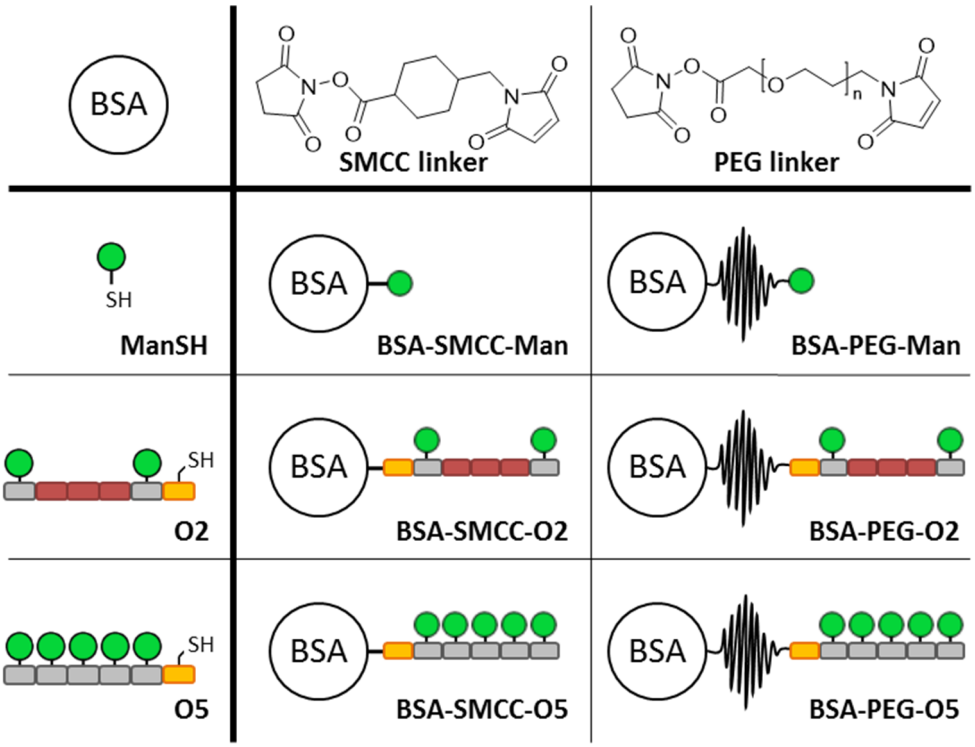

Figure 55- Overview of the synthesized NGPs in a single-pot reaction. BSA protein served as a scaffold on where to load mannose bearing molecules through two length heterobifunctional linkers. The fluorescent label was introduced in its isotiocianate form; not represented.

3.2.3.1 Quantification of NGP degree of functionalization

Neoglycoproteins were characterized regarding composition, quantifying the contents of sugar and fluorescent label per molecule of BSA, using UV-Vis spectroscopy as previously described in section 3.1.2.2. As described in section 3.1.2.2, the presence of Man for non-functionalized samples (BSA and BSA-RhodB) was attributed to the glycosylation of BSA and the interferences of RhodB in the digestion process. On average, there are two sugar-moieties on functionalized BSA, while there are 9 Man units on BSA with the lowest degree of functionalization (monovalent ManSH). The sugar units detected on BSA are not necessarily specifically binding to Con A, and it is not clear if the colorimetric test was misleading. Therefore, the sugar units detected on non-

functionalized BSA were subtracted from the Man-functionalization degree for the functionalized BSA as a means of correction. The corrected Man functionalization degree is calculated by deducing the respective contributions, Table 5.

Table 5- Characterization of BSA scaffolds after mannose (Man) functionalization with two linker lengths and fluorescent labeling. The concentration of solutions is determined by the mass of the present BSA indifferently of its functionalization. The degree of Rhodamine B and Man functionalization are expressed in a molar ratio to the BSA. Man correction corresponds to the Man functionalization degree after deducing the contribution of BSA and the proportional of the fluorescent label. Functionalization refers to the final substitution degree of BSA.

	BSA mg/ml	RhodB mol/mol BSA	Man mol/mol BSA	Man Correction mol/mol BSA	Functionalization mol/mol BSA
BSA	0.80	0.00_1	2.28	0.00	
BSA-RhodB	0.75	0.22_5	7.27	0.00	
NGPs with SMCC linker					
Man	0.46	0.16	9.25	3.42	3.58
O2	0.82	0.09	51.48	47.20	23.69
O5	0.73	0.06	116.38	112.77	22.61
NGPs with PEG linker					
Man	1.03	0.10	8.98	4.48	4.58
O2	1.02	0.04	86.83	83.66	41.87
O5	0.89	0.03	170.33	167.38	33.51

The NGPs functionalized with ManSH expose in average four sugar moieties per BSA achieving the pursued multivalency while functionalizing with **O2** and **O5** presents greater amounts of Man; more than 10 and 20 times. The fluorescent labeling shows a similar but inverted trend since fluorescent labeling competes with linker for the same functional groups. The differences in fluorescence functionalization degree and the fact that free BSA (BSA-RhodB) shows the highest intensity is therefore expected. The total functionalization degree of BSA scaffolds results from adding the corrected ratio of Man/BSA divided by its oligomer valence, plus the ratio fluorescent dye/BSA. The found highest functionalization degree of 42 molecules per BSA was achieved for BSA-PEG-O2. This value is smaller than the total amount of amino acids presenting free amine groups for functionalization, such as lysine (60x) or asparagine (14x). This is expected since some of these moieties are buried in the protein and not available for functionalization.

Note, that the NGPs functionalized with oligomers present 7-times higher functionalization degrees than with ManSH. In addition, NGPs functionalized with ligands conjugated with the long PEG linker show consistently higher degrees of functionalization. At this stage, a reason for different reactivity of the ligands cannot be given. However, it should be noted that the

functionalization via Maleimide-thiol reactions is prone to side reactions, e.g., dithiol formation or hydrolysis of the maleimide groups. Reactions depend on some parameters that were difficult to control in this work such as exact temperature (all reactions were performed at room temperature), the timing between coupling the linker and the ligands or the presence of active redox species (O_2) in the solution.

3.2.3.2 Fluorescence of NGPs on Con A surface

Fluorescent assays were performed with the complete series of NGPs, Figure 55, with Con A-SCP dispersions also at inhibiting conditions achieved with 10 mM MeMan, as described in the homonymous part in section 3.1.2.3, Figure 29. It was seen that NGPs functionalized with ManSH did not confirm the binding specificity of NGPs. That was first attributed to non-specific receptor clustering of the high Con A density of SCPs induced on BSA upon binding Man. This possibility was supposed to be feasible due to the low functionalization degree of the BSA. If this is so, the higher functionalization degree of NGPs synthetized with oligomers **O2,** and **O5** could overcome the non-specific binding with BSA. After several attempts, the fluorescent tests did not provide a constant or remarkable decrement while inhibiting the interaction, Figure 56.

Although many samples along the repetitions slightly decreased the fluorescence intensity under inhibitory media, the decrement was not greater than some fluorescent increments achieved under inhibition, e.g., BSA-PEG-O2 Round No.2, Figure 56. Subsequently, the specificity remained unresolved.

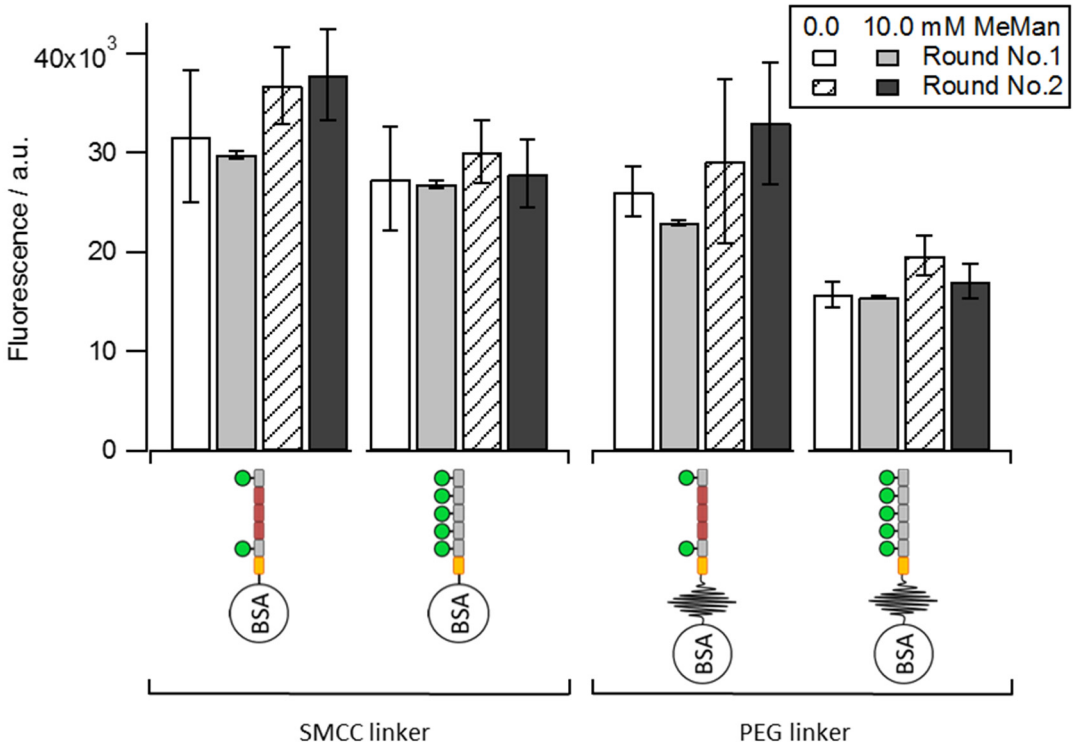

Figure 56- Fluorescent values of the whole series of NGPs testing for specific lectin-sugar binding. Example of a couple of repetition results of surface fluorescence of SCPs after incubation with NGPs under different inhibiting conditions. Experiments were performed with Con A functionalized SCPs (Con A-SCP) in solutions of NGPs functionalized with the short (SMCC), and long (PEG) linkers increasing the carbohydrate density.

3.2.3.3 Clustering rate as a function of ligand density; comparison to single molecule AFM experiments

Here, the turbidity measurements after mixing Con A with BSA-ligand scaffolds (Neoglycoproteins) and individual ligands (glycooligomers) are presented and discussed in the following section 3.2.3.4.

Neoglycoproteins. NGPs show different rates and amounts of turbidity at the experimental conditions (3.33 µM Con A and 1.33 µM NGP). For monovalent functionalized NGPs it was previously seen that mixing of Con A and NGP leads to a turbid solution. Turbidity was presented for the short linker NGP, but not for the long linker NGP, Figure 28 in section 3.1.2.3. This fact highlights that multivalent activity is affected by the linker length and flexibility.

The turbidity of NGP ligands varying the quantity and density of epitopes through the long PEG linker is shown in Figure 57. These NGPs present greater clustering rates while increasing the valence of the ligand. As well, the maximum signal is greater for higher valent NGPs. Therefore, the absent activity for BSA-PEG-Man, firstly attributed to the linker length, can be overcome by increasing the ligand valence and density.

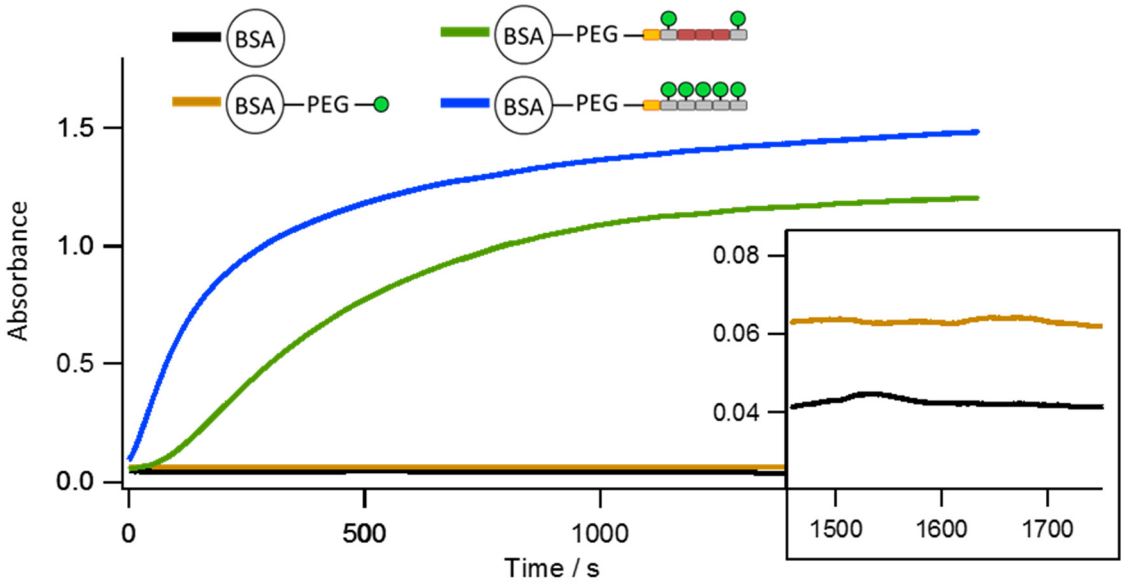

Figure 57- Turbidity of the NGPs functionalized through the longer PEG linker in terms of absorbance. Tests were performed with 1.33 µM NGP and 3.33 µM Con A solutions, both in LBB pH 7.4. It can be seen from the curve slope that the greater sugar valence, the faster the chelation is produced. The absorbance value is related to the sugar density of the aggregate, and it is greater for higher valence products. Note that the activity is influenced by the ligand density.

The turbidity of NGPs synthesized through the short SMCC linker can be seen in Figure 58. It can be appreciated that every ligand leads to significant turbidity. In the first 500 seconds, two NGPs (produced with ManSH and **O2**) have almost reached their maximum signal. It can be seen by comparing Figure 57 and Figure 58 that the turbidity for SMCC linker NGPs occurs faster than for PEG linker NGPs.

The faster kinetics of short linker NGPs difficult to assess their initial rate since the experimental setting did not allow collecting data in the starting seconds. The earliest tracked signal for the fastest product, ManSH NGP, already presents a 40% of its maximum turbidity. A normalization of the absorbance presents an inversion of the long linker NGP trend. For the short linker group of NGPs, ManSH shows the fastest binding, followed by **O2** and **O5** NGPs, Figure 59.

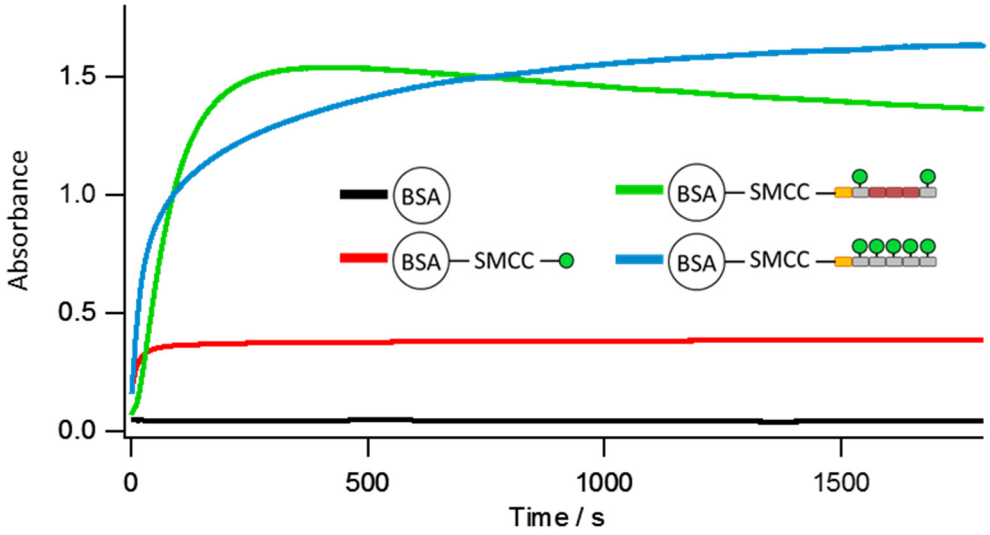

Figure 58- Turbidity of the short linker NGPs in terms of absorbance. Tests were performed with 1.33 µM NGP solutions and 3.33 µM Con A solution, both in LBB pH 7.4. It can be seen that the major part of the process occurs within the first minutes (t < 500 s). The absorbance reveals a light aggregate density for ManSH NGP. At 715 s, there is a signal cross for ***O2*** *and* ***O5*** *NGPs that is related to the aggregate precipitation of BSD.*

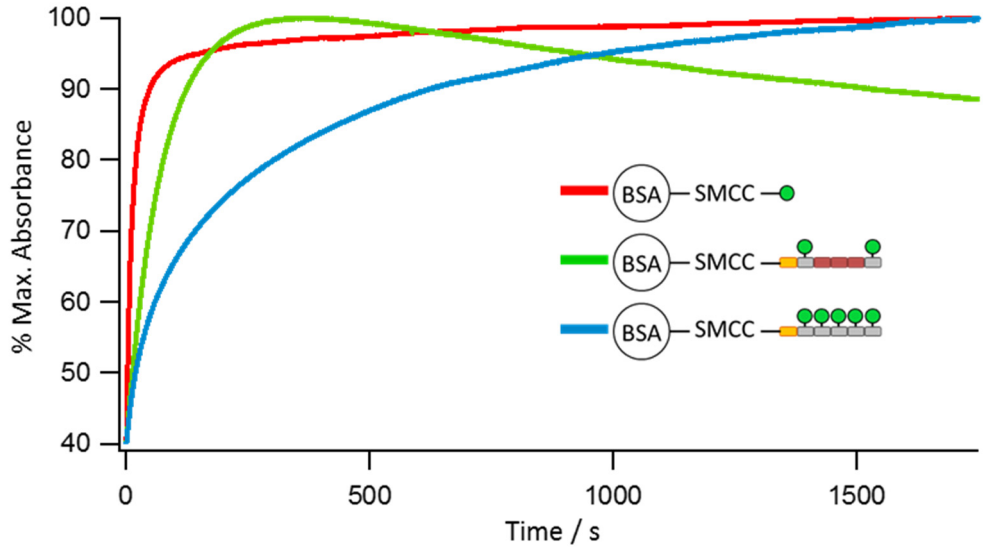

Figure 59- Normalized turbidity signal of NGPs functionalized with a short linker, from Figure 58. The initial reaction rate could not be determined due to the impossibility of tracking the first seconds. By comparing the reaction rate at the same reaction degree, it can be seen that a higher sugar degree results in a lower the rate.

Glycooligomers. As a control, the single molecule ligands used to synthesize the NGPs were analyzed via turbidity measurements in the presence of Con A to compare the binding affinity enhancement of NGPs. It was expected that monovalent single molecule ligands do not flocculate the solution due to their valence, whereas the multivalent ligands do. Turbidity tests were performed under same NGP conditions; mixing Con A (1 mL of 5 µM) with carbohydrate ligand solution (0.5 mL of 4 µM), Figure 60. This means that the multivalent ligand concentration

remained the same as the NGP experiment despite the overall concentration of Man units in the solution was significantly smaller when compared to the NGPs functionalized with glycooligomers **O2** and **O5**. It decreased by a factor of 16 and 5 respectively. As expected, the individual monovalent ligand did not show turbidity under the experimental conditions, just like multivalent oligomeric ligands did not do it either. Therefore, the experiments were repeated rising the ligand concentrations. The monovalent ligand, as expected, was not able to produce any turbidity after increasing a thousand times the concentration because there was not multivalent presentation. When increasing the oligomer concentration by a factor of 100, i.e., 6 (**O2**) and 17 (**O5**) times higher Man concentration when compared to the NGPs, no clouding was observed for the divalent oligomer **O2**. On the other hand, the pentavalent oligomer **O5** resulted in a turbid solution at the elevated concertation. It is reasonable that none of the multivalent oligomers cluster the solution at the initial lower concentration settings because Con A concentration almost triples the oligomers, despite these being multivalent. At 133.3 µM oligomer concentration, a 100 times higher starting concentration settings, the system presents 40 oligomer molecules to 1 of Con A. At this regime, the clustering behavior of oligomers differs. Since the sizes of **O2** and **O5** oligomers are similar, the clustering potential is correlated to the sugar quantity/density.

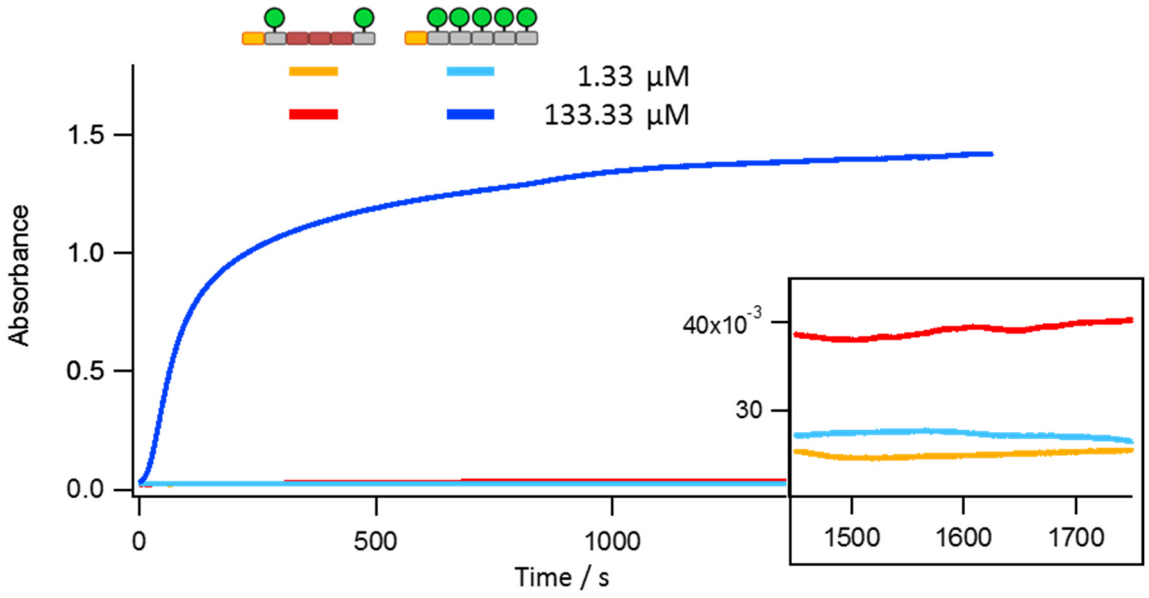

*Figure 60- Turbidity assay oligomer ligands **O2** and **O5** at the indicated concentrations chelating a 3.33 µM Con A solution in LBB pH 7.4. The absorption of light was tracked for 30 min, and only the pentavalent oligomer ligand **O5** resulted in a turbid solution at 133.3 µM; corresponding to 0.66 mM Man.*

3.2.3.4 Discussion of turbidity results and comparison of NGPs to glycooligomers

Neoglycoprotein conjugates presenting mannose (ManSH, and both glycooligomers **O2** and **O5**) showed four main results from turbidity measurements:

1) Increasing the glycooligomer valence increases the overall turbidity, i.e., affinity is increased.
2) Increasing ligand flexibility decreases affinity.
3) Binding kinetics for lower valent **O2** were slower than higher valent **O5** for longer linker NGPs; meanwhile, for shorter linker ligands, the binding kinetics were faster for **O2** as compared to **O5**.
4) Binding of NGP conjugated oligomers is more efficient as compared to free oligomers.

Increased affinity for ligands with an increment in Man presentation was often observed[51, 172-173, 176] including the SM-AFM presented here, see section 3.2.2. This is usually attributed to a statistical effect. The fact that BSA scaffold is more substituted while tethering **O2** should not hide the greater sugar presentation of the **O5** BSA constructs. Given the results from SM-AFM, where a higher dissociation force was observed for **O5** than for **O2**, the Con A clustering rate increment for BSA-PEG-O5 over BSA-PEG-O2 could also be attributed to a greater affinity by subsite binding.[49]

The effect of ligand flexibility was as well found in many studies[51, 177] and also observed in the previously presented SM-AFM; where a reduction in binding frequency was obtained for polymeric ligands, with higher molecular weights. Entropic repulsion was found as the main reason for the decreased affinity. Additionally for NGPs, the longer the linker length is, the thicker dispersant layer is present surrounding the BSA scaffold. It turns into a bigger effective volume fraction, which can lower the diffusion of the NGPs, subsequently decreasing the binding rate. This might explain the lower binding rates for the long PEG linker NGPs; what also fits with the slower rate of BSA-PEG-O2 than BSA-PEG-O5 since it is a more substituted construct and the functionalizing molecules are bigger. The facts that the functionalization degree was different and that the binding rate could be limited by diffusion, and not solely by the actual binding reaction of the tethered glycooligomers, presume similar kinetics for NGPs equally functionalized with **O2** and **O5** glycooligomers.

The differences in binding kinetics for **O5** and **O2** NGPs with the short SMCC linker are surprising. If binding affinity was purely affected by statistical effects, binding of the higher valent **O5** should be always larger. The fact that it was not larger suggests that the additional carbohydrates in **O5** did not contribute to Con A binding when compared to the divalent ligand **O2**. Rather, the slower binding of **O5** implies that the bulky sugar environment on the chain units made it difficult for the ligand to attain the optimal conformation for receptor binding. Therefore, it results in a stronger interaction, as seen in SM-AFM, section 3.2.2.4, that proceeds at a slower rate.

The BSA-SMCC-O2 NGP turbidity curve shows a maximum at around 300 seconds and then decreases. This is rather unusual, but could be explained by the formation of more homogeneous clusters between NGPs and Con A over time: At initial stages the **O2** presenting NGPs form inhomogeneous, i.e., small and large, clusters with Con A. That results in a faster growth of the turbidity since larger clusters are more efficient light scatters due to the bigger voids. The turbidity signal decay can be understood as a transient complex formation between the lower valent **O2** ligands, in which the clusters can unbind and reform over time in order to form more homogeneous and small clusters lesser scattering light. The turbidity decay is not present to the **O5** NGP. It could be attributed to a permanent cluster formation, in which the denser Man epitopes and greater binding energies hamper the unbinding and reorganization of clusters. The signal decay is not presented for ManSH NGP, despite its fastest rate, because of its small Man functionalization degree not allowing it to achieve large clusters with strong light scattering.

Finally, the achieved enhancement of affinity of NGP-presented ligands over their forming glycomolecules is due to the increased local density of ligands and multivalency as well as the non-specific interactions between BSA and Con A leading to stronger clustering when compared to free ligands. Therefore, NGPs are a valid tool to increase multivalent effects offering additional control by tuning the size and flexibility with a linker, as well as the sugar density on the scaffold.

3.2.4 Cellular scale – Adhesion inhibition of SCPs with NGPs and oligomers

SCP-adhesion has been shown to be capable for determining the ligand-receptor adhesion energy of objects with a size range from 10 to 100 µm, which is in the size range of cells. The SCPs approach serves to study the adhesion energies or the inhibitory potential of ligands both by blocking the lectin binding pockets before the SCP addition and by removing the SCP adhesion adding the ligands. Here the second approach is performed, Figure 61.

Man-SCPs adhered to Con A functionalized surfaces, a series with NGPs presenting single Man units and oligomers were added to study the reduction of SCPs adhesion due to competitive binding of NGPs. These tests were carried out as a function of time to characterize the NGP binding, Figure 61.

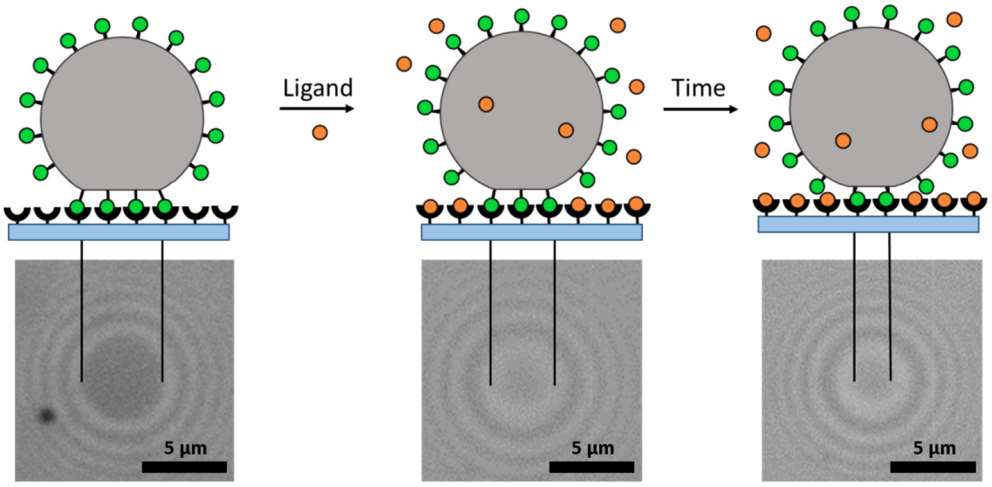

Figure 61- Scheme of adhesion inhibition test. The presence of ligands decrease by competition the adhesion energy of already adhered Man-SCPs onto a Con A functionalized surface. Orange color is used for clarity despite the Man presentation of competitors.

3.2.4.1 Adhesion inhibition with NGPs

Assays were performed in LBB pH 7.4 on Con A functionalized surfaces by chemical adsorption using GLYMO providing improved protein stability. Man-SCPs were then added, and after 60 min of incubation, the adhesion energy was measured to determine the maximum adhesion as a reference in the absence of NGP inhibitors. Then, NGP solutions were added, and a decrement in adhesion was observed.

The complete set of NGPs produced as mesoscale ligands were tested as inhibitors/competitors, see section 3.2.3, Figure 55 and Table 5. The final inhibitory concentration for all of the NGPs ligands was set at 0.05 mg/mL referring to the BSA scaffold. The adhesion energy was determined after 60 min and 600 min of ligand addition.

The reference test (REF), which remained free from inhibitory molecules, presents constant adhesion energy along the whole time frame, proving the stability of SCPs and surface, Figure 62. The blank test with BSA-RhodB results in a small decrease in adhesion energy of 17 percent. This indicated that pure BSA could interact with Con A, either by non-specific interactions or by undocumented glycosylation.

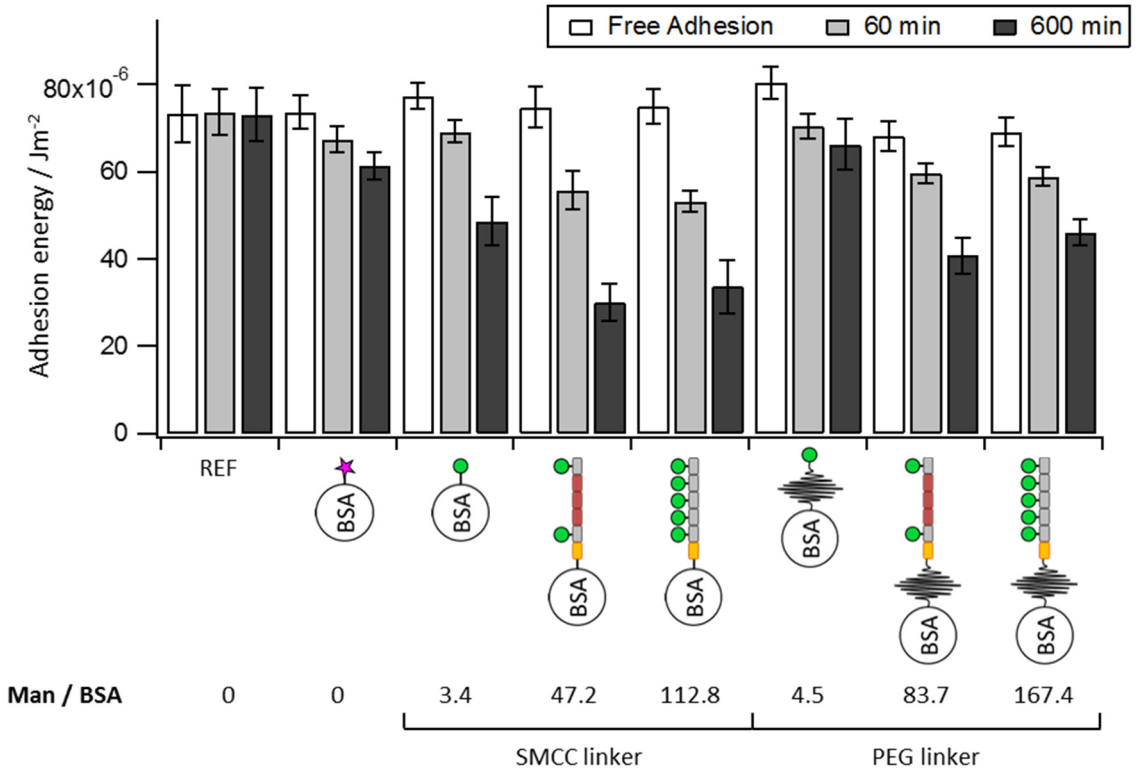

Figure 62- Adhesion energy of Man-SCPs on Con A surfaces in LBB pH 7.4. The adhesion energy was determined after 60 min of SCP addition while the media remains free of competitors and SCPs express their maximum adhesion (t=0 Free Adhesion), after 60 and 600 min of inhibition with NGPs (0.05 mg/mL). It is indicated the concentration of mannose moieties per scaffold unit. All NGPs are fluorescently labeled; only represented for Man free BSA. Note the constant adhesion energy on Con A surface without competing ligands (REF).

ManSH NGPs reduce SCP adhesion less than the oligomer NGPs presumably because of the smaller Man-functionalization degree. On the other hand, the higher Man amount of **O5** NGP compared to **O2** NGP does not result in greater adhesion inhibition, Figure 62. The trend was observed for both SMCC and PEG linkers. Therefore, adhesion inhibition does only correlate with the number of presented Man units up to a certain threshold of Man density. Importantly, however, NGPs tethering the ligands with the long PEG linker (BSA-PEG-O5 and BSA-PEG-O2) show reduced adhesion inhibition when compared to NGPs with the SMCC linker. This might be due to the overall lower affinity of the Man units at the PEG linker owing to greater steric

repulsion as also seen in direct binding experiments, see mesoscale ligands section 3.1.2.3 Figure 28 and macroscale ligands section 3.1.2.2 Figure 44.

3.2.4.2 Adhesion inhibition with oligomers and monovalent mannoses

The monovalent sugars MeMan and ManSH, together with the divalent and pentavalent oligomers (**O2** and **O5**) were tested at the final inhibitory concentration of 62.5 µM. From IC_{50} inhibition experiments on monovalent Man, it is known that inhibiting the interaction with Con A takes place at almost 1 mM and this value decreases to 69.4 µM with a divalent Man-dendrimer.[178] Therefore, different inhibitory activities are expected for the multivalent ligands at the chosen concentration.

It can be seen that all the ligands compete against the Man-SCPs for Con A binding sites and reduce the adhesive contact, Figure 63. Generally, there is larger inhibition of adhesion for multivalent ligands compared to monovalent ligands. Since multivalent oligomers result in similar decrement, it appears that increased Man multivalency alone does not achieve greater inhibition. Alternatively, the increased molecular weight (backbone length) of oligomers compared to monovalent ManSH and MeMan might be responsible for increased inhibition. Given that the ligand binds with sufficient affinity to Con A, increased backbone length results in increased entropic repulsion and therefore increased inhibition. Also for monovalent ligands, the inhibition of ManSH was slightly larger when compared to MeMan. This could be explained by the formation of disulfide bonds for ManSH increasing the valence and the molecular weight.

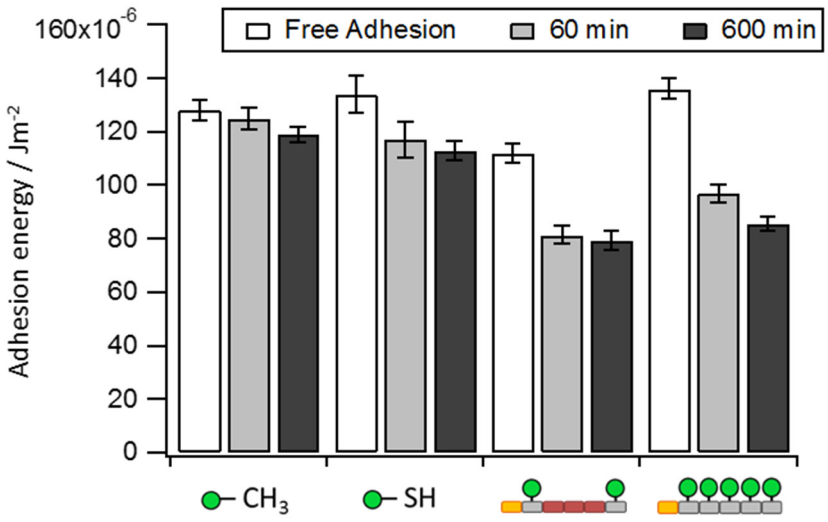

Figure 63- Adhesion energy of Man-SCPs on Con A surfaces in LBB pH 7.4. The adhesion energy was determined after 60 min of SCP addition while the media remains free of competitors and SCPs express their maximum adhesion (t=0 Free Adhesion), after 60 and 600 min of inhibition with monomolecular ligands (62.5 µM).

3.2.4.3 The inhibitory strength of monovalent ligands, oligomers, and neoglycoproteins

Here, the inhibitory strength of monovalent Man units, oligomers, and Man-bearing NGP scaffolds are compared, Table 6. Additionally, the normalized inhibitory strength with the Man concentration is presented in order to extract the effect of backbone length, Figure 64. From these data the following main results can be extracted:

1. Adhesion inhibition for the multivalent oligomer systems is roughly twice compared to the monovalent ligands.
2. The adhesion inhibition achieved by oligomers (**O2** and **O5**) is almost similar.
3. Similar trends were observed for NGPs, but here the inhibition appears stronger when compared to oligomers.
4. When tethering ligands through long PEG linker, inhibition is attenuated.
5. Although NGPs are found to be more efficient, they seem to inhibit at slower rates compared to molecular ligands, Figure 65.

The inhibition of adhesion appears to be size dependent with small ligands, for which a ManSH dimer greater inhibits the adhesion in comparison to MeMan and it is half of the achieved inhibition with oligomers. Then, at oligomer size, the valency also contributes, as seen in SM-AFM section 3.2.2.4, where a greater oligomer valency results in greater rupture forces i.e. in greater affinities, making **O5** a better inhibitor than **O2**, which hydrodynamic radius is greater, section 3.2.1.1.

For NGPs the size contribution is still present and the oligomer-functionalized BSA better inhibit the adhesion than the ManSH-functionalized BSA. The size contribution for inhibition is attenuated for the NGPs presenting the long linker, for which the entropic repulsion reduces the binding affinity as seen in turbidimetry, section 3.1.2.3; notice that BSA-PEG-ManSH lesser inhibits the adhesion than **O2** and **O5** oligomers. With the achieved size increment of NGPs, there are higher odds to simultaneously reach two Con A binding pockets through the linked functionality and it results in greater affinities lesser contributing the valency.

Overall, these results suggest that not only multivalency achieves improved adhesion inhibition, but also the backbone size and steric repulsion play an important role, where larger scaffolds achieve increased inhibitions, improving the Man efficiency. It is supported by the fact that neither oligomers nor NGPs fully removed the adhesion of the SCP ligand. Further studies should be done in this area to determine the contribution of each parameter, valence, size and steric repulsion, for the optimization of the Man activity and later considering diffusion to improve the kinetics.

Table 6- Percentage decrement in adhesion energy and their sugar correlation of Man-SCPs from Con A functionalized surfaces with molecular ligands and NGPs after 60min (Δ1) and 600 min (Δ2) of their addition.

	Δ1 / %	Δ2 / %	Man / µM	Δ1/[Man]	Δ2/[Man]
Molecular ligands					
MeMan	2.30	6.64	62.50	0.04	0.11
ManSH	12.82	15.85	62.50	0.21	0.25
O2	27.65	29.48	125.00	0.22	0.24
O5	28.70	36.87	312.50	0.09	0.12
NGPs with SMCC linker					
ManSH	10.54	37.06	2.59	4.07	14.30
O2	25.17	59.60	35.76	0.70	1.67
O5	28.95	54.93	85.43	0.34	0.64
NGPs with PEG linker					
ManSH	12.58	17.79	3.40	3.70	5.24
O2	12.32	40.22	63.38	0.19	0.63
O5	15.00	33.21	126.81	0.12	0.26

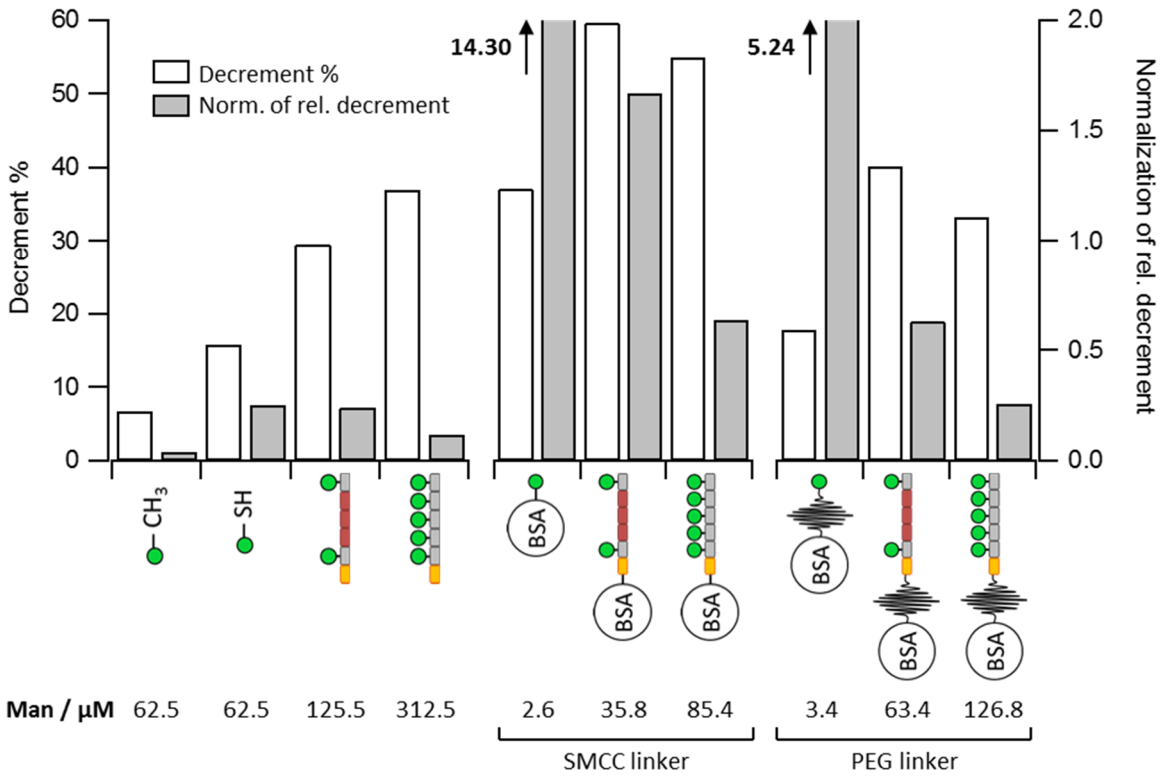

Figure 64- Relative decrease in adhesion energy of Man SCPs on Con A surfaces (white bars, left y-axis) and normalization of relative decrement with the sugar concentration (grey bars, right y-axis) after 600 min of inhibition with molecular ligands and NGPs, from Table 6.

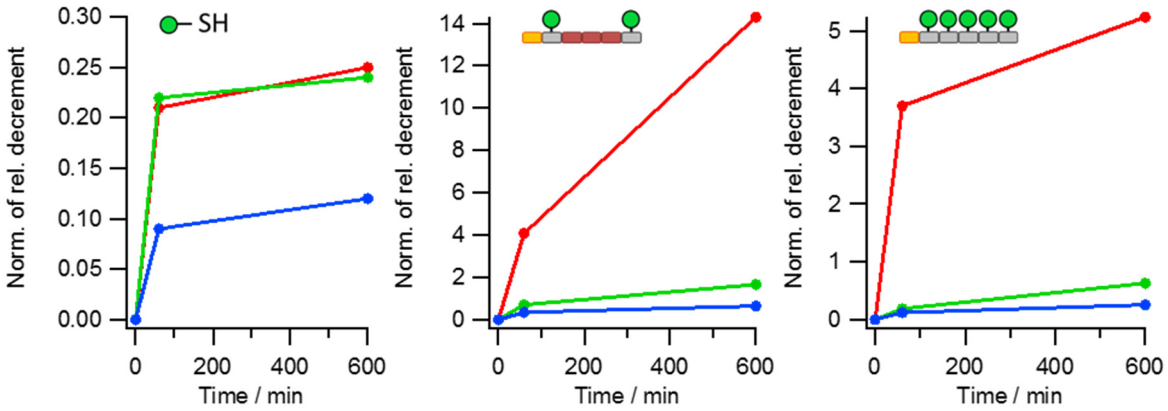

*Figure 65- Kinetics of relative decrement in adhesion energy with the mannose normalization values, from Table 6. The process kinetics can be compared through the line slopes between adhesion energy decrements at 0, 60 and 600 min. Meanwhile, the kinetics for individual ManSH is similar to the BSA-SMCC-Man but greater than BSA-PEG-Man, both individual oligomers **O2** and **O5** are much faster than the relative NGPs. Representation of the individual ligands (red), the short SMCC linker NGPs (green) and long PEG linker NGPs (blue).*

4 CONCLUSIONS AND PERSPECTIVES

In this thesis, the multivalent ligand-receptor interactions of carbohydrate ligands and lectin receptors were studied from molecular scale to cellular scale because the size of the interacting area is believed to be crucial for multivalent binding effects, as well as triggering biological functions. Among with the variation of scale, also the density of presented ligands together with the length and flexibility of ligand tethers were varied.

The well-studied ligand/receptor pair mannose (Man)/concanavalin A (Con A) lectin was chosen as a model system to perform the assays. The scale variation of ligand systems was achieved through the presentation of multiple Man units on different scaffolds. Therefore, linear oligomer and polymer ligands, proteins, hydrogel microparticles and glass coverslips were functionalized to present Man bearing molecules with different valencies. In order to take control over the multivalency and mechanical flexibility of the attachment, the scaffolds were functionalized with varying number of Man moieties, through different linkers with different lengths.

In the first part, a set of techniques was developed and validated to specifically quantify the weak interactions between Man and Con A at different scale ranges. In the second part, the developed techniques were used to study systematically Man-Con A interactions and the effect of Man presentation. For gain control over Man valency and spacing a series of multivalent precision glycooligomers and polymers were used. The sequence-defined oligomers were synthesized using solid phase synthesis techniques, previously established in Hartmann group[172], introducing 1 to 5 Man moieties on oligomer chains (up to 2.6 kDa) to later functionalize the scaffolds of larger sizes, i.e. proteins and microgels. In addition, glycooligomers were polymerized to form larger linear multiblock scaffolds (up to 30.8 kDa) also in the Hartmann group.[173]

On the single molecular scale, the assays were performed using Single-Molecule Atomic Force Microscopy (SM-AFM) by presenting oligomers and polymers on the apex of an AFM tip. Measuring the weak Man-Con A binding was possible since AFM allows observing interactions down to a few tens of pN. In order to achieve the single molecule presentation, the ligand was linked through a PEG spacer (~80 nm) improving the selectivity and providing a smaller surface density of reacting sites simultaneously. Since the adhesive forces between the tip and substrate were affected by non-specific interaction, the SM-AFM data was treated by the force and tip-sample separation of the rupture events, ensuring the detection of specific dissociation of Con A and Man complexes. The method was approved by observing the reduction in dissociation events in the presence of inhibiting Man ligands.

Interestingly, both oligomers and polymers showed a low frequency of rupture events per retraction curve regardless of their valence. This was explained by the short oligomer length not reaching consecutive binding sites, while for polymers this was due to their coiled conformation, which was confirmed by Dynamic Light Scattering (DLS). DLS revealed smaller coils for increasing Man density on oligomers, attributed to the shorter Man building block and hydrogen bonding of the carbohydrates in the coil. On the other hand, the greater Man density on polymers hampered the intramolecular hydrogen bonding expanding the coils. The smaller frequency for polymers to result in binding events in comparison to oligomers arose from their increased size of the coils, in which sugar residues could have been hidden, and the resulting increased steric (entropic) repulsion.

However, the dissociation force for identified single molecule complexes grew with the valency of the ligands. This could be caused by subsite binding effect in particular for oligomers. On the other hand for polymers, chelate-like binding could not be dismissed since the size of the coil may have reached consecutive Con A binding sites spacing 7.2 nm. Importantly, however, from AFM investigation there was no indication for oligomer or polymer uncoiling by forced detachment from the Con A surface possibly due to strong hydrogen bonding within the coils.

At mesoscale, measurements were performed using carbohydrate functionalized BSA proteins, so-called neoglycoproteins. Single Man and oligomers bearing 2 and 5 Man units were introduced through heterobifunctional linkers of different length. Excess of reactive ligands achieved high valency, usually pursued by these compounds. The reaction of linker and Man with the BSA was successful in a single step due to the orthogonality of active ester-amine and maleimide-thiol reactions. Fluorescent labeling was conducted to determine the binding of functionalized BSA to Con A functionalized substrates. Overall, these experiments showed a rather low specificity, possibly due to the non-specific interaction between Con A and BSA.

Nevertheless, turbidity measurements showed that the binding is reduced for longer flexible PEG linker (10 kDa) when compared to the shorter linker used (334 Da). Again, it could be assumed that increased coiling and steric repulsion hampered binding for the longer linker. Differences in binding strength between divalent and pentavalent oligomers at the long-linker BSA scaffold could be compensated by a higher degree of functionalization, which then resulted in similar binding for both types of oligomers. In case of the short-linker BSA, the valency increment did not affect the activity since the binding strength of all prepared neoglycoproteins was large enough to bind the maximum amount of Con A, which might indicate chelate-like binding. The BSA functionalized with the monovalent molecule reached more quickly its maximum binding, which was smaller than the achieved by oligomer functionalization, further indicating coiling of the

oligomers. Overall, these experiments showed that at mesoscopic scale reduction of affinity by using more flexible (longer) tethers can be compensated by a higher density of ligand units resulting on clustering of the receptors. It could be supposed that upon receptor clustering the ligand flexibility is broadly reduced due to confinement, i.e., enthalpy of binding dominates potential entropic effects.

In cellular and macroscopic scales, the assays were performed via Soft Colloidal Probe-adhesion (SCP-adhesion); a biosensor-based technique using functionalized hydrogel particles (SCPs) of approximately the same size of cells to represent better the biological context. The molecular binding events of the SCPs were converted into a quantifiable signal applying the JKR model of adhesion. The specificity of the adhesion signal was tested by inhibition, and the robustness of the technique was assessed by looking at the effect of handling conditions, e.g., harsh rinsing of surfaces. Man-functionalized SCPs showed adhesion reduction upon rinsing on physisorbed Con A surfaces, which was not present for covalently functionalized surfaces. The binding affinity of Man-presenting molecules and protein scaffold ligands were tested by their potential to decrease the established adhesion of Man-SCPs on Con A-surfaces. It was shown that not only the number of added Man units but also the scale of the scaffold affects adhesion inhibition of the SCPs. The increased inhibitory activity of larger ligands was probably due to additional steric repulsion enforced against the adhered SCP networks. This effect is potentially relevant for the design of antiadhesive drugs for pathogen treatment or inhibition of biofilms. Concerning the macroscopic Man-presenting surfaces, more work has to be done since their specific binding to Con A could not be confirmed. This was potentially due to a low degree of functionalization of the surfaces with Man ligands.

Taken together, a set of techniques was developed that is suitable for the measurement of multivalent binding at different size scales with high sensitivity to study weak carbohydrate interactions. They allow analyzing the contribution of valency for which an increment did not always improve the activity enhancement, e.g., due to coiling of linear multivalent scaffolds. In addition, the steric repulsion inherent to the flexibility of the ligands can also be studied. Increased flexibility was shown to overall decrease ligand binding, in particular on the single-molecule scale. For larger scaffolds this effect could be compensated while clustering of proteins due to the higher enthalpic gains associated with it. With the presented techniques, deeper studies of the individual material parameters can be performed in order to broaden the knowledge of their effects. In order to get more detailed insights, the conformation and positioning of the ligands in contact with the proteins should be analyzed. This could be achieved by spin or FRET labels at the binding partners. In terms of applications, the observed increased

inhibition of carbohydrate adhesion for larger, but not necessarily higher valent inhibitors may open new routes toward anti-adhesive agents for pathogen treatment.

5 REFERENCES

1. Choi, S. K.; Mammen, M.; Whitesides, G. M., *Chem Biol* **1996,** *3* (2), 97-104.

2. Sigal, G. B.; Mammen, M.; Dahmann, G.; Whitesides, G. M., *J. Am. Chem. Soc.* **1996,** *118* (16), 3789-3800.

3. Kingery-Wood, J. E.; Williams, K. W.; Sigal, G. B.; Whitesides, G. M., *J. Am. Chem. Soc.* **1992,** *114* (18), 7303-7305.

4. Vonnemann, J.; Liese, S.; Kuehne, C.; Ludwig, K.; Dernedde, J.; Böttcher, C.; Netz, R. R.; Haag, R., *J. Am. Chem. Soc.* **2015,** *137* (7), 2572-2579.

5. Martinez-Avila, O.; Hijazi, K.; Marradi, M.; Clavel, C.; Campion, C.; Kelly, C.; Penades, S., *Chemistry* **2009,** *15* (38), 9874-88.

6. Papp, I.; Sieben, C.; Sisson, A. L.; Kostka, J.; Bottcher, C.; Ludwig, K.; Herrmann, A.; Haag, R., *ChemBioChem* **2011,** *12* (6), 887-95.

7. Vonnemann, J.; Sieben, C.; Wolff, C.; Ludwig, K.; Bottcher, C.; Herrmann, A.; Haag, R., *Nanoscale* **2014,** *6* (4), 2353-60.

8. Rademacher, T. W.; Parekh, R. B.; Dwek, R. A., *Annu. Rev. Biochem.* **1988,** *57*, 785-838.

9. Muller, D. J.; Helenius, J.; Alsteens, D.; Dufrene, Y. F., *Nature Chemical Biology* **2009,** *5* (6), 383-390.

10. Bertozzi, C. R.; Kiessling; L., L., *Science* **2001,** *291* (5512), 2357-2364.

11. Drickamer, K.; Taylor, M. E., *Trends Biochem. Sci.* **1998,** *23* (9), 321-4.

12. Vornholt, W.; Hartmann, M.; Keusgen, M., *Biosensors & bioelectronics* **2007,** *22* (12), 2983-2988.

13. Rudiger, H.; Gabius, H. J., *Glycoconj J* **2001,** *18* (8), 589-613.

14. Wang, L.; Wang, L.; Huang, M.; Zhang, H.; Song, L., *Isj-Invertebrate Survival Journal* **2011,** *8* (2), 241-246.

15. Zhang, X. W.; Xu, W. T.; Wang, X. W.; Mu, Y.; Zhao, X. F.; Yu, X. Q.; Wang, J. X., *Mol Immunol* **2009,** *46* (8-9), 1626-37.

16. Lis, H.; Sharon, N., *Chem. Rev.* **1998,** *98* (2), 637-674.

17. Naismith, J. H.; Emmerich, C.; Habash, J.; Harrop, S. J.; Helliwell, J. R.; Hunter, W. N.; Raftery, J.; Kalb , A. J.; Yariv, J., *Acta Crystallographica Section D* **1994,** *50* (6), 847-858.

18. Palacios, R., *J Immunol* **1982,** *128* (1), 337-42.

19. Lam, S. K.; Ng, T. B., *Appl. Microbiol. Biotechnol.* **2011,** *89* (1), 45-55.

20. Ji, X.; Gewurz, H.; Spear, G. T., *Mol Immunol* **2005,** *42* (2), 145-52.

21. Abdullaev, F. I.; de Mejia, E. G., *Nat. Toxins* **1997,** *5* (4), 157-63.

22. Gray, R. D.; Glew, R. H., *J. Biol. Chem.* **1973,** *248* (21), 7547-7551.

23. Goldstein, I. J.; Hollerman, C. E.; Merrick, J. M., *Biochim. Biophys. Acta* **1965,** *97* (1), 68-76.

24. Baron, R.; McCammon, J. A., *Annu. Rev. Phys. Chem.* **2013,** *64*, 151-75.

25. Breiten, B.; Lockett, M. R.; Sherman, W.; Fujita, S.; Al-Sayah, M.; Lange, H.; Bowers, C. M.; Heroux, A.; Krilov, G.; Whitesides, G. M., *J. Am. Chem. Soc.* **2013,** *135* (41), 15579-84.

26. Weis, W. I.; Drickamer, K., *Annu. Rev. Biochem.* **1996,** *65*, 441-73.

27. Baron, R.; Setny, P.; McCammon, J. A., *J. Am. Chem. Soc.* **2010,** *132* (34), 12091-12097.

28. Rose, A. S.; Bradley, A. R.; Valasatava, Y.; Duarte, J. M.; Prli, A.; #263; Rose, P. W., Web-based molecular graphics for large complexes. In *Proceedings of the 21st International Conference on Web3D Technology*, ACM: Anaheim, California, 2016; pp 185-186.

29. Rose, A. S.; Hildebrand, P. W., *Nucleic Acids Res.* **2015,** *43* (W1), W576-W579.

30. Kitov, P. I.; Bundle, D. R., Thermodynamic Models of the Multivalency Effect. In *Carbohydrate-Based Drug Discovery*, Wong, C., Ed. 2005.

31. Mammen, M.; Choi, S. K.; Whitesides, G. M., *Angewandte Chemie-International Edition* **1998,** *37* (20), 2755-2794.

32. Ackermann, T., *Berichte der Bunsengesellschaft für physikalische Chemie* **1987,** *91* (12), 1398-1398.

33. Perlmutter-Hayman, B., *Acc. Chem. Res.* **1986,** *19* (3), 90-96.

34. Du, X.; Li, Y.; Xia, Y.-L.; Ai, S.-M.; Liang, J.; Sang, P.; Ji, X.-L.; Liu, S.-Q., *International Journal of Molecular Sciences* **2016,** *17* (2), 144.

35. Newton, A. C.; Groenewold, J.; Kegel, W. K.; Bolhuis, P. G., *J. Chem. Phys.* **2017,** *146* (23), 10.

36. Hong, S.; Leroueil, P. R.; Majoros, I. J.; Orr, B. G.; Baker, J. R.; Banaszak Holl, M. M., *Chem. Biol.* **2007,** *14* (1), 107-115.

37. Rao, J.; Lahiri, J.; Isaacs, L.; Weis, R. M.; Whitesides, G. M., *Science* **1998,** *280* (5364), 708-711.

38. Kramer, R. H.; Karpen, J. W., *Nature* **1998,** *395* (6703), 710-3.

39. Mulder, A.; Huskens, J.; Reinhoudt, D. N., *Org. Biomol. Chem.* **2004,** *2* (23), 3409-3424.

40. Pieters, R. J., *Org. Biomol. Chem.* **2009,** *7* (10), 2013-2025.

41. Pertici, F.; Pieters, R. J., *Chem. Commun.* **2012,** *48* (33), 4008-4010.

42. Schwefel, D.; Maierhofer, C.; Beck, J. G.; Seeberger, S.; Diederichs, K.; Moller, H. M.; Welte, W.; Wittmann, V., *J. Am. Chem. Soc.* **2010,** *132* (25), 8704-8719.

43. Jiang, W.; Nowosinski, K.; Low, N. L.; Dzyuba, E. V.; Klautzsch, F.; Schafer, A.; Huuskonen, J.; Rissanen, K.; Schalley, C. A., *J. Am. Chem. Soc.* **2012,** *134* (3), 1860-1868.

44. Mangold, S. L.; Cloninger, M. J., *Org. Biomol. Chem.* **2006,** *4* (12), 2458-2465.

45. Deniaud, D.; Julienne, K.; Gouin, S. G., *Org. Biomol. Chem.* **2011,** *9* (4), 966-979.

46. Kitov, P. I.; Sadowska, J. M.; Mulvey, G.; Armstrong, G. D.; Ling, H.; Pannu, N. S.; Read, R. J.; Bundle, D. R., *Nature* **2000,** *403* (6770), 669-72.

47. Kane, R. S., *Langmuir* **2010,** *26* (11), 8636-8640.

48. Vrasidas, I.; Andre, S.; Valentini, P.; Bock, C.; Lensch, M.; Kaltner, H.; Liskamp, R. M. J.; Gabius, H. J.; Pieters, R. J., *Org. Biomol. Chem.* **2003,** *1* (5), 803-810.

49. Naismith, J. H.; Field, R. A., *J. Biol. Chem.* **1996,** *271* (2), 972-976.

50. Dam, T. K.; Brewer, C. F., *Biochemistry* **2008,** *47* (33), 8470-6.

51. Gestwicki, J. E.; Cairo, C. W.; Strong, L. E.; Oetjen, K. A.; Kiessling, L. L., *J. Am. Chem. Soc.* **2002,** *124* (50), 14922-14933.

52. Kiessling, L. L.; Pohl, N. L., *Chem. Biol.* **1996,** *3* (2), 71-77.

53. Sigal, G. B.; Mammen, M.; Dahmann, G.; Whitesides, G. M., *J. Am. Chem. Soc.* **1996,** *118* (16), 3789-3800.

54. Lees, W. J.; Spaltenstein, A.; Kingerywood, J. E.; Whitesides, G. M., *J. Med. Chem.* **1994,** *37* (20), 3419-3433.

55. Jayaraman, N., *Chem. Soc. Rev.* **2009,** *38* (12), 3463-3483.

56. Merrifield, R. B., *J. Am. Chem. Soc.* **1963,** *85* (14), 2149-2154.

57. Bejugam, M.; Flitsch, S. L., *Org. Lett.* **2004,** *6* (22), 4001-4004.

58. Woller, E. K.; Cloninger, M. J., *Org. Lett.* **2002,** *4* (1), 7-10.

59. Loka, R. S.; Sadek, C. M.; Romaniuk, N. A.; Cairo, C. W., *Bioconjugate Chem.* **2010,** *21* (10), 1842-1849.

60. Fasting, C.; Schalley, C. A.; Weber, M.; Seitz, O.; Hecht, S.; Koksch, B.; Dernedde, J.; Graf, C.; Knapp, E. W.; Haag, R., *Angewandte Chemie-International Edition* **2012,** *51* (42), 10472-10498.

61. Biessen, E. A. L.; Broxterman, H.; Vanboom, J. H.; Vanberkel, T. J. C., *J. Med. Chem.* **1995,** *38* (11), 1846-1852.

62. Thoma, G.; Duthaler, R. O.; Magnani, J. L.; Patton, J. T., *J. Am. Chem. Soc.* **2001,** *123* (41), 10113-10114.

63. Lundquist, J. J.; Debenham, S. D.; Toone, E. J., *J. Org. Chem.* **2000,** *65* (24), 8245-8250.

64. Ladmiral, V.; Melia, E.; Haddleton, D. M., *Eur. Polym. J.* **2004,** *40* (3), 431-449.

65. Ting, S. R. S.; Chen, G. J.; Stenzel, M. H., *Polym. Chem.* **2010,** *1* (9), 1392-1412.

66. Ladmiral, V.; Mantovani, G.; Clarkson, G. J.; Cauet, S.; Irwin, J. L.; Haddleton, D. M., *J. Am. Chem. Soc.* **2006,** *128* (14), 4823-4830.

67. Chen, G. J.; Amajjahe, S.; Stenzel, M. H., *Chem. Commun.* **2009,** (10), 1198-1200.

68. David, A.; Kopeckova, P.; Rubinstein, A.; Kopecek, J., *Bioconjugate Chem.* **2001,** *12* (6), 890-899.

69. Geng, J.; Lindqvist, J.; Mantovani, G.; Chen, G.; Sayers, C. T.; Clarkson, G. J.; Haddleton, D. M., *Qsar & Combinatorial Science* **2007,** *26* (11-12), 1220-1228.

70. Ambrosi, M.; Cameron, N. R.; Davis, B. G., *Org. Biomol. Chem.* **2005,** *3* (9), 1593-1608.

71. Hasegawa, T.; Kondoh, S.; Matsuura, K.; Kobayashi, K., *Macromolecules* **1999,** *32* (20), 6595-6603.

72. Cloninger, M. J., Glycodendrimers and other Macromolecules Bearing Multiple Carbohydrates. In *Molecular Recognition and Polymers: Control of Polymer Structure and Self-Assembly*, Rotello, V. M.; Thayumanavan, S., Eds. 2008.

73. Chabre, Y. M.; Roy, R., *Curr. Top. Med. Chem.* **2008,** *8* (14), 1237-1285.

74. Papp, I.; Dernedde, J.; Enders, S.; Haag, R., *Chem. Commun.* **2008,** (44), 5851-5853.

75. Yi, D.; Lee, R. T.; Longo, P.; Boger, E. T.; Lee, Y. C.; Petri, W. A.; Schnaar, R. L., *Glycobiology* **1998,** *8* (10), 1037-1043.

76. Appeldoorn, C. C. M.; Joosten, J. A. F.; el Maate, F. A.; Dobrindt, U.; Hacker, J.; Liskamp, R. M. J.; Khan, A. S.; Pieters, R. J., *Tetrahedron-Asymmetry* **2005,** *16* (2), 361-372.

77. Ashton, P. R.; Hounsell, E. F.; Jayaraman, N.; Nilsen, T. M.; Spencer, N.; Stoddart, J. F.; Young, M., *J. Org. Chem.* **1998,** *63* (10), 3429-3437.

78. Woller, E. K.; Walter, E. D.; Morgan, J. R.; Singel, D. J.; Cloninger, M. J., *J. Am. Chem. Soc.* **2003,** *125* (29), 8820-8826.

79. Monsigny, M.; Kieda, C.; Roche, A. C., *Biology of the Cell* **1983,** *47* (1), 95-110.

80. Lee, Y. C.; Stowell, C. P.; Krantz, M. J., *Biochemistry* **1976,** *15* (18), 3956-3963.

81. Kieda, C.; Delmotte, F.; Monsigny, M., *FEBS Lett.* **1977,** *76* (2), 257-261.

82. Aplin, J. D.; Wriston, J. C.; Lee, Y. C., *Critical Reviews in Biochemistry* **1981,** *10* (4), 259-306.

83. Wagh, P. V.; Bahl, O. P.; Elbein, A. D., *Critical Reviews in Biochemistry* **1981,** *10* (4), 307-377.

84. Gabius, H. J., *Angew. Chem. Int. Ed.* **1988,** *27* (10), 1267-1276.

85. Kataoka, M.; Tavassoli, M., *J. Histochem. Cytochem.* **1984,** *32* (10), 1091-8.

86. Mouricout, M.; Petit, J. M.; Carias, J. R.; Julien, R., *Infect Immun* **1990,** *58* (1), 98-106.

87. Ofek, I.; Hasty, D. L.; Sharon, N., *FEMS Immunol. Med. Microbiol.* **2003,** *38* (3), 181-91.

88. Gabius, H. J., *Biochim. Biophys. Acta* **1991,** *1071* (1), 1-18.

89. Bovin, N. V.; Gabius, H. J., *Chem. Soc. Rev.* **1995,** *24* (6), 413-&.

90. Ogura, A.; Kurbangalieva, A.; Tanaka, K., *Glycoconj J* **2014,** *31* (4), 273-9.

91. Wichterle, O.; LÍM, D., *Nature* **1960,** *185*, 117.

92. Bajpai, A. K.; Bajpai, J.; Saini, R.; Gupta, R., *Polymer Reviews* **2011,** *51* (1), 53-97.

93. Kawaguchi, H., *Prog. Polym. Sci.* **2000,** *25* (8), 1171-1210.

94. Oh, J. K.; Drumright, R.; Siegwart, D. J.; Matyjaszewski, K., *Prog. Polym. Sci.* **2008,** *33* (4), 448-477.

95. Hammer, D. A.; Discher, D. E., *Annual Review of Materials Research* **2001,** *31* (1), 387-404.

96. Behra, M.; Azzouz, N.; Schmidt, S.; Volodkin, D. V.; Mosca, S.; Chanana, M.; Seeberger, P. H.; Hartmann, L., *Biomacromolecules* **2013,** *14* (6), 1927-35.

97. Pussak, D.; Ponader, D.; Mosca, S.; Ruiz, S. V.; Hartmann, L.; Schmidt, S., *Angew. Chem. Int. Ed.* **2013,** *52* (23), 6084-7.

98. Raman, R.; Raguram, S.; Venkataraman, G.; Paulson, J. C.; Sasisekharan, R., *Nature Methods* **2005,** *2*, 817.

99. Alvarez, R. A.; Blixt, O., Identification of Ligand Specificities for Glycan-Binding Proteins Using Glycan Arrays. In *Methods Enzymol.*, Academic Press: 2006; Vol. 415, pp 292-310.

100. Bojarova, P.; Rosencrantz, R. R.; Elling, L.; Kren, V., *Chem. Soc. Rev.* **2013,** *42* (11), 4774-4797.

101. Liang, C.-H.; Wu, C.-Y., *Glycan array: a powerful tool for glycomics studies, Expert Rev. Proteomics 6, 631-645*. 2009; Vol. 6, p 631-45.

102. Oyelaran, O.; Gildersleeve, J. C., *Curr. Opin. Chem. Biol.* **2009,** *13* (4), 406-413.

103. Schallus, T.; Jaeckh, C.; Feher, K.; Palma, A. S.; Liu, Y.; Simpson, J. C.; Mackeen, M.; Stier, G.; Gibson, T. J.; Feizi, T.; Pieler, T.; Muhle-Goll, C., *Mol Biol Cell* **2008,** *19* (8), 3404-14.

104. Manimala, J. C.; Roach, T. A.; Li, Z.; Gildersleeve, J. C., *Glycobiology* **2007,** *17* (8), 17c-23c.

105. Li, Q.; Anver, M. R.; Butcher, D. O.; Gildersleeve, J. C., *Mol Cancer Ther* **2009,** *8* (4), 971-9.

106. Blixt, O.; Kumagai-Braesch, M.; Tibell, A.; Groth, C. G.; Holgersson, J., *American Journal of Transplantation* **2009,** *9* (1), 83-90.

107. Wang, C. C.; Huang, Y. L.; Ren, C. T.; Lin, C. W.; Hung, J. T.; Yu, J. C.; Yu, A. L.; Wu, C. Y.; Wong, C. H., *Proc Natl Acad Sci U S A* **2008,** *105* (33), 11661-6.

108. Chandra, H.; Reddy, P. J.; Srivastava, S., *Expert Rev Proteomics* **2011,** *8* (1), 61-79.

109. Ratto, T. V.; Rudd, R. E.; Langry, K. C.; Balhorn, R. L.; McElfresh, M. W., *Langmuir* **2006,** *22* (4), 1749-1757.

110. Marshall, B. T.; Long, M.; Piper, J. W.; Yago, T.; McEver, R. P.; Zhu, C., *Nature* **2003,** *423* (6936), 190-3.

111. Merkel, R., *Physics Reports* **2001,** *346* (5), 343-385.

112. Binnig, G.; Rohrer, H., *Helvetica Physica Acta* **1982,** *55* (6), 726-735.

113. Binnig, G.; Quate, C. F.; Gerber, C., *Phys. Rev. Lett.* **1986,** *56* (9), 930-933.

114. Israelachvili, J. N., *Intermolecular and surface forces*. Academic Press: London, 1992.

115. Garcia, R.; Calleja, M.; Rohrer, H., *J. Appl. Phys.* **1999,** *86* (4), 1898-1903.

116. Rugar, D.; Hansma, P., *Physics Today* **1990,** *43* (10), 23-30.

117. Hansma, H. G.; Pietrasanta, L., *Curr. Opin. Chem. Biol.* **1998,** *2* (5), 579-584.

118. Binnig, G.; Rohrer, H., *Reviews of Modern Physics* **1999,** *71* (2), S324-S330.

119. Evans, E.; Ritchie, K., *Biophys. J.* **1997,** *72* (4), 1541-1555.

120. Merkel, R.; Nassoy, P.; Leung, A.; Ritchie, K.; Evans, E., *Nature* **1999,** *397* (6714), 50-53.

121. Burnham, N. A.; Chen, X.; Hodges, C. S.; Matei, G. A.; Thoreson, E. J.; Roberts, C. J.; Davies, M. C.; Tendler, S. J. B., *Nanotechnology* **2003,** *14* (1), 1-6.

122. Florin, E.; Moy, V.; Gaub, H., *Science* **1994,** *264* (5157), 415-417.

123. Moy, V.; Florin, E.; Gaub, H., *Science* **1994,** *266* (5183), 257-259.

124. Lee, G. U.; Chrisey, L. A.; Colton, R. J., *Science* **1994,** *266* (5186), 771-773.

125. Oberhauser, A. F.; Marszalek, P. E.; Erickson, H. P.; Fernandez, J. M., *Nature* **1998,** *393* (6681), 181-185.

126. Carrion-Vazquez, M.; Oberhauser, A. F.; Fowler, S. B.; Marszalek, P. E.; Broedel, S. E.; Clarke, J.; Fernandez, J. M., *Proceedings of the National Academy of Sciences of the United States of America* **1999,** *96* (7), 3694-3699.

127. Dammer, U.; Popescu, O.; Wagner, P.; Anselmetti, D.; Guntherodt, H. J.; Misevic, G. N., *Science* **1995,** *267* (5201), 1173-1175.

128. Misevic, G. N., *Microsc. Res. Tech.* **1999,** *44* (4), 304-309.

129. Harada, Y.; Kuroda, M.; Ishida, A., *Langmuir* **2000,** *16* (2), 708-715.

130. Schonherr, H.; Beulen, M. W. J.; Bugler, J.; Huskens, J.; van Veggel, F.; Reinhoudt, D. N.; Vancso, G. J., *J. Am. Chem. Soc.* **2000,** *122* (20), 4963-4967.

131. Johnson, K. L.; Kendall, K.; Roberts, A. D., *Proc. Royal Soc. A* **1971,** *324* (1558), 301-313.

132. Derjaguin, B., *Kolloid-Zeitschrift* **1934,** *69* (2), 155-164.

133. Schmidt, S.; Wang, H.; Pussak, D.; Mosca, S.; Hartmann, L., *Beilstein J. Org. Chem.* **2015,** *11*, 720-729.

134. Fenz, S. F.; Merkel, R.; Sengupta, K., *Langmuir* **2009,** *25* (2), 1074-1085.

135. Smith, A.-S.; Sengupta, K.; Goennenwein, S.; Seifert, U.; Sackmann, E., *Proc. Natl. Acad. Sci. U.S.A.* **2008,** *105* (19), 6906-6911.

136. Curtis, A. S., *J. Cell Biol.* **1964,** *20*, 199-215.

137. Zilker, A.; Engelhardt, H.; Sackmann, E., *J. Phys. France* **1987,** *48* (12), 2139-2151.

138. Radler, J.; Sackmann, E., *J. Phys. II* **1993,** *3* (5), 727-748.

139. Limozin, L.; Sengupta, K., *Chemphyschem* **2009,** *10* (16), 2752-68.

140. Schilling, J.; Sengupta, K.; Goennenwein, S.; Bausch, A. R.; Sackmann, E., *Phys Rev E Stat Nonlin Soft Matter Phys* **2004,** *69* (2 Pt 1), 021901.

141. Born, M.; Wolf, E., *Principles of Optics: Electromagnetic Theory of Propagation, Interference and Diffraction of Light*. 7th ed.; Cambridge University Press: Cambridge, 1999.

142. Cornelesetenvelde, I.; Bonnet, J.; Tanke, H. J.; Ploem, J. S., *Journal of Microscopy-Oxford* **1990,** *159*, 1-13.

143. Theodoly, O.; Huang, Z. H.; Valignat, M. P., *Langmuir* **2010,** *26* (3), 1940-8.

144. Kühner, M.; Sackmann, E., *Langmuir* **1996,** *12* (20), 4866-4876.

145. Kiessling, L. L.; Gestwicki, J. E.; Strong, L. E., *Curr. Opin. Chem. Biol.* **2000,** *4* (6), 696-703.

146. Ratto, T. V.; Langry, K. C.; Rudd, R. E.; Balhorn, R. L.; Allen, M. J.; McElfresh, M. W., *Biophys. J. 86* (4), 2430-2437.

147. Cruje, C.; Chithrani, D. B., *Journal of Nanomedicine Research* **2014,** *1* (1).

148. Shafer, D. E.; Inman, J. K.; Lees, A., *Anal. Biochem.* **2000,** *282* (1), 161-164.

149. Bano, F.; Banerji, S.; Howarth, M.; Jackson, D. G.; Richter, R. P., *Scientific Reports* **2016,** *6*, 34176.

150. Sim, S.-L.; He, T.; Tscheliessnig, A.; Mueller, M.; Tan, R. B. H.; Jungbauer, A., *J. Biotechnol.* **2012,** *157* (2), 315-319.

151. Rajendra, R. B.; Jan, G., *Nanotechnology* **2007,** *18* (2), 025301.

152. Rabe, M.; Verdes, D.; Seeger, S., *Adv. Colloid Interface Sci.* **2011,** *162* (1), 87-106.

153. Siegbahn, K., *Science* **1982,** *217* (4555), 111-21.

154. Touhami, A.; Hoffmann, B.; Vasella, A.; Denis, F. A.; Dufrêne, Y. F., *Langmuir* **2003,** *19* (5), 1745-1751.

155. Majorek, K. A.; Porebski, P. J.; Dayal, A.; Zimmerman, M. D.; Jablonska, K.; Stewart, A. J.; Chruszcz, M.; Minor, W., *Mol Immunol* **2012,** *52* (3-4), 174-82.

156. Sumner, J. B.; Gralen, N.; Eriksson-Quensel, I. B., *Science* **1938,** *87* (2261), 395-6.

157. Yin, L.; Wang, W.; Wang, S.; Zhang, F.; Zhang, S.; Tao, N., *Biosensors & bioelectronics* **2015,** *66*, 412-416.

158. Jeyachandran, Y. L.; Mielczarski, E.; Rai, B.; Mielczarski, J. A., *Langmuir* **2009,** *25* (19), 11614-20.

159. Wang, H.; Jacobi, F.; Waschke, J.; Hartmann, L.; Löwen, H.; Schmidt, S., *Adv. Funct. Mater.* **2017,** *27* (41), 1702040.

160. Jacobi, F.; Camaleno de la Calle, A.; Boden, S.; Grafmuller, A.; Hartmann, L.; Schmidt, S., *Biomacromolecules* **2018**.

161. Hertz, H., *Journal fur die Reine und Angewandte Mathematik* **1882,** *1882* (92), 156-171.

162. Butt, H.-J.; Cappella, B.; Kappl, M., *Surf. Sci. Rep.* **2005,** *59* (1), 1-152.

163. Castells, V.; Yang, S.; R Van Tassel, P., *Surface-induced conformational changes in lattice model proteins by Monte Carlo simulation*. 2002; Vol. 65, p 031912.

164. Tarasevich, Y. I.; Monakhova, L. I., *Colloid J.* **2002,** *64* (4), 482-487.

165. McLeod, A. G.; Walker, I. R.; Zheng, S.; Hayward, C. P., *Haemophilia* **2000,** *6* (2), 89-92.

166. Tzannis, S. T.; Hrushesky, W. J.; Wood, P. A.; Przybycien, T. M., *Proc. Natl. Acad. Sci. U.S.A.* **1996,** *93* (11), 5460.

167. Grigera, J. R.; McCarthy, A. N., *Biophys. J.* **2010,** *98* (8), 1626-31.

168. Cohen, M.; Varki, A., Modulation of Glycan Recognition by Clustered Saccharide Patches. In *International Review of Cell and Molecular Biology, Vol 308*, Jeon, K. W., Ed. Elsevier Academic Press Inc: San Diego, 2014; Vol. 308, pp 75-125.

169. Diehl, H.; Horchak-Morris, N., *Talanta* **1987,** *34* (8), 739-741.

170. Vogelsang, J.; Cordes, T.; Forthmann, C.; Steinhauer, C.; Tinnefeld, P., *Proc Natl Acad Sci U S A* **2009,** *106* (20), 8107-12.

171. Anand, G.; Sharma, S.; Dutta, A. K.; Kumar, S. K.; Belfort, G., *Langmuir* **2010,** *26* (13), 10803-11.

172. Ponader, D.; Wojcik, F.; Beceren-Braun, F.; Dernedde, J.; Hartmann, L., *Biomacromolecules* **2012,** *13* (6), 1845-1852.

173. Gerke, C.; Ebbesen, M. F.; Jansen, D.; Boden, S.; Freichel, T.; Hartmann, L., *Biomacromolecules* **2017,** *18* (3), 787-796.

174. Patrick, B.; Bettina, N.; Valentin, W.; Malte, D., *Angew. Chem. Int. Ed.* **2011,** *50* (36), 8428-8431.

175. Han, X.; Qin, M.; Pan, H.; Cao, Y.; Wang, W., *Langmuir* **2012,** *28* (26), 10020-10025.

176. Ponader, D.; Maffre, P.; Aretz, J.; Pussak, D.; Ninnemann, N. M.; Schmidt, S.; Seeberger, P. H.; Rademacher, C.; Nienhaus, G. U.; Hartmann, L., *J. Am. Chem. Soc.* **2014,** *136* (5), 2008-2016.

177. Kiessling, L. L.; Strong, L. E.; Gestwicki, J. E., *Annual Reports in Medicinal Chemistry, Vol 35* **2000,** *35*, 321-330.

178. Page, D.; Zanini, D.; Roy, R., *Bioorg. Med. Chem.* **1996,** *4* (11), 1949-61.

179. Gerchako.Sm; Hatcher, P. G., *Limnology and Oceanography* **1972,** *17* (6), 938-943.

180. Glaubitz, M.; Medvedev, N.; Pussak, D.; Hartmann, L.; Schmidt, S.; Helm, C. A.; Delcea, M., *Soft Matter* **2014,** *10* (35), 6732-41.

181. Skirtenko, N.; Richman, M.; Nitzan, Y.; Gedanken, A.; Rahimipour, S., *Chem. Commun.* **2011,** *47* (45), 12277-12279.

182. Grandjean, C.; Rommens, C.; Gras-Masse, H.; Melnyk, O., *Tetrahedron Lett.* **1999,** *40* (40), 7235-7238.

183. Ebbesen, M. F.; Gerke, C.; Hartwig, P.; Hartmann, L., *Polym. Chem.* **2016,** *7* (46), 7086-7093.

184. Felix, W.; G., O. B. A.; Sebastian, G.; H., S. P.; Laura, H., *Chem. Eur. J.* **2013,** *19* (9), 3090-3098.

185. Jensen, F. R.; Bushweller, C. H.; Beck, B. H., *J. Am. Chem. Soc.* **1969,** *91* (2), 344-351.

6 EXPERIMENTAL

6.1 MATERIALS

Standard commercial grade reagents and solvents were used without further purification.

PEG linker was obtained from Rapp Polymere (Tübingen, Germany). SMCC linker was acquired from TCI Deutschland GmbH. Methyl α-D-mannopyranoside (Me-Man) was purchased from Alfa Aesar by Thermo Fisher Scientific. Bovine serum albumin (BSA), concanavalin A (Con A), (3-aminopropyl)triethoxysilane (APTES) (≥ 98.0%), (3-glycidyloxypropyl) trimethoxysilane (GLYMO) (≥ 98.0%) and all other chemicals were purchased from Sigma-Aldrich. All water used was produced by the purification system (Barnstead™ MicroPure™ Thermo Scientific™, Germany) with a resistivity higher than 18.2 MΩ·cm at 25 °C.

6.2 METHODS

Glass surface functionalization

For Con A coating, 25 mm diameter round glass slides (Menzel-GmbH, Braunschweig) were cleaned by RCA treatment (water, ammonia, hydrogen peroxide 30%, 5:1:1, 70 °C) for 20 min and then rinsed with water. Then, glass slides were immersed in a mixture of 182.4 mL ethanol, 9.6 mL water, 192 µL acetic acid, and 1920 µL of (3-glycidyloxypropyl)trimethoxysilane, shaken for 120 min, flushed with ethanol, followed by annealing for 180 min at 80 °C. Con A incubation was carried for 60 min at 0.05 mg/mL in PBS pH 7.4, the unreacted proteins were removed by flushing with PBS pH 7.4, 10 mM HEPES pH 7.4 and LBB pH 7.4. Surfaces were held in homemade polytetrafluoroethylene (PTFE) ring-holders sealing a well.

For Con A coating, 8 well glass bottom µ-slides (IBIDI, Martinsried) were cleaned by UV irradiation for 30 min in a UV chamber (Nano Bio Analytics UVC-1014). Then, IBIDI slides were equally treated as described above. Slides were directly used on the microscope.

For carbohydrate ligand coating, 8 well glass bottom µ-slides (IBIDI, Martinsried) were cleaned by UV irradiation as described above. Then, IBIDI slides were immersed in a mixture of 90.0 mL isopropanol, 10.0 mL water, and 466 µL of (3-aminopropyl)triethoxysilane (APTES), shaken for 60 min, flushed with isopropanol, followed by annealing for 180 min at 80 °C. Heterobifunctional linkers were incubated for 60 min at 5 mM; succinimidyl 4-(*N*-maleimidomethyl)cyclohexane-1-carboxylate (SMCC) in DMSO and α-maleinimidohexanoic-ω-NHS PEG (PEG) in PBS pH 8.0, the unreacted linkers were removed by flushing with water. Thiol-functionalized sugar molecules

were incubated for 60 min at 5 mM in PBS pH 7.4. For surface sugar dilution 2-mercaptoethanol and 1,4-dithio-D-threitol were used to lower the sugar concentration. Unreacted molecules were removed by flushing with PBS pH 7.4, 10 mM HEPES pH 7.4 and LBB pH 7.4.

Preparing AFM tips for Single Molecule – Atomic Force Microscopy

Silicon cantilevers of nominal spring constant of 0.2 N/m (HQ:XSC11/No Al μMash, Estonia) were cleaned by UV irradiation for 15 min in a UV chamber (Nano Bio Analytics UVC-1014). Instantly after, cantilevers were immersed in a solution of 13.5 mL propan-2-ol, 1.2 mL water and 70 μL of (3-aminopropyl)triethoxysilane (APTES) for 30 min and latterly rinsed with isopropanol, dried under nitrogen and annealed for 30 min at 110 °C. The cantilevers were cooled down to RT and immersed in heterobifunctional PEG linker solution (40 μL of 50 mM α-maleinimidohexanoic-ω-NHS PEG in PBS pH 8.0) for 60 min, immediately after, flushed with water, dried under nitrogen and immersed in the sample solution made of 4 μL of 100 μM thiol functionalized glicomacromolecule, 16 μL of 100 μM 2,2'-(ethylenedioxy)diethanethiol, both in water, and 20 μL of PBS pH 7.4 for 120 min at room temperature. Then, cantilevers were flushed with PBS pH 7.4 and water, and preserved in 4 °C water until used within following 48 h.

Single-Molecule – Atomic Force Microscopy

AFM force curves were tracked operating in "force map" mode using the previously described modified silicon cantilevers. Experiments were run in LBB pH 7.4 at RT after 30 min equilibration step. The force curves (n>500) were recorded at constant speed mode of 1 μm/s for both approaching and retracting motion, an extended delay of 5 s at constant force delay mode, a sampling rate of 5000 Hz, a release setpoint force of 0.5 nN and a z-piezo-range of 3 nm. The thermal noise calibration for real spring constant was performed with the second harmonic; correction factor 0.251. Force curves were corrected and treated with the software supplied by the AFM manufacturer by 1) deflection recalibration, sensitivity, and spring constant adjustment, 2) baseline subtraction, 3) distance offset adjustment, 4) slope and height of curves fitting and offset correction, and 5) height for cantilever bending correction. Unspecific interactions between the tip and substrate were discarded by individually selecting curves reaching the baseline before further disconnection steps (baseline criteria) and only these disconnection steps were later considered. A second constrain delimited the tip-substrate height at which disconnections steps were considered due to glycomacromolecule sizes (distance criteria: 50–100 nm for oligomers, 50–200 nm for polymers). The last constraint in energy discarded non-representative disconnection events over 400 pN. The inhibiting concentrations while validation were 0, 10 and 100 mM MeMan.

Synthesis of neoglycoproteins

NGPs were synthesized starting from a 1 mg/mL BSA solution in LBB pH 7.4 that was mixed overnight. 100 µL of 1.5 mg/mL SMCC in DMSO for NGPs functionalized with the sort crosslinker or 100 µL of 5 mg/mL heterobifunctional PEG in LBB pH 7.4 for the NGPs functionalized with the long crosslinker were reacted for 30 min at room temperature while mixing. Immediately afterward, 900 µL of 5 mM thiol functionalized sugar ligand in PBS pH 7.4 were added to the reaction and mixed for 15 min after which and without delay, 15 µL of RBITC at 1 mg/mL in DMSO were added and mixed in the dark overnight. NGP solutions were individually crossed through LBB pH 7.4 equilibrated desalting columns (PD-10 desalting columns, GE Healthcare) in spin mode to get rid of unreacted molecules and possible precipitates. The recovered eluents were considered stock NGPs solutions for further applications.

Neoglycoproteins for ^{1}H-NMR characterization

The chemical procedure to obtain NGPs was tested by means of NMR. A ^{1}H nmR spectrum was performed either to the bare starting BSA protein and the final NGP lacking the fluorescent marker; with a Bruker AVANCE III - 600. For that, neoglycoprotein without the fluorescent label was synthesized with the multivalent glycooligomer **O2** and the short SMCC linker (BSA-SMCC-O2 sample, see Figure 55) through the method mentioned above. BSA-SMCC-O2 sample for ^{1}H NMR was dialyzed with a 5 kDa molecular weight cut-off membrane (Vivaspin® 2, Sartorius) to ensure complete removal of unreacted sugar, linker and sugar-linker molecules from the system; which highest molecular weight was of 2.1 kDa. BSA-SMCC-O2 was freeze-dried after the dialysis, 7.8 mg were recovered and re-dissolved in 600 µL D_2O. The same amount of stock BSA was dissolved in 600 µL D_2O for the NMR test. The linked multivalent glycooligomer **O2** presents two mannose moieties grafted to the backbone through Copper(I)-catalyzed azide-alkyne cycloaddition (CuAAC). The comparison of spectra unambiguously revealed imidazole proton signals for BSD sample, which are the result of the CuAAC reaction proving the unambiguous synthesis of NGPs, see ^{1}H NMR spectra of BSA and BSA-SMCC-O2 in Figure 26.

Characterization of Neoglycoproteins via UV-Vis

UV-Vis spectra for neoglycoprotein characterization was performed in a UV-Vis spectrometer filling a QX quartz crystal cuvette. Absorption values were integrated for 10 ms, with 1 nm slit, at 10 nm/s and Δλ of 0.1 nm covering the spectral range from 200 to 700 nm. Deuterium/halogen lamp change was produced at 320 nm. A reference baseline with LBB was set for correcting. For determination of protein concentration and fluorescence degree of labeling the stock neoglycoprotein solutions from size exclusion purification were analyzed and correlated through

their extinction coefficients. BSA: λ_{max}=280 nm, ε=43824 $M^{-1}cm^{-1}$. RBITC: λ_{max}=555 nm, ε=106000 $M^{-1}cm^{-1}$, correction factor of 0.34. For mannose determination, the procedure was adapted from[179]. 167 µL of the stock sample was digested with 167 µL of a 5% phenol in water solution and 835 µL of 95% sulfuric acid for 30 min in a bath at 30 °C. The maximum absorption of complex products at λ=490 nm was determined and correlated with a calibration line in the range of 5-100 µg/mL, Figure 66.

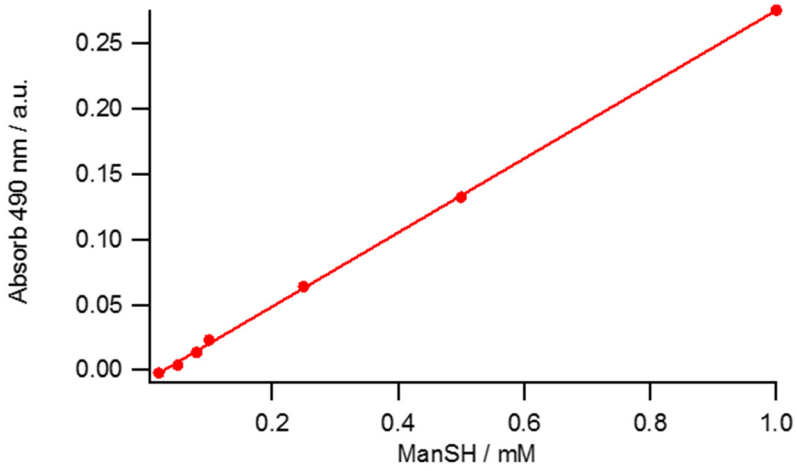

Figure 66- Calibration line and fitting for mannose determination in the range of 5-100 µg/mL. The absorption was determined at λ=490 nm for digested samples with a 5% vol. solution of phenol in water and 95% sulfuric acid solution in a 1:1:5 ratio. The mixture was incubated for 30 min at 30 °C. The fitting line was calculated by the least squares method resulting in the following values ± standard error. Slope: 0.28304015 ± 0.001963375, interception: -0.008297736 ± 0.000857597 and r^2: 0.999759466.

Turbidity assay

Turbidity assay via UV−Vis spectroscopy was performed with a 0.55 mg/ml Con A dissolved in LBB pH 7.4 solution and tracked at λ=420 nm. A reference baseline of LBB was set. 1 mL of Con A solution was transferred to a 1.5 mL QX quartz crystal cuvette and placed in the spectrometer. For 5 min the absorption was recorded to prove the steady state. 0.5 mL of 4 µM sample solution in LBB pH 7.4 were added, mixed thoroughly by pipetting and immediately after, the absorbance was recorded over a period of 30 min, missing the starting seconds. Absorption values were integrated for 100 ms, with 1 nm slit, at 5 Hz.

Fluorescence assay

A DM IRE2 inverted microscope (Leica, Germany) was used to determine the fluorescence of the SCP surface from the binding of fluorescent NGPs. For illumination, a xenon lamp (Leica, Germany) was used as a light source in series with Rhodamine fluorescence filters (R/G – TRITC). An HCX PL APO 63x/1.32-0.6 oil objective (Leica, Germany), fluorescent free immersion oil

(Cargille, USA) and AxioCam MRc (Zeiss, Germany) were used to determine the fluorescent intensity. Focusing at the half height of the respective particles two images were obtained for each SCP. First, a transmission mode image was taken to determine the area on where later to integrate the fluorescent intensity in terms of grayscale. The second image was taken in fluorescent mode at the same focal plane by simply changing the filter with an integration time of 500 ms, a gain of 200 and an offset of 240. Images with fluorescent intensities were integrated using a public image processing software (ImageJ, USA).

Individually in 50 µL of Con A-SCP solution in LBB pH 7.4 either at 0.0 mM and 10.0 mM MeMan, 10 µL of the respective NGP solutions were added and mixed thoroughly by pipetting. The mixture was incubated overnight at 4 °C in the dark and equilibrated at room temperature before determining the fluorescence. For fluorescence determination, 20 µL were transferred into a microscope well (µ-slide 18 well flat, IBIDI, Martinsried).

Synthesis and functionalization of Soft Colloidal Probes

The macromonomer Poly(ethylene glycol)-diacrylamide[1] (PEG-dAAm) stored at –20 °C under a nitrogen atmosphere was warmed up to room temperature. 50 mg of PEG-dAAm and 1.2 mg Irgacure® 2595 were diluted in 10 mL of 1 M sodium sulfate solution and shaken to create a microparticle dispersion. The dispersion was transferred into a glass vial and particles were polymerized irradiating for 180 s in a UV chamber HiLite power (Heraeus Kulzer, Germany). The resulting PEG SCP dispersion was 10x washed with type I water to remove the sulfate solution. The washing process was performed by centrifuging each round for 15 min at 3000 RCF, shaking the dispersion for 30 min in between rounds.

Grafting crotonic acid. The water SCP dispersion was gradually exchanged with 2:1, 1:1, 1:2 mixtures of water/ethanol in vol. into pure ethanol by centrifugation and the following protocol was repeated three times in a row. SCPs were redispersed in 10 mL ethanol containing 25 mg benzophenone and 150 mg crotonic acid. The dispersion was transferred into a glass vial and 6x irradiated for 180 s in a UV chamber. Degasification was performed bubbling nitrogen for 60 s at the beginning and 30 s in between rounds. After the very last irradiation step (18^{th}), the dispersion was 15x washed with pure ethanol, shaking for 30 min in between rounds. Finally, the SCPs were gradually dispersed into water with 2:1, 1:1, 1:2 in vol. mixtures of ethanol/water. All the SCP samples achieved CA functionalization degrees over 45 µmoles/g.

[1] Poly(ethylene glycol)-diacrylamide was synthesized and characterized by Hanqing Wang (Ph.D. student, group of Prof. Dr. Laura Hartmann, Heinrich-Heine-Universität Düsseldorf).

Functionalization of SCPs with amine functionalized carbohydrates. 3 mL CA-SCP dispersion in water were exchanged into dimethylformamide (DMF) by 3x centrifugation. 3.12 mg (6 µmol) benzotriazol-1-yl-oxytripyrrolidinophosphonium hexafluorophosphate (PyBOP) and 0.45 mg (3 µmol) hydroxybenzotriazole (HOBt) were added to the dispersion and dissolved. Then, 1.05 µL (6 µmol) *N*,*N*-diisopropylethylamine (DIPEA) were added to the dispersion and shaken for 5 min. 5.57 mg (6 µmol) of amino-functionalized mannose were added and reacted for 180 min while shaking. Afterward, SCPs were washed 3x with DMF and 3x with methanol. 0.65 mg (12 µmol) of sodium methoxide were added, and the dispersion was shaken for 30 min. SCPs were washed 3x with methanol and 3x with water. Sugar functionalized SCPs were stored at 4 °C in water containing 0.01% sodium azide.

Functionalization of CA-SCPs with Con A. 2 mL CA-SCPs in water were dispersed in MES buffer pH 5.5 (0.1 M 2-(*N*-morpholino) ethanesulfonic acid) 3x exchanging the solvent by centrifugation. 23.02 mg (0.1 M) *N*-Hydroxysuccinimide (NHS) and 38.2 mg (0.1 M) 1-Ethyl-3-(3-dimethylaminopropyl) carbodiimide (EDC) were added into the dispersion and shaken for 60 min at room temperature. The dispersion was 3x washing with MES buffer. Then, the SCP pellet was resuspended in a previously prepared 10 mg/mL protein solution in phosphate buffer pH 8.0 (0.1 M sodium phosphate). The unreacted proteins were 3x washed with PBS pH 7.4 (10 mM sodium phosphate, 2.7 mM potassium chloride and 137 mM sodium chloride). The dispersion of SCPs in PBS buffer was firstly 3x exchanged with water, then 3x with HEPES (10 mM) pH 7.4 and finally 3x with LBB pH 7.4. Con A functionalized SCPs were stored at 4 °C in LBB containing 0.01% sodium azide.

Young's Modulus determination of Soft Colloidal Probes

AFM force measurements were performed in combination with an optical microscope. First, a tipples cantilever with a spring constant of 0.3 N/m (Nanoworld AG, Switzerland) was cleaned for 30 min in a UV Ozone chamber (Nano Bio Analytics UVC-1014). Then, a glass bead (diameter: 4.75 µm) was adhered with epoxy glue onto the cantilever.

For the measurement, 20 µL of the SCP dispersion were added into 3 mL of LBB pH 7.4 in a petri dish. Images at the half height of the SCPs were recorded to determine their respective diameter with the image processing software ImageJ. Being R_{SCP} the radius of the SCP, and R_{tip} the radius of the glass bead, the effective tip radius R_{eff} can be calculated with the following equation:

$$\frac{1}{R_{eff}} = \frac{1}{R_{tip}} + \frac{1}{R_{SCP}} \qquad (8)$$

Knowing the sensitivity of the tip, the spring constant of the tip and effective radius, the force curve was fitted with the Hertzian model developed by Glaubitz et al.[180] to determine the elastic modulus. The sensitivity of the tip was calibrated every time the tip entered into the aqueous phase. Ten SCPs were analyzed for each batch, and their average was determined as the corresponding Young's modulus.

Toluidine Blue O colorimetric test

Approximately 0.5 mL of carboxylic group functionalized SCPs dispersion were washed with ethanol and dried for 6 h under vacuum at 35 °C until a stable weight of the dry SCPs. A 12.5 mM toluidine blue O (TBO) solution was prepared at pH 10–11 with 1 M NaOH. 1 mL of a 1:40 dilution with type I water pH 10.5 of the prepared TBO solution was added to the dry SCPs and shaken overnight in the dark. The stained SCP dispersion was centrifuged and 0.3 mL of the supernatant was diluted with 1.7 mL of type I water. As a reference, 0.3 mL of the 1:40 diluted TBO solution were newly diluted with 1.7 mL of type I water. The absorbance at λ=633 nm of both solutions was determined with a UV-VIS spectrometer and compared. All the SCP samples achieved CA functionalization degrees over 45 µmoles/g.

Determination of adhesion energy of Soft Colloidal Probes – SCP-Adhesion

An inverted microscope was used to obtain images of the contact area between the SCPs and the glass coverslip surfaces. For illumination, objective and camera see the instrumentation part. In order to conduct the JKR measurements of the adhesion energies, the contact radius was determined, and the particle radius was calculated from the interference fringe pattern. Images with RICM patterns were read out using self-written image analysis software, contact areas and particle profiles were evaluated using scripted peak finding algorithms (IgorPro Wavemetrics, USA).

Protein surface stability. The SCPs were added after 5 min equilibration, and the images of the adhesion area were tracked afterward. Series of slightly aggressive water flushing steps, buffer equilibration and determine the adhesion energy determination were steadily performed. In the very last round, a 10 mM MeMan solution in LBB was used to equilibrate and inhibit the protein surface.

Carbohydrate surface density. Experiments were performed in 8 well glass bottom µ-slides containing 300 µL LBB. SCPs were added and after an equilibration time of 60 min images of adhesion area were tracked (t=0). Sets of 15 SCP images were tracked after 120 min (t=1) and 600 min (t=2) of SCP addition.

Adhesion inhibition with NGPs, oligomers and monovalent ligands. Experiments were performed in 8 well glass bottom µ-slides containing 300 µL LBB. 20 µL SCP solution were added and after an equilibration time of 60 min and images of adhesion area were tracked (t=0). Afterward, about 20 µL of the appropriate NGP solutions to reach a final concentration of 0.05 mg/mL were carefully added. In competition tests with oligomers, 20 µL of 1 mM solution in LBB were added reaching a final concentration of 62.5 µM. Sets of 15 SCP images were tracked after 60 min (t=1) and 600 min (t=2) of NGP or oligomer addition.

Determination of hydrodynamic radius

The hydrodynamic radius of oligomer and polymer samples was determined by dynamic light scattering. Sample solutions of 10 mg/mL were prepared in MilliQ water and analyzed for 5 min. The experiments were run with a channel width of 4.3 µs, at 20 °C and a scattering detection angle of 90°. The liquid viscosity was assumed as 1 CP and the refraction index as 1.344. The data analysis was performed using an exponential fit with cumulant.

Synthesis of thiol-terminated mannose oligomers[2,3] and polymers[4]

The oligomers were synthesized via solid phase synthesis following the established protocols of the Hartmann group.[172] Tailor-made functional building blocks were gradually reacted in a sequence-defined backbone. Then, azide functionalized mannose moieties were introduced via 1,3-dipolar cycloaddition. The obtained yields for the oligomers were between 27 and 34% with greater purities than 92% after cleavage from the resin and double precipitation in diethyl ether as determined by RP-HPLC. Glycooligomers were also analyzed by ^{1}H-NMR and HRMS. For all the analysis see section 7.2 Characterization of sequence-define glycooligomers. The batch sizes for synthesizing the oligomers using solid phase synthesis were of 0.1 mmol for SM-AFM assays, section 3.2.2, and 0.3 mmol for NGP assays, section 3.2.3; both resulted in the same purity and analysis. The yield for **O5** in the batch for NGP assays decreased in an 8% due to the presence of a compound fraction missing one TDS building block with its corresponding Man moiety.

[2] Thiol-terminated mannose oligomers for SM-AFM assays, section 3.2.2, were synthesized and characterized (NMR, RP-HPLC and MALDI-TOF) by Jennifer Materlik (BSc student, group of Prof. Dr. Laura Hartmann, Heinrich-Heine-Universität Düsseldorf).

[3] Thiol-terminated mannose oligomers for NGP assays, section 3.2.3, were re-synthesized and characterized (NMR, RP-HPLC and MALDI-TOF) by the author of this thesis.

[4] Thiol-terminated mannose polymers were synthesized and characterized (NMR, RP-HPLC and MALDI-TOF) by

Christoph Gerke (PhD student, group of Prof. Dr. Laura Hartmann, Heinrich-Heine-Universität Düsseldorf).

The polymers were synthesized via photoinduced thiol−ene coupling (TEC) by the protocol of Gerke et al.[173] Sequence-defined mannose-bearing oligomers were alternated with another hydrophilic spacer oligomer resulting into the final polymers. For detailed analytical data of the glycopolymers, see Supporting Information from previous work.[173]

For the synthesis of oligomers and polymers in the present work, EDS[183], DDS[184], TDS[172] building blocks are employed as well as and 2-azidoethyl-α-D-Mannopyranoside.[172]

Synthesis of thiol-functionalized mannose

Mannose thiol was synthetized glycosylating 2-bromoethanol with peracylated mannose and later reacting it with thioacetic acid; applying the protocols of Skirtenko et al.[181], Figure 67. The starting peracetylated mannose was synthesized with the procedure of Grandjean et al.[182] The obtained batch size was of 20 mmol. Mannose thiol was analyzed by ^{1}H NMR and HRMS, see section 7.1.

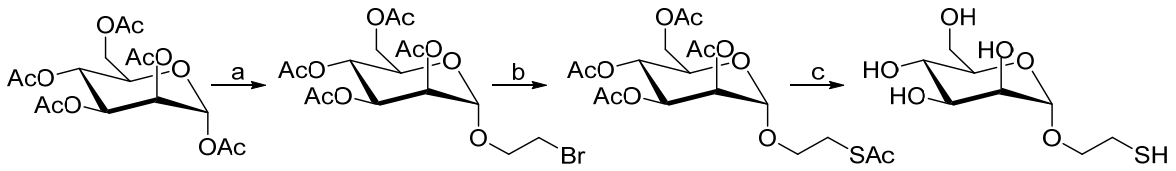

Figure 67- Synthesis of mannose thiol. Reagents and conditions: a. 2-bromo propanol, BF3.Et2O, CH2Cl2, 72h, rt, 65%; b. Cesium carbonate, thioacetic acid, DMF 0 °C, 12h, rt, 66%; c. NaOMe, MeOH, 89%.

6.3 INSTRUMENTATION

X-ray Photoelectron Spectroscopy (XPS)

XPS spectra for lectin and sugar surface functionalization protocols were recorded with an ESCALAB 5 device (VG-Instruments). The X-ray source was operated at an electron acceleration voltage of 11 keV at a current of 20 mA with resulting photon energy of 1486.7 eV (Al-Kα) and a step energy of 0.5 eV. The analyzer pass energy was set to 50 eV. Every sample was scanned three times with a Dwell of 200 ms. Spectra were treated with CasaXPS software. Background and line fitting shape information is not provided due to the non-quantitative purposes.

Atomic Force Microscopy (AFM)

Force-distance curves for SM-AFM and elastic moduli determination were tracked on a Nanowizard III (JPK Instruments AG, Berlin, Germany) operating in force mode (trade mark by JPK instruments AG). The sensible parameters for the assays such as speed, extended delay, sampling rate, set point force and data treatment are described in the corresponding method section.

Ultra Violet – Visible spectroscopy (UV-Vis)

All UV-Vis spectra for neoglycoprotein characterization, turbidity, and TBO colorimetric assays were performed in a Spedcord® 210 PLUS dual-beam spectrometer (Analytik JENA AG) with a QX quartz crystal cuvette. The analytical parameters of each assay are previously described in the method section.

Optical Microscopy

An IX 73 inverted microscope (Olympus, Japan) was used to conduct the SCP-Adhesion assay. For illumination, a monochromatic collimated LED (530 nm, Thorlabs, Germany, M530L2-C1) was used as a light source. An UPlanFL N 60x/0.90 dry objective (Olympus Corporation, Japan), and uEye CMOS camera (IDS Imaging Development Systems GmbH, Germany) were used to image.

Nuclear Magnetic Resonance spectroscopy (NMR)

All ^{1}H NMR spectra were recorded on a Bruker AVANCE III – 600 MHz. The chemical shifts of all NMR spectra were reported in parts per million (ppm). The solvent for ^{1}H NMR analysis was deuterated water, used as an internal standard (4.79 ppm). Being the following abbreviations used in the Supporting Information to indicate the multiplicities: s, singlet; d, doublet; t, triplet; m, multiplet.

Reversed Phase – High Pressure Liquid Chromatography – Mass Spectrometry (RP-HPLC-MS)

Measurements were completed with an Agilent 1260 Infinity. The device integrates a variable wavelength detector (VWD) set at 214 nm and a 6120 Quadrupole LC/MS with an Electrospray Ionization (ESI) source operating in positive ionization mode. The used HPLC column was a MZ-Aqua Perfect C18 (3.0×50 mm, 3 µm) RP Column from MZ Analysetechnik. The mobile phases A and B were respectively H_2O/ACN (95/5) and H_2O/ACN (5/95), both containing 0.1% of formic acid. The analysis flow rate was of 0.4 mL/min starting at 100% mobile phase A. The linear gradient reached 50% mobile phase B at 30 min. The temperature of the column was of 25 °C. UV and MS spectral analysis was done within the OpenLab ChemStation software for LC/MS from Agilent Technologies.

Preparative Reversed Phase – High Pressure Liquid Chromatography (Preparative RP-HPLC)

Purification of glycooligomers was performed with an Agilent 1260 Infinity instrument. The device integrates a variable wavelength detector (VWD) set at 214 nm and an automated fraction collector (FC). The used RP-HPLC column was a CAPCELL PAK C18 (20×250 mm, 5 µm). The mobile phases A and B were respectively H_2O and ACN. The process flow rate was of 20 mL/min, and the gradients were varied for each compound.

Ultra High Resolution – Mass Spectrometry (UHR-MS)

UHR-MS measurements were performed with a Bruker UHR-QTOF maXis 4G instrument with a direct inlet via syringe pump, an ESI source and a quadrupole followed by a Time Of Flight (QTOF) mass analyzer.

Dynamic Light Scattering (DLS)

DLS analysis was performed with a PSS Nicomp ZLS Z3000 device using a laser illumination at 660 nm.

7 SUPPORTING INFORMATION

7.1 CHARACTERIZATION OF THIOL-FUNCTIONALIZED MANNOSE

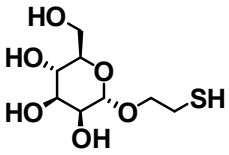

Mannose thiol (ManSH) was obtained in a yield of 36%. ^{1}H nmR (600 MHz, D_2O): 4.92 (d, *J*=1.64 Hz, 1H, anomeric), 3.97 (dd, *J*=1.75 Hz, 3.50 Hz, 1H, H2), 3.89 (d of d, *J*=1.97 Hz, 11.85 Hz, 1H, H3), 3.87 – 3.80 (m, 2H), 3.79 – 3.63 (m, 4H, next to O), 3.02-2.72 (t + m, 2H, Cα to -SH). The anomeric proton signal appears doubled (Δ*J*=4.85 Hz) while the ring protons present a complex multiplicity as a consequence of the cyclohexane conformations [185]. Not integrated signals correspond to solvent traces.

HR-ESI-MS for $C_8H_{16}O_6S$ (exact monoisotopic mass 240.0668): $[M+Na]^{1+}$ calcd. 263.0565, found 263.0560, mass accuracy -0.05 ppm.

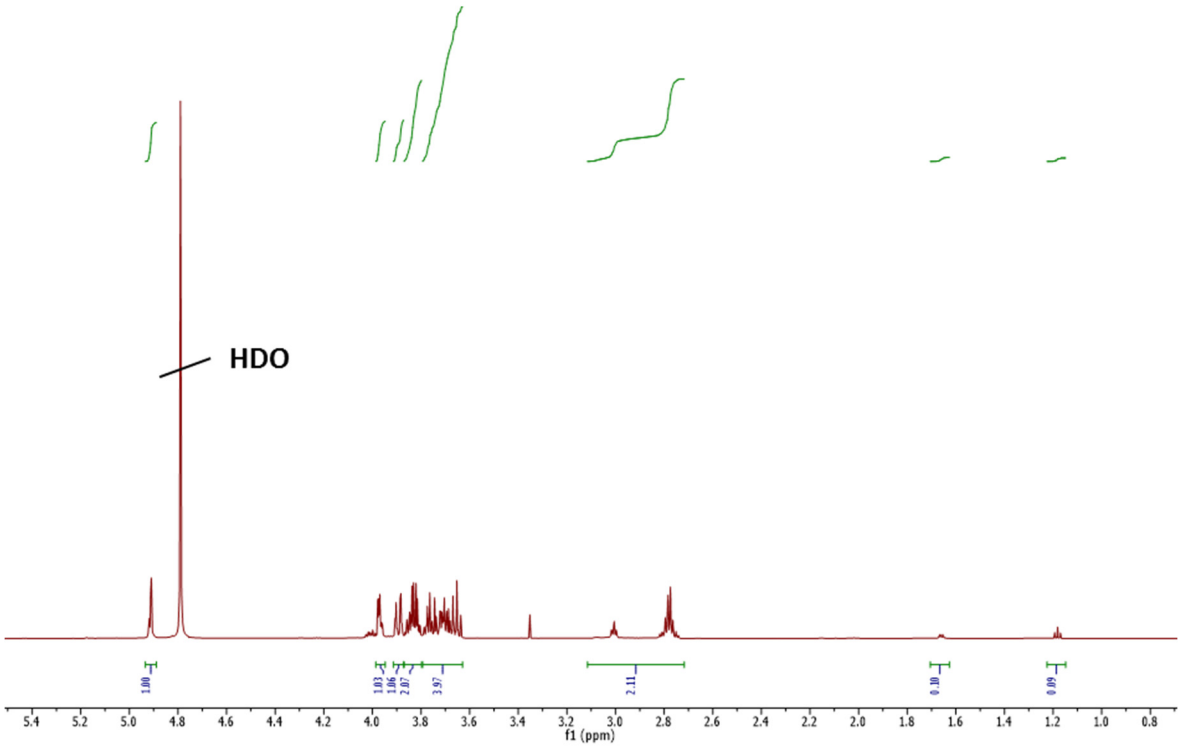

Figure SI 1- ^{1}H-NMR (600 MHz, D_2O) of compound ManSH.

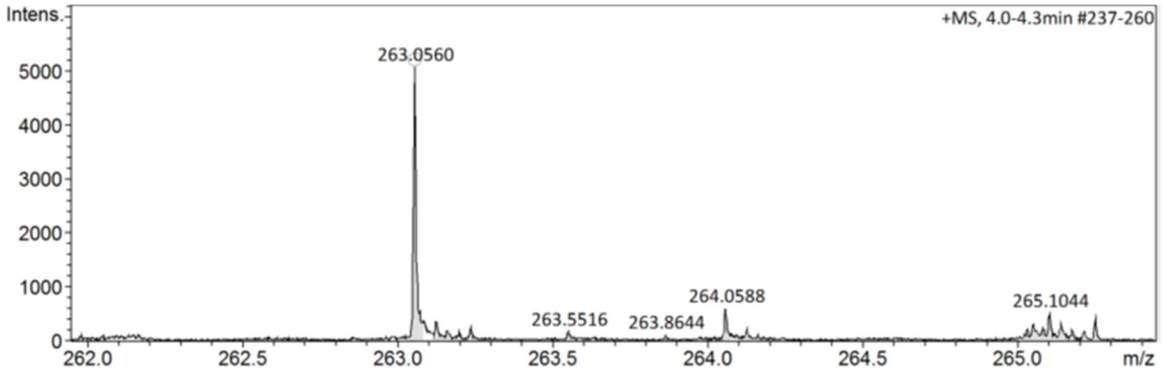

Figure SI 2- HR-MS (ESI) of compound ManSH.

7.2 CHARACTERIZATION OF SEQUENCE-DEFINE GLYCOOLIGOMERS

Glycooligomer O1

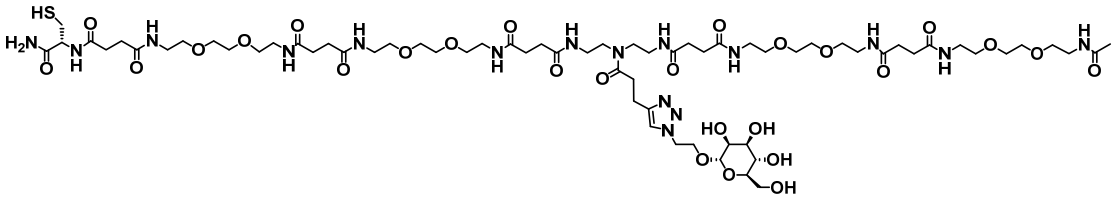

Glycooligomer **O1** was purified via preparative HPLC obtaining a yield of 31%. The anomeric proton of mannose (A) could not be examined in ^{1}H-NMR due to the overlaying signal from the residual solvent. ^{1}H nmR (600 MHz, D_2O): δ 7.88 (s, 1H), 4.70 – 4.58 (m, 2H), 4.53 – 4.47 (m, 1H), 4.15 – 4.04 (m, 1H), 3.96 – 3.90 (m, 1H), 3.88 – 3.83 (m, 1H), 3.77 – 3.71 (m, 1H), 3.71 – 3.58 (m, 35H), 3.52 – 3.44 (m, 4H), 3.43 – 3.32 (m, 20H), 3.06 – 3.02 (m, 1H), 3.01 (t, *J*=7.4 Hz, 2H), 2.98 – 2.88 (m, 2H), 2.80 (t, *J*=7.3 Hz, 2H), 2.67 – 2.43 (m, 20H), 2.00 (s, 3H) ppm.

HR-ESI-MS for $C_{66}H_{116}N_{16}O_{27}S$ (exact monoisotopic mass 1596.7917): $[M+2H]^{2+}$ calcd. 799.4031, found 799.4028, mass accuracy -0.38 ppm.

RP-HPLC (linear gradient from 0 - 50% eluent B in 30 min at 25 °C): Compound **O1** t_R=12.0 min (89%) and dimer of compound **O1** due to a disulfide formation t_R=13.1 min (7%). Determined purity (Sum of compound **O1** and its dimer): 96%.

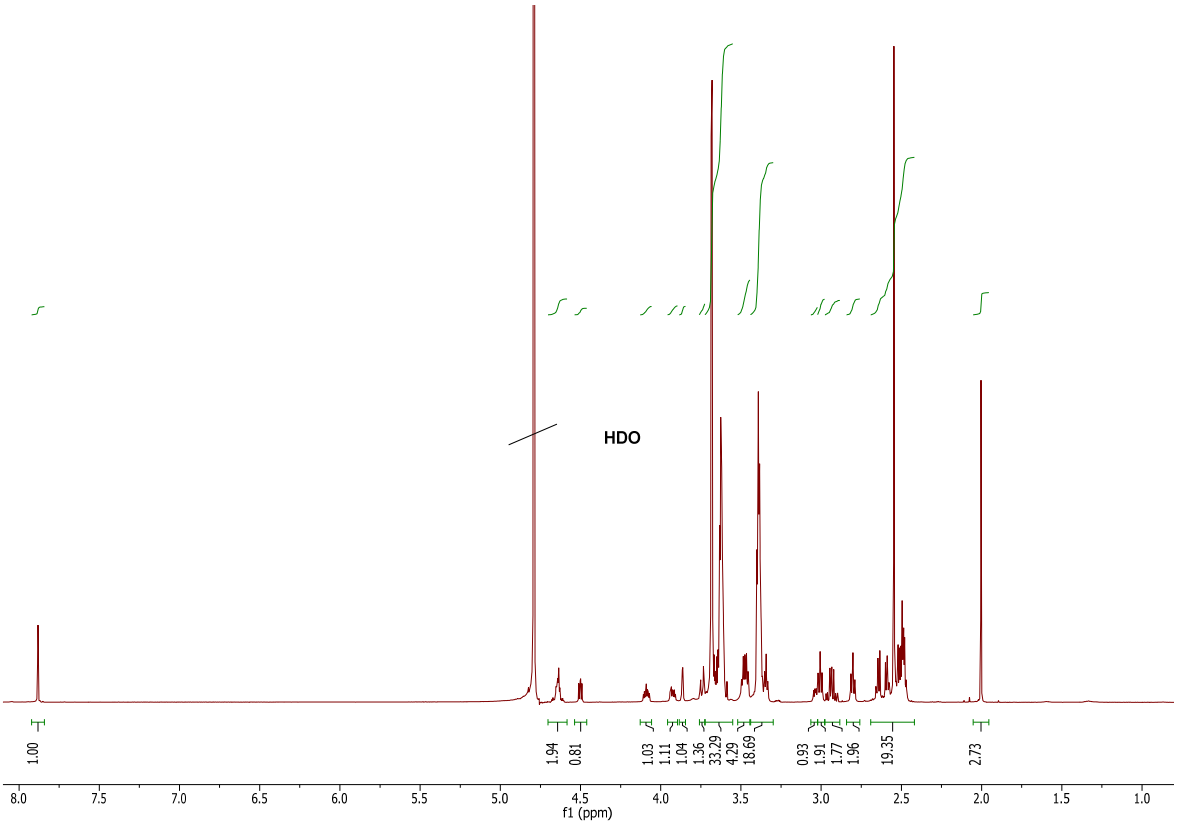

*Figure SI 3- ^{1}H-NMR (600 MHz, D_2O) of compound **O1**.*

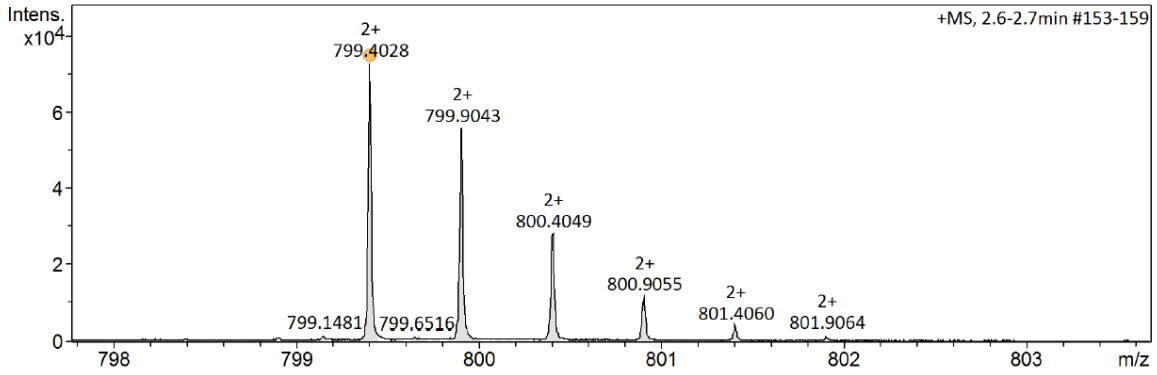

*Figure SI 4- HR-MS (ESI^{+} Q-TOF) of compound **O1**.*

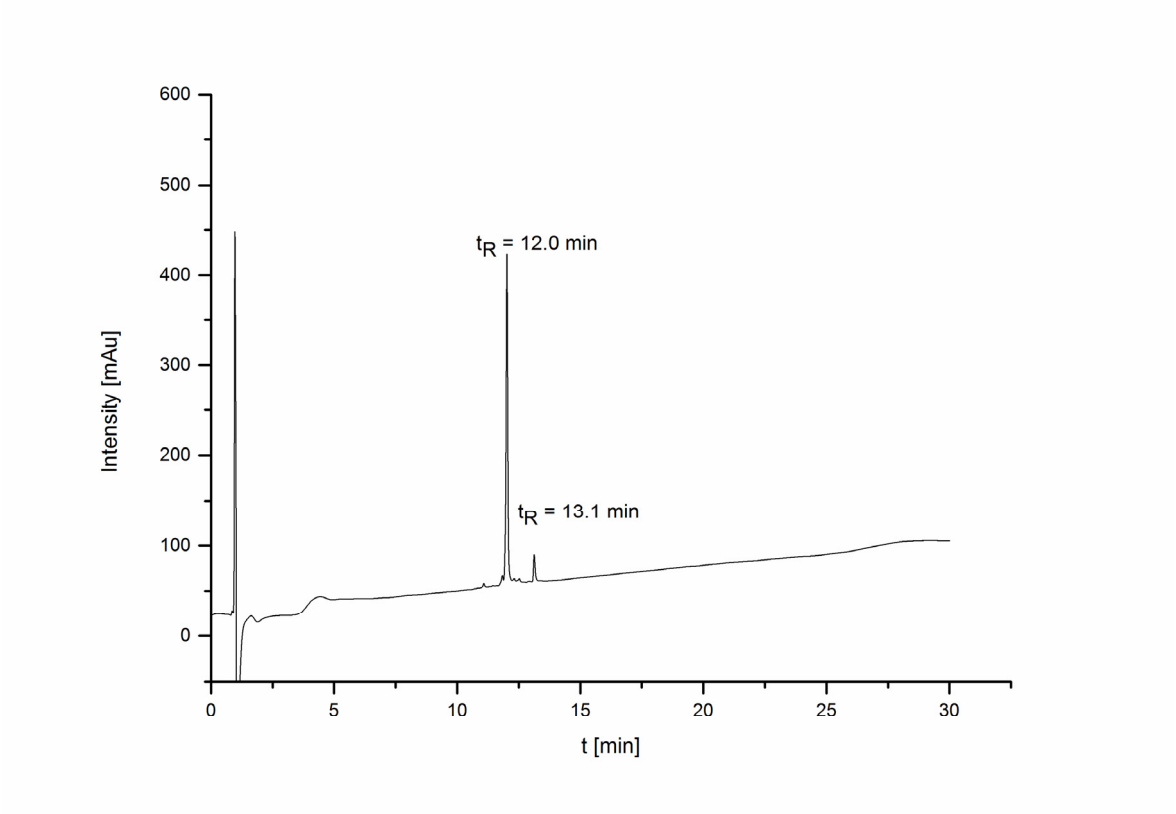

*Figure SI 5- RP-HPLC analysis (linear gradient from 0 - 50% eluent B in 30 min at 25 °C) chromatogram of compound **O1** and its dimer due to disulfide formation with their retention times.*

Glycooligomer O2

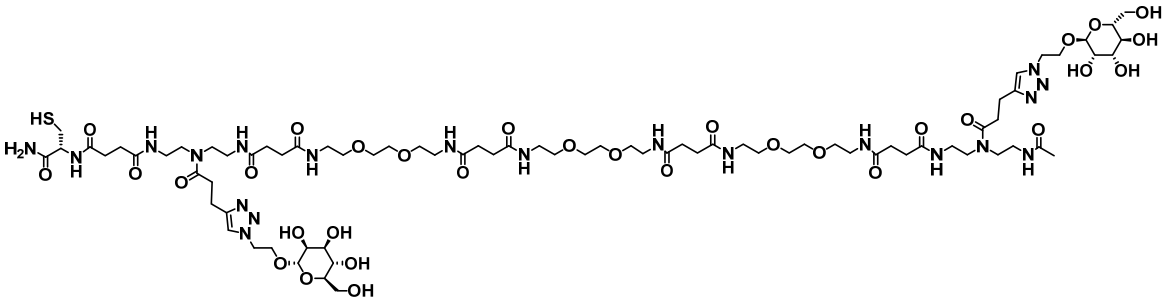

Glycooligomer **O2** was purified via preparative HPLC obtaining a yield of 27%. The anomeric proton of mannose (A) could not be examined in ^{1}H-NMR due to the overlaying signal from the residual solvent. For the acetyl group on the N-terminal end, we observed two singlets with a ratio of 1:1 that we assign to two rotational isomers in equal amounts. The presence of rotational isomers was identified in ^{1}H-NMR experiments at higher temperatures (data not shown). ^{1}H nmR (600 MHz, D_2O): δ 7.87 (s, 2H), 4.69 – 4.58 (m, 4H), 4.52 – 4.45 (m, 1H), 4.13 – 4.05 (m, 2H), 3.96 – 3.89 (m, 2H), 3.88 – 3.84 (m, 2H), 3.77 – 3.71 (m, 2H), 3.71 – 3.54 (m, 30H), 3.53 – 3.43 (m, 8H), 3.43 – 3.30 (m, 20H), 3.09 – 3.03 (m, 2H), 3.01 (t, *J*=7.4 Hz, 4H), 2.97 – 2.88 (m, 2H), 2.84 – 2.77 (m, 4H), 2.65 – 2.44 (m, 20H), 1.95 + 1.93 (2s, 3H) ppm.

HR-ESI-MS for $C_{77}H_{132}N_{20}O_{32}S$ (exact monoisotopic mass 1880.9037): $[M+3H]^{3+}$ calcd. 627.9752, found 627.9751, mass accuracy -0.16 ppm.

RP-HPLC (linear gradient from 0 - 50% eluent B in 30 min at 25 °C): Compound **O2** t_R=11.5 min (78%) and dimer of compound **O2** due to a disulfide formation t_R=12.4 min (17%). Determined purity (Sum of compound **O2** and its dimer): 95%.

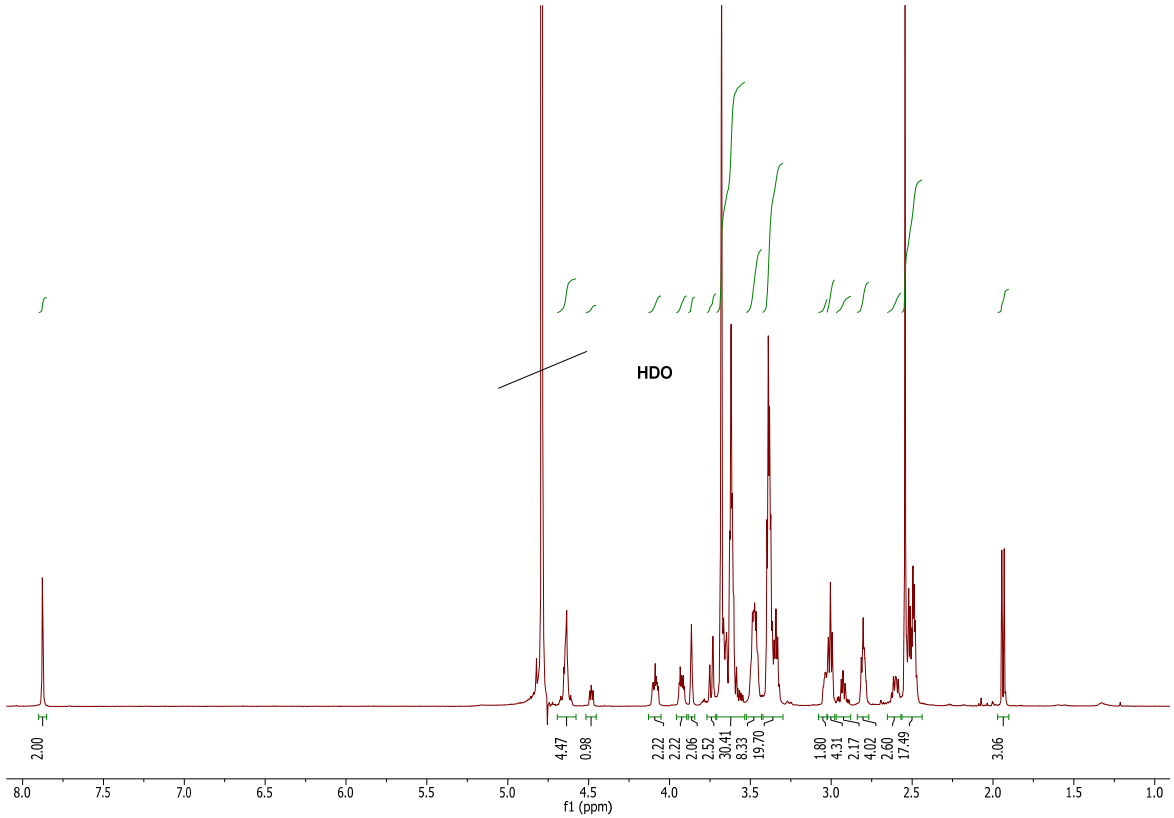

*Figure SI 6- ^{1}H-NMR (600 MHz, D_2O) of compound **O2**.*

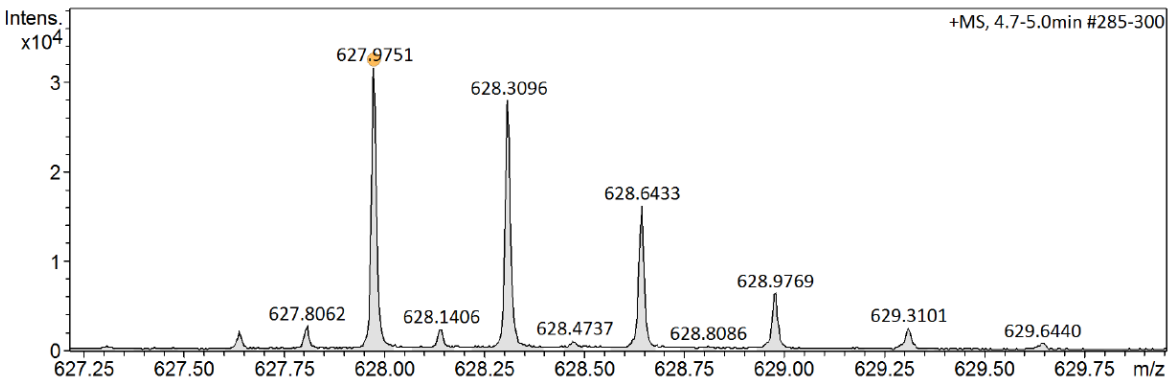

*Figure SI 7- HR-MS (ESI^{+} Q-TOF) of compound **O2**.*

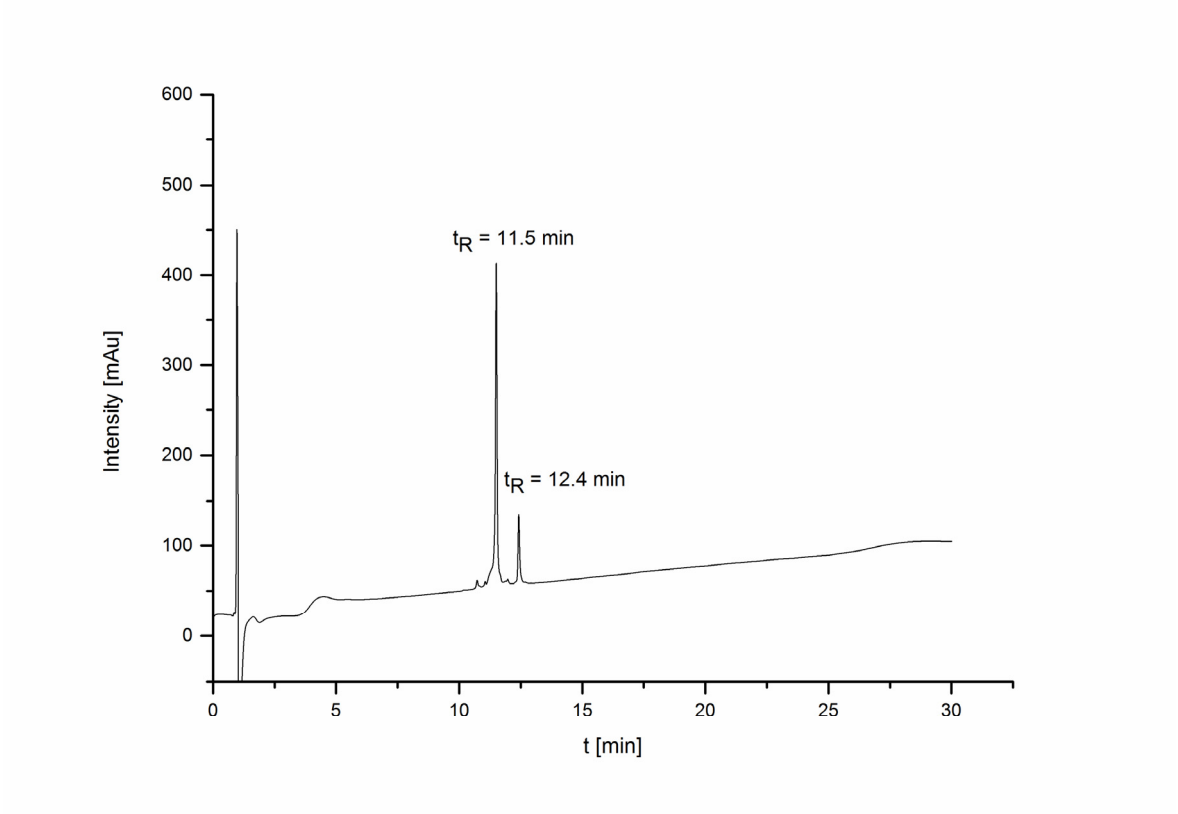

*Figure SI 8- RP-HPLC analysis (linear gradient from 0 - 50% eluent B in 30 min at 25 °C) chromatogram of compound **O2** and its dimer due to disulfide formation with their retention times.*

Glycooligomer O3

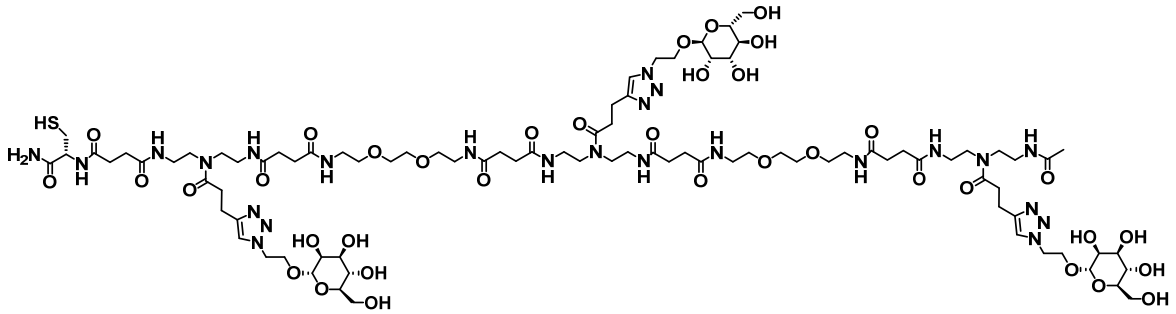

Glycooligomer **O3** was purified via preparative HPLC obtaining a yield of 29%. The anomeric proton of mannose (A) could not be examined in ^{1}H-NMR due to the overlaying signal from the residual solvent. For the acetyl group on the N-terminal end, we observed two singlets with a ratio of 1:1 that we assign to two rotational isomers in equal amounts. The presence of rotational isomers was identified in ^{1}H-NMR experiments at higher temperatures (data not shown). ^{1}H nmR (600 MHz, D_2O): δ 7.87 (s, 3H), 4.68 – 4.59 (m, 6H), 4.51 – 4.46 (m, 1H), 4.14 – 4.04 (m, 3H), 3.98 – 3.89 (m, 3H), 3.88 – 3.85 (m, 3H), 3.77 – 3.72 (m, 3H), 3.68 – 3.54 (m, 25H), 3.51 – 3.43 (m, 12H), 3.41 – 3.31 (m, 20H), 3.06 – 3.02 (m, 3H), 3.00 (t, *J*=7.3 Hz, 6H), 2.97 – 2.88 (m, 2H), 2.85 – 2.76 (m, 6H), 2.63 – 2.45 (m, 20H), 1.94 + 1.93 (2s, 3H) ppm.

HR-ESI-MS for $C_{88}H_{148}N_{24}O_{37}S$ (exact monoisotopic mass 2165.0158): $[M+3H]^{3+}$ calcd. 722.6792, found 722.6788, mass accuracy -0.55 ppm.

RP-HPLC (linear gradient from 0 - 50% eluent B in 30 min at 25 °C): Compound **O3** t_R=10.9 min (91%) and dimer of compound **O3** due to a disulfide formation t_R=11.7 min (3%). Determined purity (Sum of compound **O3** and its dimer): 94%.

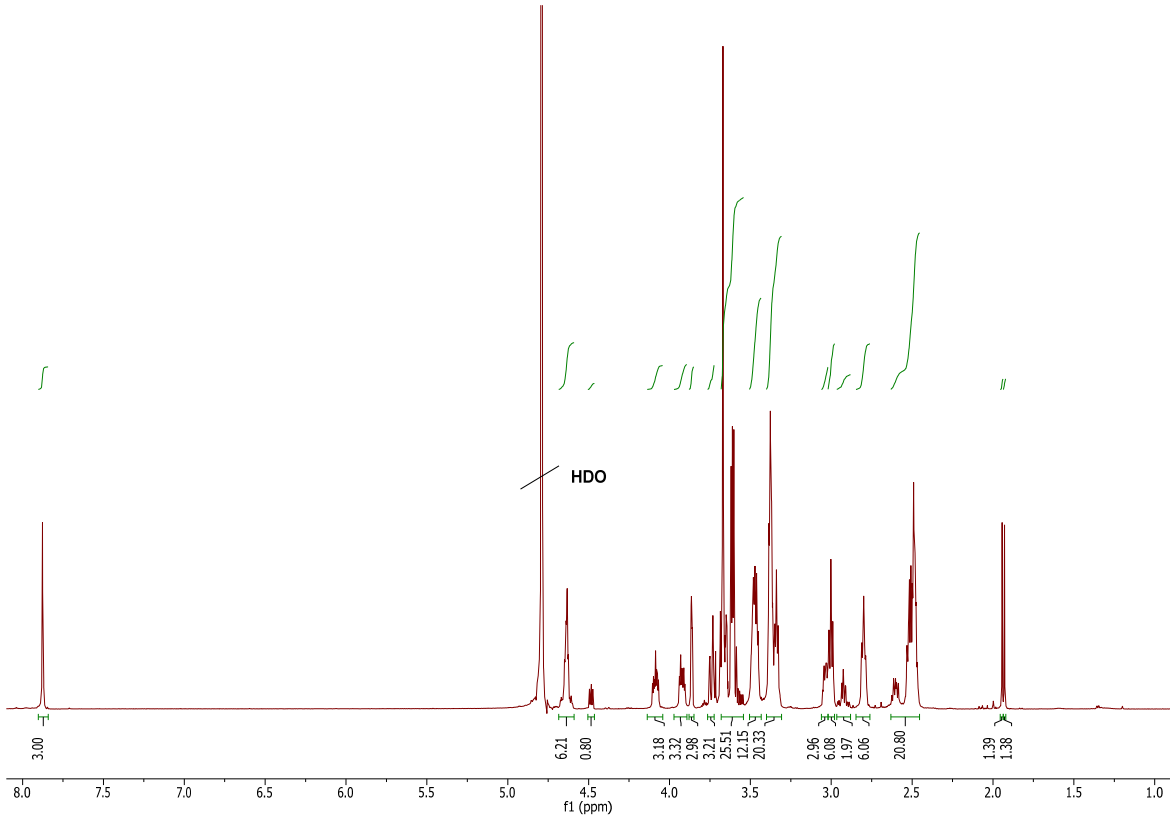

*Figure SI 9- ^{1}H-NMR (600 MHz, D_2O) of compound **O3**.*

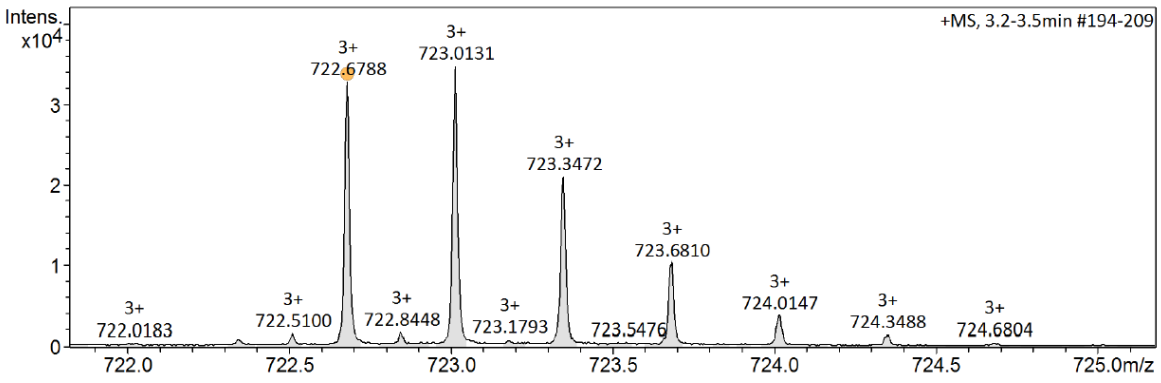

*Figure SI 10- HR-MS (ESI^{+} Q-TOF) of compound **O3**.*

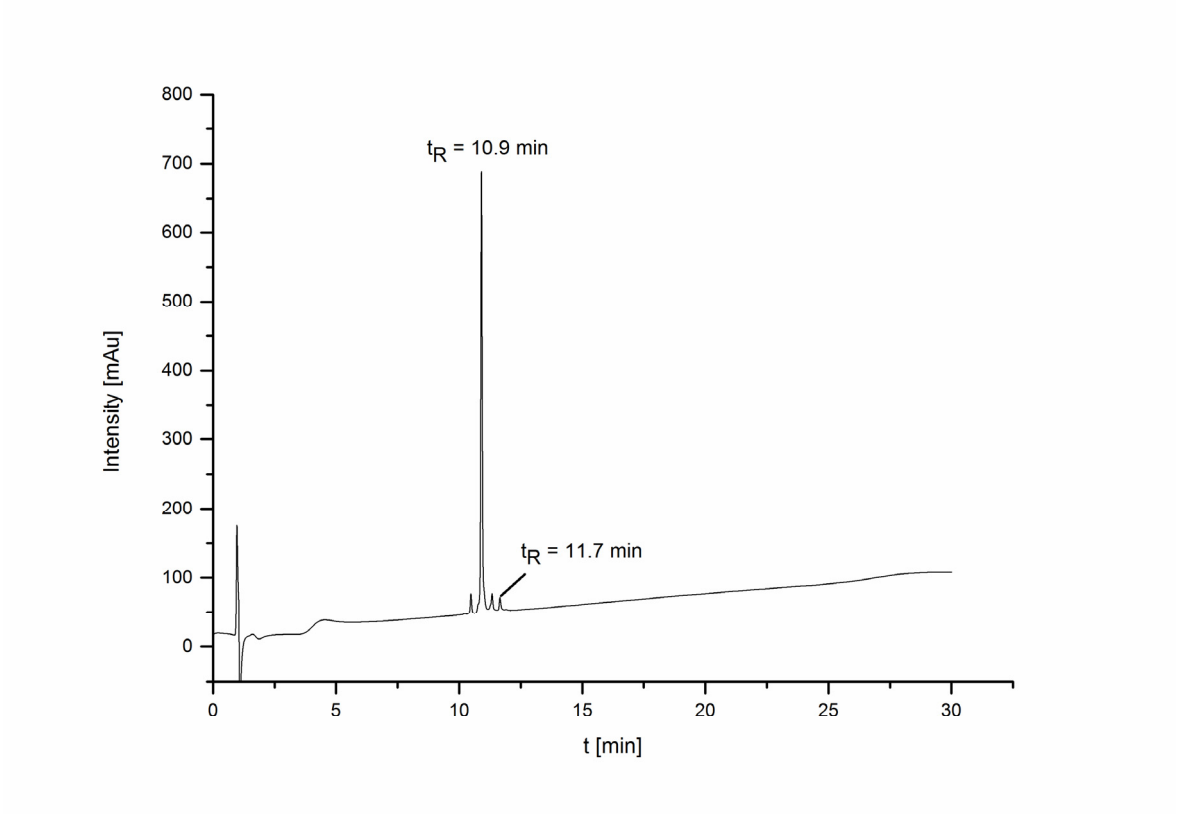

*Figure SI 11- RP-HPLC analysis (linear gradient from 0 - 50% eluent B in 30 min at 25 °C) chromatogram of compound **O3** and its dimer due to disulfide formation with their retention times.*

Glycooligomer O5

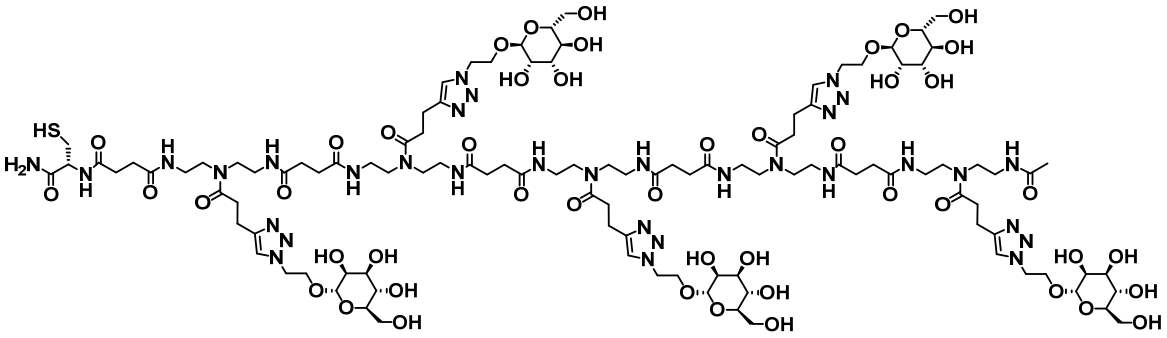

Glycooligomer **O5** was purified via preparative HPLC obtaining a yield of 34%. The anomeric proton of mannose (A) could not be examined in ^{1}H-NMR due to the overlaying signal from the residual solvent. For the acetyl group on the N-terminal end, we observed two singlets with a ratio of 1:1 that we assign to two rotational isomers in equal amounts. The presence of rotational isomers was identified in ^{1}H-NMR experiments at higher temperatures (data not shown). ^{1}H nmR (600 MHz, D_2O): δ 7.87 (s, 5H), 4.69 – 4.58 (m, 10H), 4.51 – 4.46 (m, 1H), 4.11 – 4.04 (m, 5H), 3.96 – 3.89 (m, 5H), 3.88 – 3.84 (m, 5H), 3.77 – 3.71 (m, 5H), 3.70 – 3.57 (m, 15H), 3.52 – 3.41 (m, 20H), 3.40 – 3.27 (m, 20H), 3.06 – 3.01 (m, 5H), 3.01 – 2.95 (m, 10H), 2.95 – 2.88 (m, 2H), 2.82 – 2.75 (m, 10H), 2.63 – 2.40 (m, 20H), 1.94 + 1.92 (2s, 3H) ppm.

HR-ESI-MS for $C_{110}H_{180}N_{32}O_{47}S$ (exact monoisotopic mass 2733.2399): $[M+3H]^{3+}$ calcd. 912.0873, found 912.0866, mass accuracy -0.77 ppm. For the second batch (0.3 mmol) a peak at $[M+3H]^{3+}$ 741.0085 was found corresponding to an incomplete reaction of the last TDS building block.

RP-HPLC (linear gradient from 0 - 50% eluent B in 30 min at 25 °C): Compound **O5** t_R=10.2 min (89%) and dimer of compound **O5** due to a disulfide formation t_R=10.8 min (3%). Determined purity (Sum of compound **O5** and its dimer): 92%.

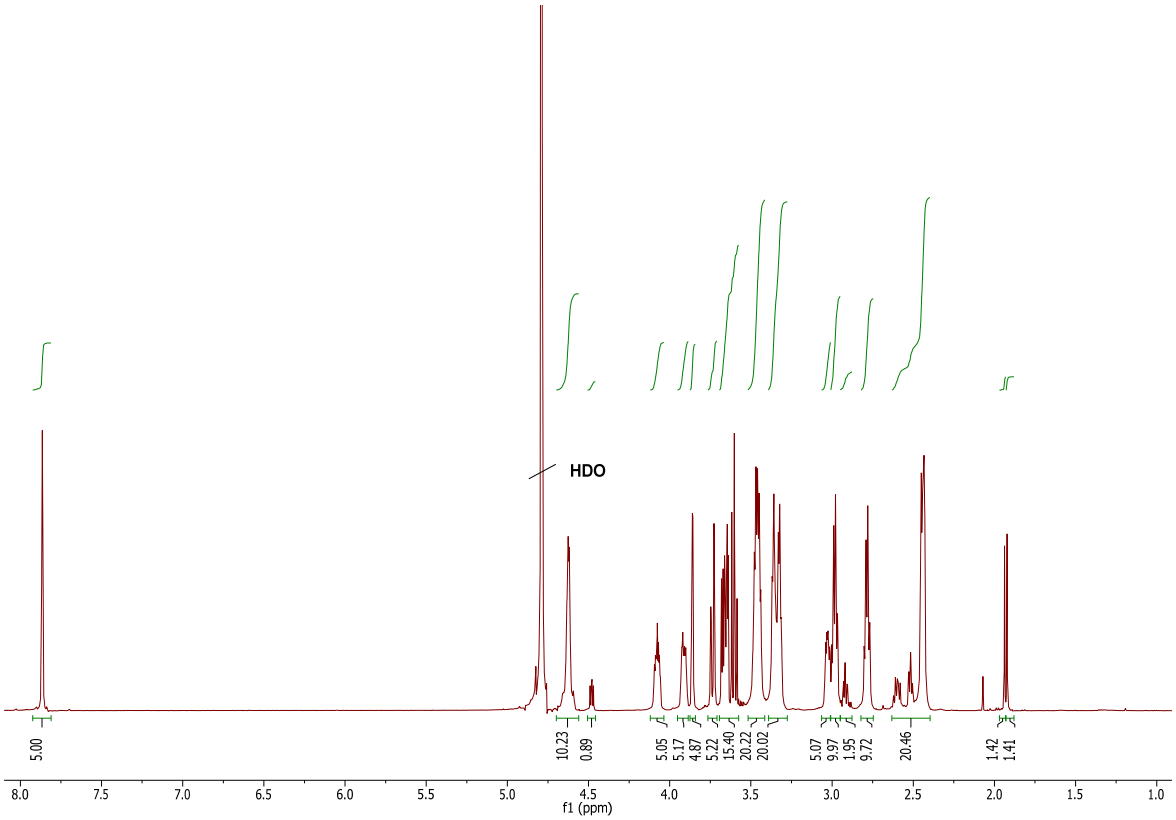

*Figure SI 12- ^{1}H-NMR (600 MHz, D_2O) of compound **O5**.*

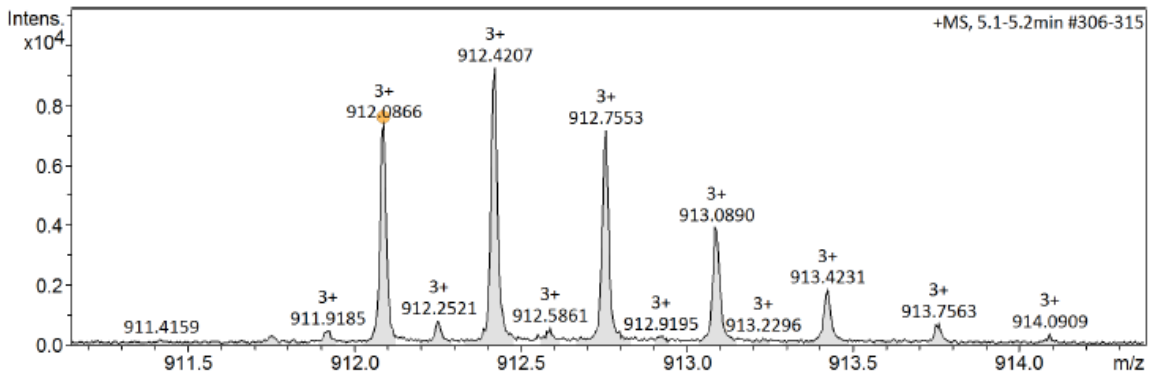

*Figure SI 13- HR-MS (ESI^{+} Q-TOF) of compound **O5**.*

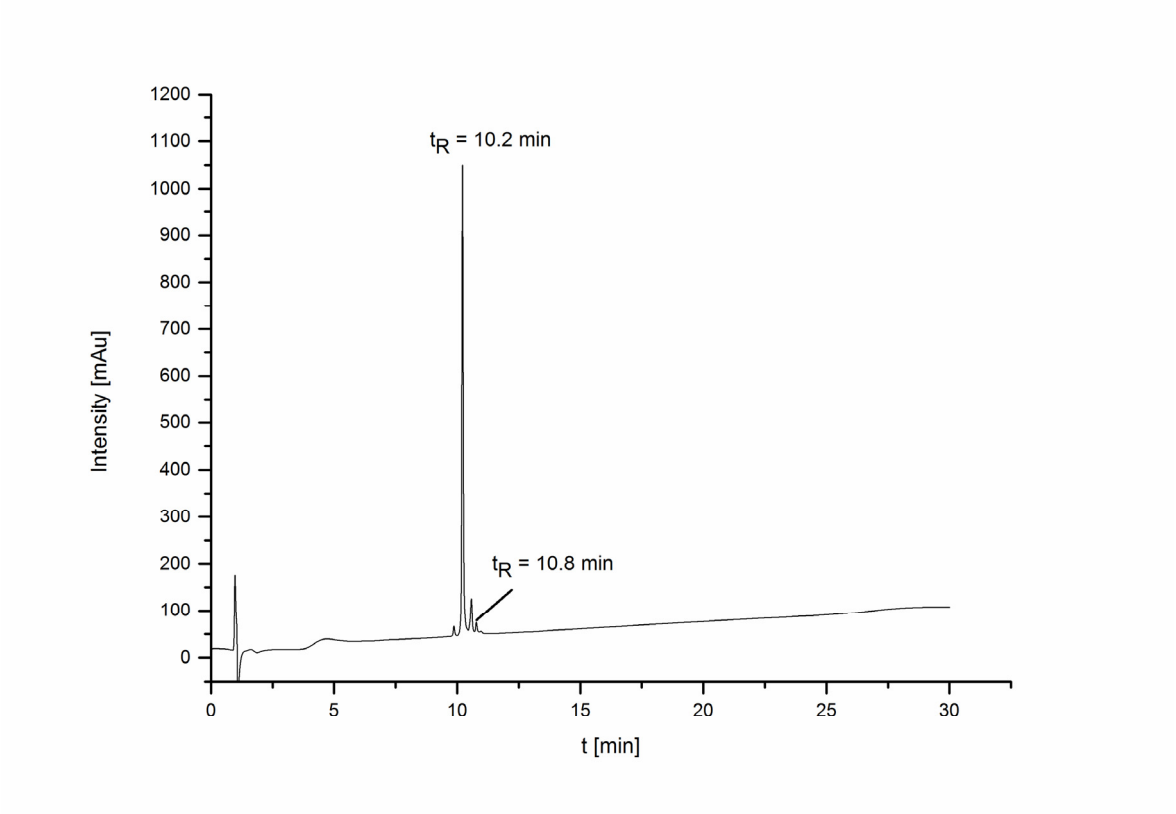

*Figure SI 14- RP-HPLC analysis (linear gradient from 0 - 50% eluent B in 30 min at 25 °C) chromatogram of compound **O5** and its dimer due to disulfide formation with their retention times.*

7.3 VALUES OF GRAPHICS IN FIGURES

Table SI 1- Adhesion energy of CA-SCPs at sugar-functionalized surface steps, Figure 18.

Surface	APTES	Linker
Adhesion Energy / μJm^{-2}	193 ± 8.83	8.8 ± 0.78

Table SI 2- Adhesion energy of Man-SCPs on GLYMO-Con A functionalized surface under inhibitory conditions, Figure 18.

MeMan / mM	0	10	100
Adhesion Energy / μJm^{-2}	120.65 ± 6.88	42.92 ± 6.27	36.09 ± 4.66

Table SI 3- Percentages of retraction curves (n=512) presenting specific rupture events over 50 nm (Single Molecule) and not showing any interaction (Flat) under inhibiting conditions, Figure 24.

MeMan / mM	0	10	100
Single Molecule / %	38.9	21.7	16.4
Flat / %	8.4	26.9	17.1

Table SI 4- Number of specific Man-Con A disruptive events within the single molecule curves under inhibition, Figure 24.

MeMan / mM	0	10	100
Single Molecule	228	118	93

Table SI 5- Mean ± std. deviation of rupture force for the specific Man-Con A events determined in single molecule curves under inhibiting conditions, Figure 24.

MeMan / mM	0	10	100
Rupture force / pN	136.5 ± 109.1	81.2 ± 51.6	83.5 ± 68.11

Table SI 6- Surface fluorescence of SCPs incubated with NGPs and BSA under different inhibiting conditions, Figure 30. Fluorescent values are expressed in arbitrary units and reduced a thousand times (10^{-3}).

MeMan / mM	CA-SCP BSA	Con A-SCP BSA	Con A-SCP BSA-SMCC-Man	Con A-SCP BSA-PEG-Man
0	43.13 ± 3.53	43.36 ± 3.52	27.81 ± 3.45	31.69 ± 4.17
10	46.39 ± 3.77	46.66 ± 3.79	22.45 ± 2.15	28.52 ± 3.14

Table SI 7- Repetitions of surface fluorescence of Con A-SCPs incubated with NGPs under different inhibiting conditions, Figure 31. Fluorescent values are expressed in arbitrary units and reduced a thousand times (10^{-3}).

MeMan / mM	BSA	BSA-SMCC-Man	BSA-PEG-Man
0	64.64 ± 1.19	40.66 ± 3.53	49.51 ± 4.89
10	63.56 ± 2.99	41.29 ± 5.62	52.95 ± 7.89

Table SI 8- Adhesion energy of Man-SCPs on Con A-functionalized surface along different reaction steps, Figure 37.

Surface	Glass	P-ConA	GLYMO	C-ConA
Adhesion Energy / μJm^{-2}	68.4 ± 4.41	100 ± 3.14	196 ± 7.78	134 ± 7.09

Table SI 9- Adhesion energy between Man-SCPs and Con A functionalized surfaces, by physisorption and chemisorption, after flushing steps and a final inhibition with 10 mM MeMan, Figure 39.

Round	0	1	2	3	4
Phisisorption	63.37 ± 2.21	58.89 ± 3.57	62.50 ± 1.91	64.07 ± 2.18	63.88 ± 2.28
Chemisorption	127.85 ± 2.96	107.07 ± 6.65	86.81 ± 3.65	73.31 ± 3.32	72.36 ± 2.66

5	6	7	8	9	Inhibition
62.46 ± 2.72	66.05 ± 1.88	62.73 ± 3.02	65.63 ± 3.68	63.25 ± 2.86	34.69 ± 4.88
70.97 ± 2.72	68.30 ± 1.73	71.26 ± 2.17	75.88 ± 1.85	68.40 ± 2.55	53.22 ± 2.89

Table SI 10- Adhesion energy of fresh Man-SCPs on Con A functionalized surfaces after "pushing" previous SCPs away from the observed area, Figure 41.

Round	1	2	3	4	5
Physisorption	110.12 ± 4.66	97.81 ± 3.88	91.85 ± 6.51	84.35 ± 3.98	64.96 ± 2.46
GLYMO	44.79 ± 2.06	45.07 ± 2.87	42.97 ± 1.47	41.65 ± 2.04	46.86 ± 1.61

6	7	8	9	10
87.02 ± 7.56	74.45 ± 4.05	68.48 ± 3.89	61.42 ± 2.61	54.12 ± 1.92
44.61 ± 2.29	42.37 ± 2.50	51.53 ± 1.61	43.27 ± 2.82	41.36 ± 1.95

Table SI 11- Adhesion energy for thoroughly mixed and re-precipitated Man-SCPs on physisorbed Con A surfaces, Figure 42.

Round	1	2	3	4
0 mM MeMan	112.17 ± 3.7	227.13 ± 33.0	228.00 ± 25.3	147.25 ± 10.3
10 mM MeMan	77.16 ± 2.88	82.66 ± 4.49	73.25 ± 3.76	73.16 ± 4.67

Table SI 12- Adhesion energy of Con A-SCPs on sugar functionalized surfaces with SMCC linker and the indicated density of mannose diluted with 2-mercaptoethanol, Figure 44.

	100%	50%	25%	0%
0 mM MeMan	42.1 ± 1.66	48.6 ± 3.28	49.8 ± 1.50	48.5 ± 8.05
10 mM MeMan	23.2 ± 2.37	32.5 ± 1.96	29.1 ± 2.23	26.3 ± 2.50

Table SI 13- Adhesion energy of Con A-SCPs on sugar functionalized surfaces with PEG linker and the indicated density of mannose diluted with 2-mercaptoethanol, Figure 44.

	100%	50%	25%	0%
0 mM MeMan	92.3 ± 2.29	15.9 ± 2.09	18.2 ± 1.23	15.2 ± 2.44
10 mM MeMan	12.3 ± 1.08	11.5 ± 1.12	8.46 ± 2.55	12.1 ± 1.55

Table SI 14- Adhesion energy of Con A-SCPs on sugar functionalized surfaces with SMCC linker and the indicated density of mannose diluted with dithiothreitol, at different times after SCP addition, under inhibiting conditions, Figure 45.

ManSH	MeMan / mM	60 min	120 min	600 min
100%	0	26.5 ± 1.65	26.7 ± 1.06	25.8 ± 1.36
	10	10.9 ± 2.25	16.2 ± 1.87	18.3 ± 2.38
50%	0	49.2 ± 2.45	41.0 ± 5.50	51.3 ± 3.08
	10	24.1 ± 1.33	25.3 ± 2.14	25.5 ± 1.80
25%	0	48.6 ± 2.45	46.4 ± 3.64	50.3 ± 3.79
	10	24.9 ± 1.47	31.1 ± 1.64	31.1 ± 1.16
0%	0	49.6 ± 4.36	43.7 ± 3.85	51.6 ± 3.13
	10	24.4 ± 5.24	24.5 ± 2.64	31.9 ± 1.46

Table SI 15- Adhesion energy of Con A-SCPs on sugar functionalized surfaces with SMCC linker and the indicated density of mannose diluted with dithiothreitol with a post-acetylation of sugars, at different times after SCP addition, under inhibiting conditions, Figure 46.

ManSH	MeMan / mM	60 min	120 min	600 min
100%	0	18.0 ± 1.97	23.0 ± 1.49	26.2 ± 1.75
	10	68.4 ± 2.1	16.7 ± 2.19	18.4 ± 1.48
50%	0	27.8 ± 3.08	35.8 ± 1.91	37.7 ± 4.96
	10	16.0 ± 3.24	22.2 ± 2.66	26.1 ± 3.33
25%	0	40.1 ± 2.52	41.6 ± 2.11	13.8 ± 1.66
	10	23.6 ± 3.47	25.3 ± 1.62	26.7 ± 2.14
0%	0	34.6 ± 2.72	31.4 ± 2.57	38.1 ± 1.88
	10	22.3 ± 2.4	20.3 ± 2.12	27.1 ± 1.51

Table SI 16- Frequency of "Single Molecule" curves expressed as percentage for oligomers (n=512) and polymers (n=1024) ligands, Figure 51.

Ligand	O1	O2	O3	O5	P1	P2	P3	P5
Single Molecule / %	16.41	24.22	15.63	16.6	3.42	4.39	3.92	1.89

Table SI 17- Frequency of rupture events in "Single Molecule" curves for oligomer and polymer ligands, Figure 51.

Ligand	Ratio	Ligand	Ratio
O1	1.41 ± 0.71	P1	1.57 ± 1.18
O2	1.12 ± 0.36	P2	1.45 ± 0.69
O3	1.14 ± 0.40	P3	1.16 ± 0.56
O5	1.50 ± 0.78	P5	1.41 ± 0.78

Table SI 18- Average rupture force for the oligomer and polymer carbohydrate ligands (mean ± std. deviation), Figure 54.

Ligand	Force / pN	Ligand	Force / pN
O1	67.10 ± 46.30	P1	103.03 ± 81.11
O2	71.15 ± 45.58	P2	105.01 ± 69.88
O3	88.08 ± 45.37	P3	99.12 ± 77.09
O5	96.39 ± 65.40	P5	112.62 ± 74.76

*Table SI 19- Fluorescent values of the whole series of NGPs under different inhibiting conditions; NGPs functionalized with the short (SMCC) and long (PEG) linkers and oligomers bearing 2 (**O2**) and 5 (**O5**) Man moieties, Figure 56. Fluorescent values are expressed in arbitrary units and reduced a thousand times (10^{-3}).*

	O2		O5	
SMCC	0 mM MeMan	10 mM MeMan	0 mM MeMan	10 mM MeMan
Round 1	31.61 ± 6.64	29.79 ± 0.37	27.32 ± 5.22	26.84 ± 0.38
Round 2	36.75 ± 3.91	37.85 ± 4.56	30.10 ± 3.11	27.86 ± 3.41
PEG	0 mM MeMan	10 mM MeMan	0 mM MeMan	10 mM MeMan
Round 1	26.09 ± 2.47	22.98 ± 0.24	15.75 ± 1.28	15.46 ± 0.15
Round 2	29.14 ± 8.22	32.96 ± 6.13	19.61 ± 2.00	17.06 ± 1.71

Table SI 20- Adhesion energy of Man-SCPs on Con A determined after 60 min of SCP addition remaining the media free of competitors (Free Adhesion), and after 60 and 600 min of inhibition with NGPs (0.05 mg/mL), Figure 62.

	Free Adhesion	60 min	600 min
REF	73.3 ± 6.58	73.7 ± 5.16	73.1 ± 6.20
BSA	73.6 ± 3.94	67.4 ± 2.98	61.3 ± 3.07
BSA-SMCC-Man	77.3 ± 2.94	69.2 ± 2.52	48.6 ± 5.62
BSA-SMCC-O2	74.7 ± 4.72	55.7 ± 4.37	30.0 ± 4.22
BSA-SMCC-O5	74.9 ± 3.89	53.2 ± 2.45	33.7 ± 6.15
BSA-PEG-Man	80.4 ± 3.73	70.4 ± 2.78	66.3 ± 5.72
BSA-PEG-O2	68.1 ± 3.48	59.7 ± 2.25	40.8 ± 4.08
BSA-PEG-O5	69.2 ± 3.18	58.9 ± 2.08	46.1 ± 2.98

Table SI 21- Adhesion energy of Man-SCPs on Con A determined after 60 min of SCP addition remaining the media free of competitors (Free Adhesion), and after 60 and 600 min of inhibition with monomolecular ligands (62.5 µM), Figure 63.

	Free Adhesion	60 min	600 min
MeMan	128.00 ± 3.94	125.00 ± 4.26	119.00 ± 2.88
ManSH	134.00 ± 7.09	117.00 ± 6.62	113.00 ± 3.50
O2	112.00 ± 3.53	81.30 ± 3.31	79.30 ± 3.52
O5	136.00 ± 3.84	96.70 ± 3.41	85.60 ± 2.60

8 ACKNOWLEDGMENTS

"Que es de gratitud, al alcanzar una cima,
volver la vista sobre los hombros que te aupan"

I would like to extend thanks to all the people who positively influenced in my education and those that generously contributed to the work presented in this thesis.

Foremost, I would like to express my sincere gratitude to my supervisor Jun. Prof. Dr. Schmidt, who has successfully helped me to move forward my scientific career since we first met in Leipzig. Since then, I am very grateful for his guidance, endorsement, patience, and encouragement. I am also very thankful to Prof. Dr. Laura Hartmann for the opportunity to start at Heinrich Heine Universität Düsseldorf, for the prospect to cooperate with her group and her insightful comments. Further, I also thank Prof. Dr. Reiner Weinkauf for his courtesy and the permission to use his XPS equipment.

Besides, I would also like to thank the people that contributed to this thesis. C. Gerke, Dr. H. Wang and F. Jacobi for providing samples, and B. Deckert for the XPS instructions.

In addition, I would like to thank all the students from the Schmidt and Hartmann groups, for the good reception, for the interesting discussions, and all the fun. Together to senior scientist Dr. M. Tabatabai, lab technician S. Scheelen and secretary M. Kitza, who made working easier.

As well, my gratitude is to Letizia Cardone for her kindness, confidence, and support.

Finally, my deepest gratitude is to my parents, brother and sister.

9 AUTHORSHIP AND CONTRIBUTIONS

I hereby declare that this doctoral thesis is the result of my own work unless otherwise acknowledged in the text. All references and verbatim extracts have been quoted, and all sources of information have been specifically acknowledged. This thesis has not been submitted for any other degree. The contributions of co-authors and supervisors to this thesis are listed below.

Jun. Prof. Dr. Stephan Schmidt (Co-supervisor):

Design of research, research coordination, and collaborative data analysis. DLS measurements of sequence define oligomers and polymers (section 3.2.1.1).

Prof. Dr. Laura Hartmann (Supervisor):

Design of research and collaborative data analysis.

Dr. Hanqing Wang (Ph.D. student, group of Prof. Dr. Laura Hartmann):

Synthesis and functionalization of Con A-SCPs for Lectin functionalized surface (section 3.1.1.3) and Lectin surface stability (section 3.1.1.3). Synthesis and characterization of PEG-dAAm macromonomers used in the synthesis of Con A-SCPs for adhesion inhibition assays (section 3.2.4).

Christoph Gerke (Ph.D. student, group of Prof. Dr. Laura Hartmann):

Synthesis and characterization of building blocks. Synthesis and characterization of the sequence defined glycopolymers for SM-AFM (sections 3.1.1 and 3.2.2).

Fawad Jacobi (Ph.D. student, group of Prof. Dr. Laura Hartmann):

Synthesis and functionalization of Con A-SCPs for Adhesion inhibition assays (section 3.2.4).

Yulia Schaumkessel (B.Sc. student, group of Jun. Prof. Dr. Stephan Schmidt):

TBO characterization and functionalization of Con A-SCPs for Macroscopic scale (section 3.1.1).

Jennifer Materlik (B.Sc. student, group of Prof. Dr. Laura Hartmann):

Synthesis and characterization of the sequence defined glycooligomers for SM-AFM (section 3.2.2).

Düsseldorf, 07.12.2018

Lic. D. Alberto Camaleño de la Calle